UNIVERSITY OF BELGRADE

FACULTY OF CHEMISTRY

Stepan M. Stepanović

Density functional approximations for spin state energetics in transition-metal complexes

Doctoral Dissertation

Belgrade, 2018

UNIVERZITET U BEOGRADU

HEMIJSKI FAKULTET

Stepan M. Stepanović

Aproksimacije funkcionala gustine u proučavanju energija spinskih stanja kompleksa prelaznih metala

doktorska disertacija

Beograd, 2018

Supervisors

_____

Dr. Maja Gruden-Pavlović, Associate professor

University of Belgrade-Faculty of Chemistry, supervisor

_____

Dr. Marcel Swart, ICREA Research professor

Institut de Química Computacional i Catàlisi (IQCC)

University of Girona, Spain, supervisor

Committee members

_____

Dr. Mario Zlatović, Associate professor

University of Belgrade-Faculty of Chemistry

_____

Dr Matija Zlatar, Associate research professor

University of Belgrade- Center for Chemistry,

Institute of Chemistry, Technology and Metallurgy

_____

Dr Wesley Browne, Associate Professor

Stratingh Institute for Chemistry

University of Groningen, The Netherlands

Date _____.

Acknowledgments

On the very beginning, I would like to thank my mentor, Dr. Maja Gruden-Pavlović for extraordinary guidance, and support she has given me, not only related to this dissertation but since our first encounter. She put up with many things no other person would. I would like to thank her for her patience, unique opportunities she provided and for being by my side in most difficult times during these five years.

I want to express a special gratitude to Professor Dr. Marsel Swart for being extremely helpful many times, he and Maja designed the shape of this thesis. Also, I want to thank him for going through entire dissertation and giving his valuable contributions to its content.

Although Dr. Matija Zlatar is not formally a supervisor in this comity, he has definitely been that during my thesis. I would like to thank him for scientific knowledge that he unselfishly shared and his valuable advice, guidelines and opinions he provided, and without whom my knowledge and this this thesis would be at even lower level.

This thesis would not be a result of a great teamwork If it hadn't been for two great professors, Dr. Wesley Brownie and Dr. Mario Zlatović. Their scientific contributions regarding this thesis are priceless, and I would like to thank both of them for their time, efforts and involvement in this project.

Dr. Aleksandar Nikolic (Sasa) already knows how much his presence and behavior meant to me during some difficulties time, especially at the very beginning. Also, there are so many things I learned from him.

I would also like to give a lot of thanks to my colleges at the laboratory, Filip, Mladen, Ljubica, Marko for endless time and effort they provided so this thesis could have the life of its own and a very big thank you for providing a great environment in which we all, as a great team, were able to accomplish remarkable things. Filip, you are next.

For endless love, support and guidance I would like to thank my parents. Without them, this life would have been so much harder and my entire education, which was one of my father greatest wishes, would not be as relaxed and carefree.

Special gratitude goes to my Friends, Djordje, Marijana, Jovana and Filip. They make my life complete.

And last but not the least, I would like to thank my girlfriend Tijana because her presence gave the special purpose to everything I do. Love is the only thing that can change us to better.

This thesis is dedicated to my parents, for everything they have given me.

Ovu tezu posvećujem svojim roditeljima, zbog svega što su mi pružili.

Density functional approximations for spin state energetics in transition-metal complexes

SUMMARY

Many fascinating features of coordination chemistry originate from the fact that small changes in metal ion environment can induce big changes in the properties of the compounds. Moreover, most transition-metal (TM) ions with partially filled d-shells can manifest different spin multiplicity in the ground state that is, different spin states. The identity of the ground spin state and the analysis and description of close lying states of different multiplicity is of crucial importance for the understanding of the microscopic origin of the reactivity, electrochemistry and photochemistry in biomolecules, industrial catalysis and in spin crossover compounds. However, elucidating the role and effect of different spin states on the properties of a system, and even determining which spin state occurs naturally, is challenging task both from an experimental and theoretical point-of-view.

Density Functional Theory (DFT) has become the preferred theoretical method for complicate electronic structure of coordination compounds, mainly because it provides good compromise between the computational cost and accuracy. The challenge in application of DFT for spin states was first noted in 2001, and it was concluded that early Generalized Gradient Approximation (GGA) functionals favored low-spin states, while hybrid functionals favored high-spin states. In the following years, many density functional aproximations (DFAs) showed partial success, but mainly failures in the attempts to tackle the problem of close lying spin states in TM complexes. In 2004, the combination of a relatively new exchange functional, OPTX, with the PBE correlation part gave excellent results for the spin states of iron complexes, and hence a new DFA was born (OPBE). Since OPBE showed very good performance of for spin states, and later as well S_N2 reaction barriers, it was mixed with PBE that gives good results for weak interactions. After incorporation of Grimme's D_2 dispersion energy, the SSB-D functional was created. Future refinement to make it numerically more stable and inclusion of Grimme's D_3 dispersion energy, led to its successor S12g.

One of the driving ideas of this work was a thorough validation of these DFA's, specifically designed for spin states (OPBE, SSB-D and S12g) and to propose suitable computational recipes for accurate determination of geometries, spin states and all related properties of TM compounds.

Systematic validation study for the spin state energetics of nine iron complexes that show a diversity of experimentally observed spin ground states, and represent biomimetic molecules for P450cam and similar active sites, have been performed. This study of iron challenging systems resulted in further insight in the performance of the promising density functional approximations. The next step was a systematic analysis of the effect of the spin state and the ligand charge on coordination preferences for a Mn^{II}, Fe^{II}/Fe^{III}, Co^{II}, Ni^{II}, Cu^{II} and Zn^{II} for the 2,6-diacetylpyridinebis(semioxamazide) ligand and its mono- and di-anionic analogues. Complexes of polydentate acylhydrazone ligands with d-metals are particularly interesting since they have remarkable structural features that lead to a diversity of potential applications. The analysis showed some remarkable features, including significant effect of the spin state on the ligand coordination, and rationalized trends and behavior across the first row transition metal series. Furthermore, we analyzed and explained trends in spin state energetics in polypyrazolylborato complexes of first-row transition metals. The effects of substitution at the position 3 and 5 of pyrazolyl rings was also explored, as well as the influence of Jahn-Teller distortion on spin state switching, and altogether, the deeper insight in the chemistry of these important enzymatic mimics and SCO molecules was gained. All these validation studies direct us towards the best DFA (S12g) for the study of the mechanism of the catalytic cycle for catechol dioxygenase mimics. Full details of the catalytic cycle, with all accessible spin states and both possible pathways, intradiol and extradiol, have been explored.

With proposed methodology, obtained results and their rationalizations, we are step further to achieve explicit control of spin states of TM compounds and rational design of TM compounds with desired properties.

Keywords: Multideterminental Density Functional Theory, Spin states, Biomimetic model szstems, Jahn-Teller effect, Reaction mechanisams

Area of science: Chemistry

Sub-area of science: Inorganic chemistry

UDC number:

Aproksimacije funkcionala gustine u proučavanju energija spinskih stanja kompleksa prelaznih metala

REZIME

Mnoge fascinantne osobenosti koordinacione hemije potiču od činjenice da male promene u okruženju centralnog metala mogu izazvati velike promene u svojstvima jedinjenja. Štaviše, većina jona prelaznih metala (TM) sa delimično popunjenim d-orbitalama može manifestovati različit spinski multiplicitet u osnovnom stanju, tj. različita spinska stanja. Identitet osnovnog spinskog stanja i analiza i opis bliskih spinskih stanja različitog multipliciteta su od ključnog značaja za razumevanje mikroskopskog porekla reaktivnosti, elektrohemijskih osobina, fotohemijskog ponašanja biomolekula, industrijske katalize i *spin-crossover* (SCO) jedinjenja. Međutim, razjašnjavanje uloge i efekta različitih spinskih stanja na osobine sistema, pa čak i samo određivanje osnovnog spinskog stanja je komplikovan zadatak sa eksperimentalne kao i teorijske tačke gledišta.

Teorija funkcionala gustine (DFT) postala je ključna teorijska metoda za analizu komplikovane elektronske strukture koordinacionih jedinjenja, uglavnom zbog toga što pruža dobar kompromis između utrošenog računarskog vremena i ostvarene preciznosti. Problemi u primeni DFT-a za spinska stanja prvi put su zabeleženi 2001.godine i zaključeno je da stariji funkcionali, koje se zasnivaju na generalizovanom gradijentu (eng. Generalized Gradient Approximation - GGA) favorizuju stanja sa niskim spinom, dok hibridni funkcionali, koji imaju uključen deo interakcije izmene iz Harti-Foka, favorizuju stanja sa visokim spinom. U narednim godinama, mnogi aproksimativni funkcionali gustine (DFA) su pokazali umereni uspeh, ali uglavnom neuspehe u pokušajima da opišu problem bliskih spinskih stanja u kompleksima prelaznih metala. U 2004, kombinovanjem relativno novog funkcionala koji opisuje interakciju izmene, OPTX, sa PBE funkcionalom za opis korelacije, dobijeni su odlični rezultati za spinska stanja kompleksa gvožđa, čime je stvoren novi DFA (OPBE). Kako se OPBE pokazao vrlo dobro za opisivanje spinskih stanja, a kasnije i za S_N2 reakcione barijere, kombinovan je sa PBE koji se dobro pokazao za opis nekovalentnih interakcija. Nakon

dodavanja Grimme-ove D_2 disperzione energije, napravljen je SSB-D funkctional. Naredna podešavanja, u cilju poboljšavanja numeričke stabilnosti, kao i dodatak Grimme-ove D_3 disperzione energije, su dovele do njegovog naslednika S12g funkcionala.

Jedna od vodećih ideja ove disertacije je temeljna validacija DFA jedinstveno dizajniranih za spinska stanja (OPBE, SSB-D and S12g) i predviđanje računarskih protokola za precizno određivanje geometrija, spinskih stanja i svih povezanih svojstava TM jedinjenja.

Izvedena je sistematična validaciona studija za energije spinskih stanja devet kompleksa gvožđa koji eksperimentalno pokazuju različita osnovna spinska stanja i predstavljaju biomimetička jedinjenja P450cam i enzima sa srodnim aktivnim mestima. Proučavanje ovih komplikovanih sistema omogućilo je dublji uvid u performanse S12g DFA. Naredni korak je podrazumevao detaljnu analizu uticaja spinskih stanja i naelektrisanja liganda na koordinacionu hemiju kompleksa Mn^{II}, Fe^{II} / Fe^{III}, Co^{II}, Ni^{II}, Cu^{II} i Zn^{II} sa 2,6-diacetil-piridin-bis(semioksamazid)-nim ligadnom i njegovim mono- i di-anjonskim analozima. Kompleksi polidentatnih acilhidrazonskih liganada sa d-metalima su posebno zanimljivi jer imaju nesvakidašnje strukturne karakteristike koje dovode do izuzetno raznovrsnih aplikacija. Analize su pokazale izuzetne karakteristike, uključujući značajan uticaj spinskih stanja na koordinaciju liganda i razloge koji stoje iza opažanih trendova i ponašanja u prvoj seriji prelaznih metala. Nadalje, analizirali smo i objasnili trendove u energetici spinskih stanja u polipirazolilborato kompleksima prve serije prelaznih metala. Efekti supstitucije na položaje 3 i 5 pirazolilskog prstena su takođe istraživani, kao i uticaj Jahn-Teller-ove distorzije na redosled spinskih stanja što sve zajedno daje dublji uvid u hemiju ovih važnih enzimskih mimetika i SCO jedinjenja. Sve validacione studije su nas usmerile ka najboljem DFA (S12g) za proučavanje mehanizma katalitičkog ciklusa molekula koji su mimetici katehol-dioksigenaze. Ispitani su detalji katalitičkog ciklusa, sa svim mogućim spinskim stanjima i oba moguća katalitička puta, intradiolni i ekstradiolni.

Predstavljena metodologija, dobijeni rezultati, kao i njihova racionalizacija predstavljaju još jedan korak ka krajnjem cilju, razumevanju i dostizanju kontrole

spinskih stanja jedinjenja prelaznih metala i preciznog dizajniranja TM jedinjenja sa željenim svojstvima.

Ključne reči:, Multideterminantna Teorija funkcionala gustine, Spinska stanja, Biomimetički model sistemi, *Jahn-Teller*-ov efekat, Reakcioni mehanizmi
Naučna oblast: Hemija
Uža naučna oblast: Neorganska hemija
UDK broj:

Contents

1. Introduction

The beauty and the diversity of the transition metal chemistry lie up in the fact that small changes in the central metal environment can produce significantly different properties. The origin of this behavior can be traced back to the electronic structure. Molecular orbitals that originate from metal d-orbitals have just the right energy separation that makes various electron arrangements relatively close in energy and thus it is relatively easy to affect properties, spectra and reactions of these compounds.

From the various electron arrangements that have been mentioned, arise the states with different spin multiplicity. The understanding of the nature and behavior of these states, coupled with prediction of their influence on spectroscopy and properties of transition-metal complexes is one of the main goals of modern inorganic chemistry. Their significance arises both from the fundamental aspect and various applications in material design, biomolecular science and catalysis. It is noteworthy to mention that, despite great progress in the development of the different experimental techniques, the experimental (mainly magnetic and spectroscopic) characterization of the spin multiplicity of important intermediates and reactive species is still far from a trivial task. As a consequence, the theoretical prediction, analysis and interpretation of close lying spin states represent a natural complementary approach. Unfortunately, the theory has its own inherent problems and limitations. State of the art *ab initio* methods are very accurate, but are generally too computationally expensive for interesting transition metal systems, unless drastic simplifications and approximations are made. Density functional theory (DFT) represents a good compromise between accuracy and computational cost, but most Density Functional Approximations (DFAs), developed for main group elements show unwanted tendencies toward some particular spin state. The description of this phenomena and the rational analysis on the basis of DFT is not a trivial task, and one of the aims of this work is the thorough validation of different DFAs, specifically designed for spin states, as well as other modern DFAs on the properties of biomimetic model complexes and potential spin crossover (SCO) systems.

As a final point, the thorough analysis of different close lying spin states on a catalytic mechanism of well-described model compound that mimics the catalytic cycles of the important O_2 activating enzyme class. To do so, the level of theory that has proven to be

the most accurate in the validation studies performed in the first part of this thesis was utilized.

Whenever there is a possibility of degenerate spin state, the analysis of the Jahn-Teller effect on the spin state ordering and the overall molecular properties was also examined. The thesis is divided in an introductory part containing Chapters 2 and 3, followed by the results and discussion part, contained in Chapter 4, and general conclusion presented in Chapter 5. Chapter 2 describes the origin, misconceptions, significance and the nature of the concept of the spin states in chemistry, with special emphasis on transition metal compounds. As a methodological introduction, Chapter 3 contains theoretical basics of quantum chemical description of electronic structure, again, with special emphasis on the tendencies in the description of spin states and their fundamental origin. Challenging systems and biomimetics for the P450 pathway are analyzed and used for methodology validation (Chapter 4-1), together with exotic, first row series of biomimetic seven coordinate complexes with flexible ligand that can bind to metal in various ways and protonated forms (Chapter 4-2) and entire first row series important SCO candidates and small molecules enzyme mimetics, scorpionate complexes, 4-3. Chapter 4-4 constitutes the central part of the work and examines the effect of different close lying spin states on a catalytic cycle of catechol dioxygenase biomimetics with different selectivity.

2. Spin States in Chemistry

All but simplest one electron systems have more than one electronic state with different spin multiplicity (spin state) available. The simple illustration is given in Figure 2-1, where, for example, two electrons can be in paired (singlet, a)) state or unpaired (triplet, b)) state.

Figure 2-1 Two examples of electron arangements in two electron-two level system

Generally, the arrangement with maximal number of unpaired electrons is the high spin (HS) state, the low spin (LS) state have minimal number of unpaired electrons and any intermediate arrangement is called the intermediate (IS) spin state.[1] In coordination compounds, molecular orbitals that originate from metal d-orbitals have just the right energy separation that makes these arrangements relatively close in energy and very important for properties, spectra and reactions of these compounds. This is the reason that discussion of spin states is most often connected with transition metal chemistry, since in "everyday" bio-organic molecules all electrons are paired and other arrangements are significantly higher in energy. Close lying HS and LS spin electronic configurations of a first row, octahedral transition metal (TM) complexes is depicted in Figure 2-2.

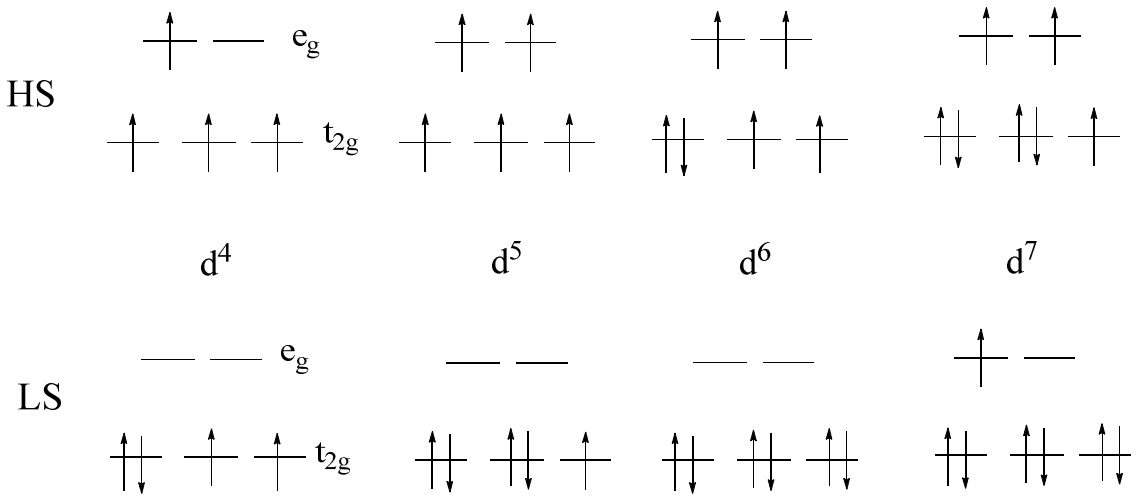

Figure 2-2 HS and LS spin electronic configurations that are relatively close in energy for a first row TM octahedral complexes

2.1. Spin states in main group chemistry

Although this area of spin state research have drawn much less attention than coordination chemistry, there are important exceptions of main group compounds that have a close lying spin states.[2-4] Among the diatomic molecules, the triplet ground state of oxygen is most important example. The relative inertness of O_2 arises from the fact that most of the everyday compounds are in a singlet ground state[i] and the reaction with $^3O_2$ is spin forbidden (otherwise, everything would just burst into flame). It is not surprising that all the enzymes in the body that utilize oxygen for certain transformations, possess a TM in their active site, since these have many close lying spin states available and can react with oxygen in a spin-allowed manner. Also, the excited $^1O_2$ is much more reactive oxidant and as such have found many application in organic synthesis.

Second important example could be carbenes which are very important intermediates in many organic reactions.[4] The structural parameters, electronic properties an reactivity are strikingly different for singlet and triplet state.[5] The simplified schematic

[i] Spin multiplicity is defined as 2S+1, where S is the spin quantum number. First few examples include:

representation of triplet and singlet carbines is given in Figure 2-3 a) and b). Bond angle can be up to 180° with triplet carbons and as low as 120° with singlet ground state. Ground state preference can be qualitatively predicted if we note that π-donor substituents (halogens, oxygen and nitrogen) stabilize singlet carbenes by electron donation to a empty orbital, Figure 2-3 c).[5] As we mentioned, the reactivity and mechanistic preferencies of singlete and triplete carbenes are complementary: while singlet carbenes often participate in concerted reactions triplet analogs follow step by step mechanisams. The experimental procedures play an important roll in determinating the spin state of carbenes, because, depending of reaction conditions, the carbene intermediate doesn't have to be formed in it's ground state.[5]

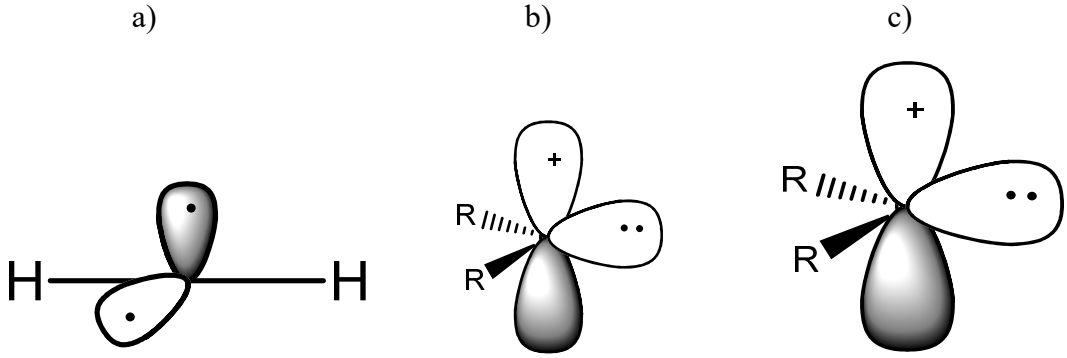

Figure 2-3 Schematic representation of: a) carbene that have triplet ground state, b) carbene that have a singlet ground state and c) stabilization interaction between π-donor group with singlet carbine.

2.2. Spin states in transition metal complexes

As already mentioned, when it comes to the coordination chemistry, its power lies in the ability to make small changes in a metal ion environment and produce significant changes when it comes to the properties.[1,6,7] Due to its various applications in medicine, catalysis and photonics, biology, studies on transition metal have achieved considerable results.[1] Also, some transition metal ions with partially filled d shells will have the ground state of different spin multiplicity in different coordination environments, and even under the influence of external factors, like pressure and temperature. Metal spin

---

Singlet (2S+1=1), doublet (2S+1=2), triplet (2S+1=3), quartet (2S+1=4)…

states represent, without a doubt, enormously significant research area, that have a central role in the important research fields, such as the function of biomolecules and their reactivity, industrial catalysis and spin crossover compounds. A lot of mentioned properties can provide excellent possibilities for novel, switchable materials with applications when it comes to the possibility of computer storage and display devices. Being able to discover, learn about and present to the scientific world the essence of spin states preferences in the manifold of close lying electron arrangements is one of the most important and challenging endeavors both from theoretical and experimental point of view.

When it comes to the current state of knowledge, spin states have very important role in enzymatic reactions, metal-oxo complexes, in spin crossover compounds and we can even talk about spin-state catalysis where different reactions take place for different spin states.[1,8,9] A wide range of heme-containing proteins perform a lot of different functions such as electron transfer, oxygen transfer and storage, gas sensing, gene regulation and catalysis.[1] When it comes to the matter of catalysis, the active complex often involves a metal-oxo (M=O) species like, for example, in horse radish peroxidase, catalase and cytochrome P450.[8,10,11] The family and subfamilies of cytochrome P450 have two wide functional roles: inside of catabolic pathways they initiate the constructive cleavage of various environmental compounds, both for usage as food or means of detoxification.[10,11] Mentioned enzymes are the main cause of the phase I metabolism of nearly 75% of known pharmaceuticals. Due to its discovery, these P450s have drawn attention of the considerable research community such as pharmacologists and medicinal chemists, biophysical chemists, toxicologists, chemists and biochemists. Most studied enzyme from this family is P450cam which shows very interesting catalytic cycle that involves a number of spin flips. One thing in particular must be mentioned: the catalytic mechanism of these enzymes is mostly poorly understood when it comes to the matter of spin state and the effect this may have on the functioning of the enzymes.[10,11]

Like many others, various reactions such as halogenation, desaturation, cyclization, epoxidation and decarboxylation can involve oxoiron species.[1] The synthesis of well-examined model compounds can provide crucial informations when it comes to the mechanism of biological and chemical oxidation reactions. Also, when it comes to the

spin states in the enzyme active center and in small molecule biomimetic, the enzymatic species are high-spin and others have intermediate spin, computational chemistry has contributed in a lot of different ways researching the properties of these reactive intermediates and their various mechanisms making the way of scientific, theoretical and experimental success.[12]

As we mentioned, one of two possible spin states can occur: high spin (HS) with a highest number of unpaired electrons or low spin (LS) with less (or none of) unpaired electrons. In a particular set of circumstances, both states are close enough in energy such that an external influence like pressure or heat can induce a spin-state change or spin crossover (SCO).[9,13] The compounds with SCO properties can be utilized as single-molecule switches/sensors.[9] The computational design of new spin crossover and Light-Induced Excited Spin State Trapped (LIESST) materials is a new field with excessive interest when it comes to data storage, molecular electronics and quantum computation.[14]

2.2.1. Crystal field theory

The first (and the simplest) theory that managed to explain the electronic structure, magnetic properties and spectra of simple TM compounds is crystal field theory (CFT).[6,7,15-17] By CFT, only atomic d-orbitals on a TM center are considered, and the effect of ligand environment is introduced as a simple electrostatic perturbation, i.e. ligands are considered as point charges. In the same time, the effect of electron-electron interaction (and spin-orbit interaction) needs to be taken into account to produce at least a qualitative model that explains the behavior of coordination compounds.

If we first introduce just the spherical electrostatic perturbation with negative "ligands", energies of all five d-orbitals increase. In octahedral environment, two orbitals have higher energy, compared to the barycenter, while three of them will be bellow this level. The splitting between the two energy levels is defined as Δo or 10 Dq (Figure 2-4).

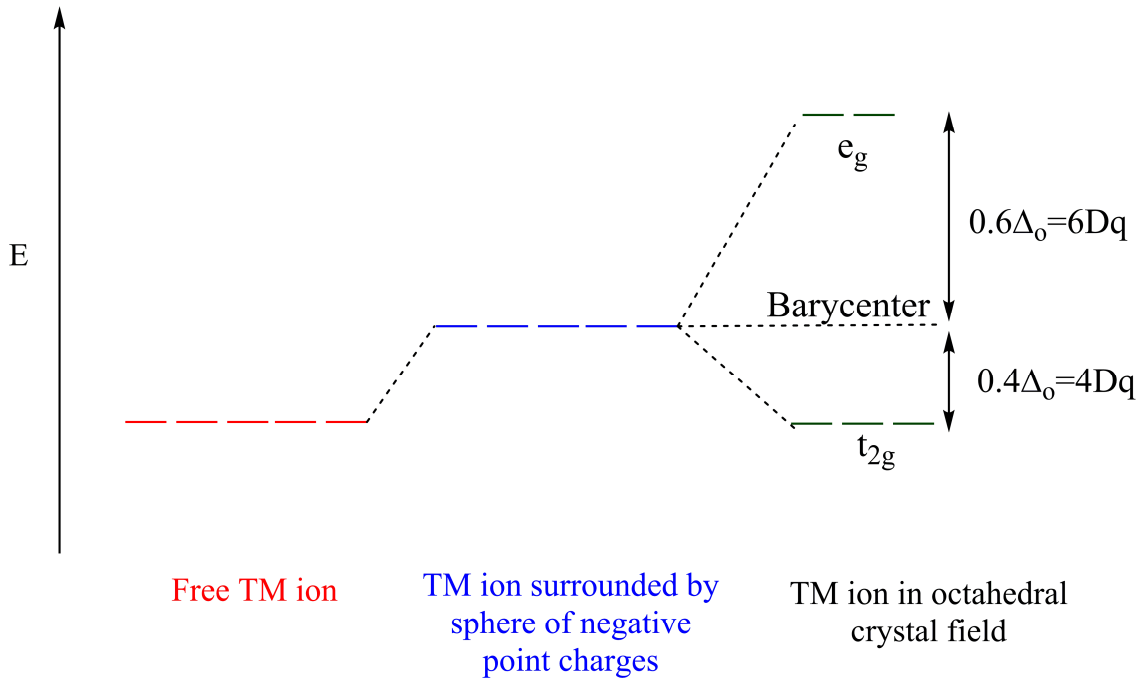

Figure 2-4 The interaction of a free metal ion in the gas phase with a sphere of negative charge causes the energy of the d-orbitals to increase. Redistribution of the negative charge in an octahedral CF causes some of the orbitals to be raised with respect to the barycenter, while others are stabilized. The splitting between the two energy levels is defined as Δ_o or 10 Dq.

The automatic interpretation suggests that if the splitting is large enough (and in CFT it depends of the metal and ligand charge and their separation) the electrons will accommodate the lower t_{2g} orbital, and if the splitting is smaller compared to pairing energy, some electrons will go to the e_g double degenerate level. The enormous simplicity, the biggest advantage of CFT formalism is also it's biggest drawback. Is is obvious that metal ligand interactions can not be properly approximated with simply considering only pure d-orbitals surrounded with just the point charges.

2.2.2. *Experimental trends*

It is a well known and universally accepted empirical fact that, for octahedral coordination, Mn^{2+} and Mn^{3+} form almost entirely HS complexes while Co^{3+} is in a LS state in all but one complex, $[CoF_6]^{3-}$.[18,19] These observation cannot be explained with simple difference in charge of the metal ion and Δ_o. Also, naively, there should be much more pronounced tendency toward the LS ground state for Fe^{3+} comparing to Fe^{2+} as a consequence of metal charge. This is not the case.[18,19]

2.2.3. *Ligand field theory*

Ligand field theory (LFT) can be regarded as extension of CFT which takes the complexity of metal-ligand interaction into account, but only implicitly (by using swichable parameters, *vide infra*).[20-23] LFT suggests the answer to CFT problems in the language of simple coordination chemistry, the electron-electron repulsion (pairing energy, Π) is different when we move from d^4 to d^7 electronic configuration (where more spin states are accessible).[6,15] Pairing energy can be defined as the energy difference between the lowest energy states of a given multiplicity (when we take in account only electron-electron interaction), divided by the number of of pairings destroyed by the low-spin → high-spin transition. Pairing energy for electronic configurations that can have close lying spin states, can be expressed using Racah parameters (Scheme 2-1):[15]

$$\Pi(d^4) = 6B + 5C$$
$$\Pi(d^5) = 7.5B + 5C$$
$$\Pi(d^6) = 2.5B + 4C$$
$$\Pi(d^7) = 4B + 4C$$

Scheme 2-1 First order expressions of Π in terms of Racah's parameters B *and* C.

If we assume that B is similar in different d^n confirgurations and that that C ≈ 4B, we can inspect the compare electron-electron repulsion for every configuration from *Figure 2-2*. As we can see the interelectronic repulsion is almost the same for d^4 and d^5 but it is much smaller for d^6 (which is close to d^7), Scheme 2-2.

$$C \approx 4B \;\Rightarrow \Pi(d^4) = 26B \;\approx\; \Pi(d^5) = 27.5B \;>\; \Pi(d^6) = 18.5B \;\approx\; \Pi(d^7) = 20B$$

Scheme 2-2 Trends of changes in Π when we go from d^4 to d^7 electronic configuration, under assumption that $C \approx 4B$.

We can account for the origin of this trend in an intuitively clear manner by simply considering the change in exchange and Coulomb contributions. But, it is important to note that this is just a qualitative consideration, and that energy two-electron contributions for multideterminenal electronic states have to be obtained by calculating the expectation value of the two electron operator.

Under the assumption of spherical symmetry (which is assumed when Racah parameters are utilized) there are only two Coulomb interactions (the stronger one is when electrons are in same orbital) and only one exchange contribution, Figure 2-5.

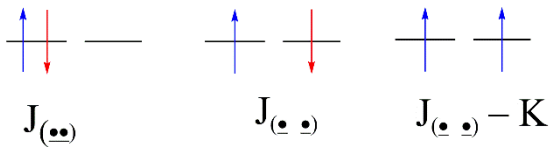

$$J_{(\bullet\bullet)} > J_{(\bullet\ \bullet)}$$

Figure 2-5 Schematic representation for only possible types of Coulomb's and Exchange interaction, under the framework of the spherical symmetry (E_g-E_g interaction is the same as E_g-T_{2g} and T_{2g}-T_{2g}). $J_{(\bullet\bullet)}$ represent Columb interaction between electrons in same orbital, $J_{(\bullet\ \bullet)}$ represent Columb interaction between electrons that are not in same orbital, and K represents exchange interaction.

Once again, we need to stress that this is just a simple, qualitative demonstrations, and that even the assumption from Figure 2-5 is far from valid. The advantage of this approach, beside simplicity, is that it's fundations lie in electron counting procedure that is very close to chemical intuition.

Now we can easily estimate the pairing energy for configurations d^4-d^7. We will obtain that d^6 and d^7 should indeed have a smaller pairing energy since one less exchange

contribution is lost than in d^4 and d^5. This provides very simple and understandable explanation to a well known and documented chemical trend and behaviour, Figure 2-6. The interactions among electrons that don't participate in the changing of the spin state (blue color) are not included since they contribute equally to both spin states and cancel out when we calculate Π. (Figure 2-6). Thus, only interaction or red electrons among themself and with blue electrons are considered (for example in d^6, placing the two red electrons in e_g contributes with 9 week Coulomb interactions- one red-red and 8 red blue, and 7 exchange interactions- 1 red-red and 6 red-blue).

Bellow are two examples of obtaining the expressions for pairing energy by counting the exchange and Coulomb contributions for HS and LS state in d^4 and d^6 configurations.

$$E_{d^4}^{HS} = 3J_{\underline{\bullet}\ \underline{\bullet}} - 3K, \qquad E_{d^4}^{LS} = J_{\underline{\bullet\bullet}} + 2J_{\underline{\bullet}\ \underline{\bullet}}$$

$$\Pi\left(d^4\right) = E_{d^4}^{LS} - E_{d^4}^{HS} = J_{\underline{\bullet\bullet}} - J_{\underline{\bullet}\ \underline{\bullet}} + 3K$$

Scheme 2-3 Derivation of pairing energy expression from Figure 2-5, for d^4 configuration.

$$E_{d^6}^{HS} = 9J_{\underline{\bullet}\ \underline{\bullet}} - 7K, \qquad E_{d^6}^{LS} = 2J_{\underline{\bullet\bullet}} + 7J_{\underline{\bullet}\ \underline{\bullet}} - 3K$$

$$\Pi\left(d^6\right) = \frac{E_{d^4}^{LS} - E_{d^4}^{HS}}{2} = J_{\underline{\bullet\bullet}} - J_{\underline{\bullet}\ \underline{\bullet}} + 2K$$

Scheme 2-4 Derivation of pairing energy expression from Figure 2-5, for d^6 configuration.

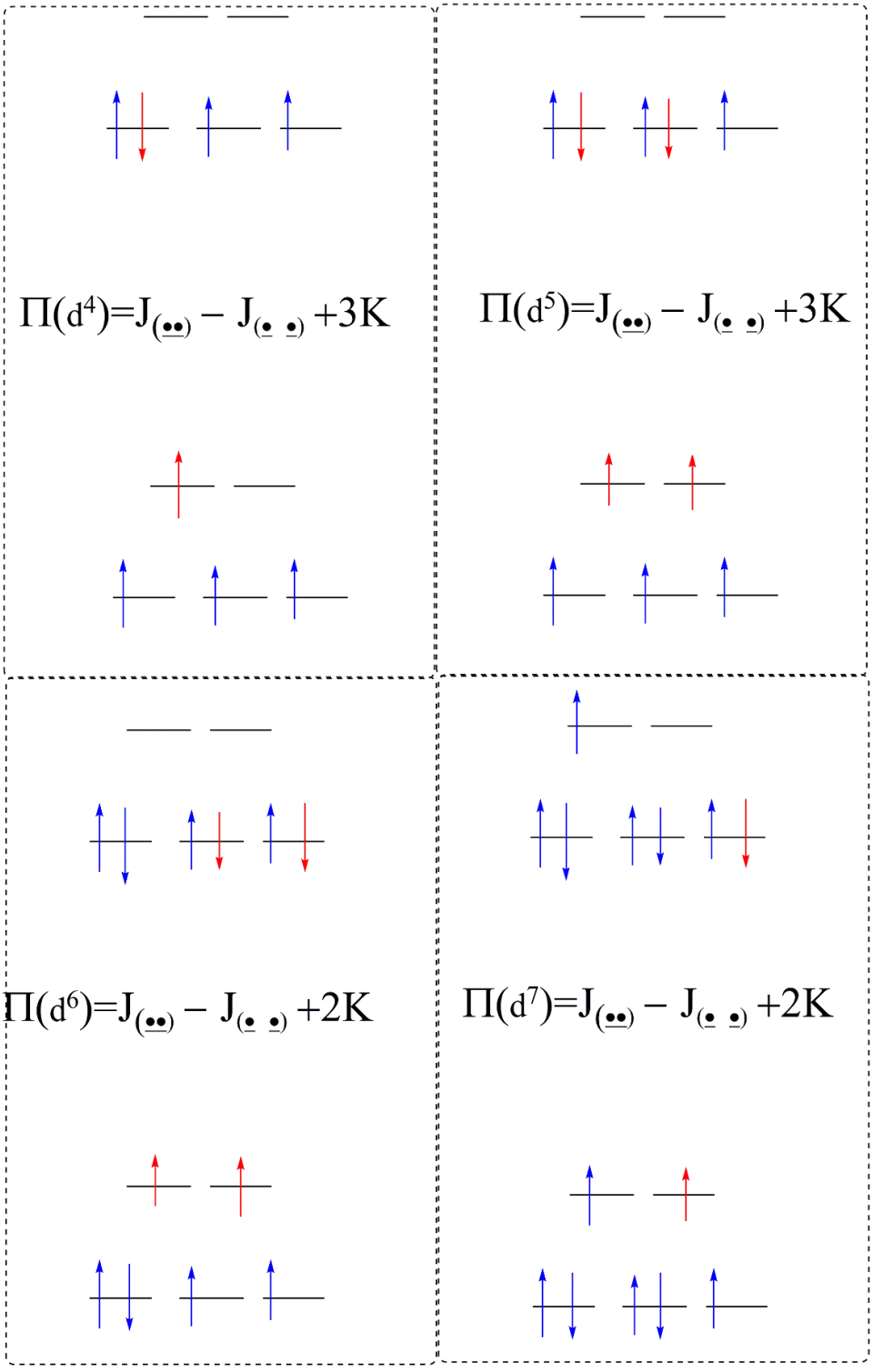

Figure 2-6 Schematic representation and qualitative explanation of different pairing energies for d^6 and d^7 vs. d^4 and d^5 configurations.

3. Theoretical and Methodological Background

Quantum mechanical (QM) modeling has become a widely accepted approach to obtain the knowledge that is either not easily available through experiments, or to reduce the cost associated with the synthesis, characterization and testing of the potential candidates for the desired application. But, most of all, it has become the mean to understand the origin of the molecular properties, and to derive the connection between the electronic structure and macroscopic observables. As a consequence, it has grown into a tool to anticipate how fine-tuning in the molecular structure can affect the phenomenon we are interested in.

The quantum mechanical methods that don't utilize any system dependent empirical parameters are often referred to as *ab initio* methods. These methods can be categorized into two main divisions:[24]

1) the ones that are wrapped around the wavefunction as a central quantity, and
2) the ones that utilize the electron density, as a much simpler and intuitively closer
   starting point

In theory, both approaches should be able to give the same exact energy and any observables we are interested in. Unfortunately, since the basic equations of quantum mechanics are not exactly solvable for anything but a few simple model systems, both methodologies are essentially trying to find the best approximate approach for QM description of real-world problems and observations. The wavefunction based approaches have the advantages that they are systematically improvable, and as a consequence, they are considered to be highly accurate and very reliable. Their disadvantage is the fact that they are very time consuming and limited by system size, thus there is a need for accurate, versatile, but less time consuming methodology.

The methodological direction that utilizes the electron density as a central quantity is based on Density Functional Theory (DFT), which originated in late 1920s in the works of Thomas, Fermi, Dirac and Wigner that stated that the electronic energy can be expressed solely in terms of the density.[24-28] In the next chapters simplified and very brief treatment of these milestones of modern molecular quantum mechanics will be given.

3.1. Schrödinger equation

The Schrödinger equation (SE) is the basic equation of the non-relativistic quantum mechanics and completely describes dynamics of micro-particles. Similarly as Newton's or Maxwell's equations, that represent the foundation of classical physics, the SE cannot be strictly derived (although there are many textbook derivations, they are more an intuitive tool to help the understanding, than a general path toward the SE). The most general form of the SE is time dependent SE:[29]

$$i\hbar\frac{\partial\psi}{\partial t} = \hat{H}\psi$$

Equation 3-1

where ψ represents the wavefunction, that encapsulates all assessable information concerning the micro-objects, and H is the Hamiltonian operator, that can be constructed by the correspondence with the classical energy expression.[ii]

If the wavefunction does not explicitly have the time dependence, the SE can be easily converted to the time independent version in which the energy is simply the eigenvalue of the Hamiltonian, with the wavefunction being the corresponding eigenfunction (eigenvector).[29,30]

$$H\psi = E\psi$$

Equation 3-2

Hamiltonian can be constructed for any system configuration, but the complexity of the obtained differential equation prevents the exact solvability, except in trivially simple cases.[29] It is instructive to note that the difficulty that arises when we attempt to solve

the SE for the system that has more than one electron is not some exotic quantum mechanical complexity but originates from the three body problem that does not have analytical solutions even in the classical mechanics. This problem is elegantly bypassed for the one electron systems even with several nucleus by translating the coordinate system to the center of mass, and assuming the fixed nuclei[iii] , thus following only the motion of electron and leading to effectively one particle problem.

To summarize, for every problem, Hamiltonian is easily constructed, but the difficulty arises in the follow up process of obtaining energy and wavefunction. Wavefunction can be a function of time, position and momentum of a system, $\psi(t,r,p)$ can be real, but is most often complex and has no physical interpretation. Following the Borns interpretation, we can assign the physical meaning to the $\psi^*\psi = \psi^2$, that is a real quantity, and can be interpreted as a probability distribution of a particle, meaning that the probability of finding a particle in a differential volume element dV is proportional to $\psi^2 dV$. The space on which Hamiltonian[iv] operate must be specified, or otherwise we would be dealing with undefined objects. A complete inner-product space (Hilbert space) takes a central position in quantum mechanics by providing the framework for the operators (that represent measurable quantites) and their corresponding eigenfunctions (that represent states of the system).[29] The fact that the state space is a vector space makes QM so different from classical physics and naturally brings many fundamental and new properties, such as the possability for a state to be linear combination of other states.

In quantum mechanics, as distinct from classical picture, different results can be obtained when order of action of some operators in reversed, i.e. if we use x and y components of angular momentum as an example, $L_x L_z \psi \neq L_z L_x \psi$. These operators do not commute (specialy, in our example $\left[L_x L_z\right] = L_x L_z - L_z L_x \neq 0$), and their eigenvalues

---

[ii] For example, in position representation, the Hamiltonian can be constructed from the energy expression if we make the substitution $x \to x, \;\; p_x \to -i\hbar \frac{d}{dx}$ (and analogous for y and z). If the Hamiltonian contains mixed terms (product of momentum and coordinate), the correspondence is more complicated.

[iii] i.e. that nuclei move much slower than electrons and that SE can be separated into electronic and nuclear part. This is a basis of the Born Oppenheimer approximation

can not be simultaneously accurately measured (Heisenberg's uncertainty principle).[29] The operators that commute with the Hamiltonian of the system, (can) have time independent expectation values and their eigenvalues are good quantum numbers.[29]

3.2. Hartree–Fock method

The three body problem prevents the solubility of the SE for any system larger than H_2^+ ion. Since almost all atoms and molecules fall into that category, it was natural that there were many attempts to develop a reliable and accurate way of obtaining approximate solutions to the SE. One of the most successful is the self-consisted field (SCF) Hartree-Fock (HF) approach, that expands the trial multielectron wavefunction as a Slater determinant (SD) composed of one electron wavefunctions (molecular orbitals).[31] As an example, the simplest version of SD for the Ne atom (electronic configuration $1s^2 2s^2 2p^6 = 1s^{\uparrow\downarrow} 2s^{\uparrow\downarrow} 2p_1^{\uparrow\downarrow} 2p_0^{\uparrow\downarrow} 2p_{-1}^{\uparrow\downarrow}$) is given below:

$$\frac{1}{\sqrt{10}}\begin{vmatrix}
1s_\uparrow(1) & 1s_\downarrow(1) & 2s_\uparrow(1) & 2s_\downarrow(1) & 2p_{1\uparrow}(1) & 2p_{0\uparrow}(1) & 2p_{-1\uparrow}(1) & 2p_{1\downarrow}(1) & 2p_{0\downarrow}(1) & 2p_{-1\downarrow}(1) \\
1s_\uparrow(2) & 1s_\downarrow(2) & 2s_\uparrow(2) & 2s_\downarrow(2) & 2p_{1\uparrow}(2) & 2p_{0\uparrow}(2) & 2p_{-1\uparrow}(2) & 2p_{1\downarrow}(2) & 2p_{0\downarrow}(2) & 2p_{-1\downarrow}(2) \\
1s_\uparrow(3) & 1s_\downarrow(3) & 2s_\uparrow(3) & 2s_\downarrow(3) & 2p_{1\uparrow}(3) & 2p_{0\uparrow}(3) & 2p_{-1\uparrow}(3) & 2p_{1\downarrow}(3) & 2p_{0\downarrow}(3) & 2p_{-1\downarrow}(3) \\
1s_\uparrow(4) & 1s_\downarrow(4) & 2s_\uparrow(4) & 2s_\downarrow(4) & 2p_{1\uparrow}(4) & 2p_{0\uparrow}(4) & 2p_{-1\uparrow}(4) & 2p_{1\downarrow}(4) & 2p_{0\downarrow}(4) & 2p_{-1\downarrow}(4) \\
1s_\uparrow(5) & 1s_\downarrow(5) & 2s_\uparrow(5) & 2s_\downarrow(5) & 2p_{1\uparrow}(5) & 2p_{0\uparrow}(5) & 2p_{-1\uparrow}(5) & 2p_{1\downarrow}(5) & 2p_{0\downarrow}(5) & 2p_{-1\downarrow}(5) \\
1s_\uparrow(6) & 1s_\downarrow(6) & 2s_\uparrow(6) & 2s_\downarrow(6) & 2p_{1\uparrow}(6) & 2p_{0\uparrow}(6) & 2p_{-1\uparrow}(6) & 2p_{1\downarrow}(6) & 2p_{0\downarrow}(6) & 2p_{-1\downarrow}(6) \\
1s_\uparrow(7) & 1s_\downarrow(7) & 2s_\uparrow(7) & 2s_\downarrow(7) & 2p_{1\uparrow}(7) & 2p_{0\uparrow}(7) & 2p_{-1\uparrow}(7) & 2p_{1\downarrow}(7) & 2p_{0\downarrow}(7) & 2p_{-1\downarrow}(7) \\
1s_\uparrow(8) & 1s_\downarrow(8) & 2s_\uparrow(8) & 2s_\downarrow(8) & 2p_{1\uparrow}(8) & 2p_{0\uparrow}(8) & 2p_{-1\uparrow}(8) & 2p_{1\downarrow}(8) & 2p_{0\downarrow}(8) & 2p_{-1\downarrow}(8) \\
1s_\uparrow(9) & 1s_\downarrow(9) & 2s_\uparrow(9) & 2s_\downarrow(9) & 2p_{1\uparrow}(9) & 2p_{0\uparrow}(9) & 2p_{-1\uparrow}(9) & 2p_{1\downarrow}(9) & 2p_{0\downarrow}(9) & 2p_{-1\downarrow}(9) \\
1s_\uparrow(10) & 1s_\downarrow(10) & 2s_\uparrow(10) & 2s_\downarrow(10) & 2p_{1\uparrow}(10) & 2p_{0\uparrow}(10) & 2p_{-1\uparrow}(10) & 2p_{1\downarrow}(10) & 2p_{0\downarrow}(10) & 2p_{-1\downarrow}(10)
\end{vmatrix}$$

Expanding the general determinant in the form of permutations of electron positions easily highlights that only single and two electron permutations contribute to the ground state energy (since different orbitals are orthogonal and these matrix elements can only *survive* if they are coupled by one- and two- electron operators).[30,31] Variational minimization of the energy expression generates a set of integro-differential eigenvalue equations called Hartree-Fock equations:[31]

[iv] and other Hermitian operators, that have only real eigenvalues and represent the observables

$$F_i\phi_i = \varepsilon_i\phi_i$$

Equation 3-3

Where F_i is so called Fock operator. ϕ_i is oneelectron wavefunction and the ε_i is the corresponding orbital energy. The three body problem is circumvented by calculating the interaction of one electron with the smeared cloud of electron density originating from all other electrons, thus obtaining density distribution of electron under consideration. The entire process is than repeated until self-consistency.

The operator for the electron in orbital *i* that takes the following form:

$$F = \sum_{i=1} h_i + \sum_{i=1}\sum_{j=1}\left(J_{ij} - K_{ij}\right)$$

Equation 3-4

With h_i being the one electron term, incorporating all the contibutions beside electron electron interactions and J_{li} and K_{li} are, respectively, Coulumb and Exchange matrix elements.

$$K_{ij} = \int \phi_j^*\left(r_1\right) K_i\left(r_1\right)\phi_j\left(r_1\right) d^3r_2 = \int\int \phi_j^*(r_1)\phi_i^*\left(r_2\right)\frac{1}{r_{12}}\phi_i\left(r_1\right)\phi_j\left(r_2\right) d^3r_1 d^3r_2$$

Equation 3-5

$$J_{li} = \int \phi_j^*\left(r_1\right) J_i\left(r_1\right)\phi_i\left(r_1\right) d^3r_2 = \int\int \phi_j^*\left(r_1\right)\phi_i^*\left(r_2\right)\frac{1}{r_{12}}\phi_i\left(r_2\right)\phi_j\left(r_1\right) d^3r_1 d^3r_2$$

Equation 3-6

Coulomb contribution represents the classical Coulomb electron-electron repulsion term and the Exchange contribution is a consequence of the antisymetrized wavefunction and the inability of two electrons of the same spin to occupy the same region of space (so called the Exchange hole).[v] The Exchange contribution stabilizes the configurations

[v] when we expand spinorbital and separate spatial and spin contributions, immediately follow that $K_{li} \neq 0$ only if two considered electrons have the same spin function, so K_{li} exists only with same spin electrons

with the maximum number same spin electrons. It should be noted that in the HF framework, the total energy is not the simple sum of orbital energies, because then the electron–electron interactions would be double counted (i.e. the interaction between electrons i and j would be accounted both in the energy of the orbital with electron i and orbitald with electron j).

Before considering interplay of these contribution on the energy of states with different spin multiplicity and inherent problems of the Hartree-Fock formalism, we are just going to note that in the expresion for the Fock operator J_{ij} and the K_{ij} are not constrained by $i \neq j$ and the term describing the interaction of electrons with itself naturally emerge, J_{ii} and K_{ii}, but, luckily, they exactly cancel out since $J_{ii} = K_{ii}$.

The main drawback of the Hartree-Fock theory is, of course, in the step where it had to approximate the exact particle-particle interaction with the interaction one electron with the smeared cloud of electron density originating from all other electrons. This incorporated the physically wrong assumption in the heart of HF theory: since the electron is interacting with the average density distribution of the other electron, there is the same probability for these two electrons to be one next to each other and at very distant points.[31] This is, naturally, not correct. The electrons correlate their motion, thus reducing the electron-electron repulsion (Coulomb hole).[32] The exchange hole is captured with the asymmetry of the starting wavefunction, but there is not enough variational flexibility in the HF formalism to capture the Coulomb hole and the HF energy is always higher then the real energy of the system under consideration. The absence of any kind of correlation between the electrons of the opposite spin, as opposed to some degree of correlation for the same spin electrons leads to the artificial stabilization of the configurations with more unpaired electrons at HF level of theory.[4]

3.3. Post-Hartree–Fock methods

All post HF methods have a goal to capture the part of electron correlation missing in the original HF methodology.[15,33,34] The electron correlation is often categorized into two divisions: static correlation (originating from inadequate single determinant description of the ground state) and dynamical correlation (which is a consequence of

electrons correlating their motion because of electron-electron repulsion).[32,33] The most popular post HF methods that are utilized in modern quantum chemical program packages are based on: various flavours of configuration interaction (CI) approach, Møller–Plesset perturbation theory (MP), coupled cluster (CC) methodology, or their combination, *vide infra*. All forms of CI are good in retrieving static correlation but differ by the amount of dynamical correlation that is taken into account. MP and CC methods in their most simple and most often used form only deal with dynamical correlation. In MP approach, Hamiltonian is expressed in a perturbative form $H = F + P$, where F is a Fock operator and P is a perturbation that represents a difference between real electron-electron repulsion and an average one:

$$F = \sum_{i=1} h_i + \overbrace{\sum_{i=1}\sum_{j=1}\left(J_{ij} - K_{ij}\right)}^{\substack{average\ \ repulsion \\ 2\left\langle V^{e-e}\right\rangle}}; \quad H = \sum_{i=1} h_i + \sum_{i=1}\sum_{j>i} \overbrace{\frac{1}{r_{ij}}}^{\substack{exact \\ repulsion}} = \sum_{i=1} h_i + V^{e-e}$$

Equation 3-7

$$P = H - F = V^{e-e} - 2\left\langle V^{e-e}\right\rangle$$

Equation 3-8

It can be easily deduced that the combination of zeroth order energy and first perturbative correction are equal to the HF energy

$$E_I^{(0)} + E_I^{(1)} = 2\sum_{i=0}\varepsilon_i + \left\langle \Psi_I^{(0)} \middle| P \middle| \Psi_I^{(0)} \right\rangle = 2\sum_{i=0}\varepsilon_i - \left\langle V^{e-e}\right\rangle = E_{HF}$$

Equation 3-9

The first contribution to the electron correlation is the second order correction (MP2):

$$E_0^{(2)} = -\sum_{J\neq 0} \frac{\left|\left\langle \Psi_J^{(0)} \middle| V^{e-e} \middle| \Psi_0^{(0)} \right\rangle\right|^2}{\left(E_0^{(0)} - E_J^{(0)}\right)}$$

Equation 3-10

MP2 captures a considerable amount of dynamical correlation and it is not significantly more computationally expensive than HF. Since MP is perturbative and not a variational approach, we don't know if our energy (regardless of order of correction) is lower or higher than the exact one. The most important source of problems are the systems where electron correlation is too large and perturbative approach is no longer applicable (and the consequence can be divergent behavior of the MP expansion).

In the full configuration interaction (FCI) the wavefunction is a linear combination of all Slater determinants obtained by all possible electron excitations:

$$\left|\Psi_{FCI}\right\rangle = C_0 \underbrace{\Phi_{HF}}_{\substack{HF\ SD \\ reference}} + \sum_{i}^{occ.}\sum_{k}^{vir.} c_i^k \underbrace{\left|\Phi_i^k\right\rangle}_{\substack{single\ excited\ SDs}} + \sum_{i}^{occ.}\sum_{k}^{vir.}\sum_{i<j}^{occ.}\sum_{k<l}^{vir.} c_{ij}^{kl} \underbrace{\left|\Phi_{ij}^{kl}\right\rangle}_{\substack{double\ excited\ SDs}} +$$

$$+\sum_{i}^{occ.}\sum_{k}^{vir.}\sum_{i<j}^{occ.}\sum_{k<l}^{vir.}\sum_{j<m}^{occ.}\sum_{l<n}^{vir.} c_{ijm}^{kln} \underbrace{\left|\Phi_{ijm}^{kln}\right\rangle}_{\substack{triple\ excited\ SDs}} + \cdots \begin{matrix} all\ \ higher \\ excitations \end{matrix}$$

Equation 3-11

where $\Phi_{i\ldots}^{k\cdots}$ are the Slater determinants with 1, 2, 3, … excited electrones. The coefficients $c_{i\ldots}^{k\cdots}$ are found by variationally optimizing the energy

$$E_{\mathrm{CI}} = \min_{\mathbf{c}} \frac{\left\langle \Psi_{FCI} \middle| \hat{H} \middle| \Psi_{FCI} \right\rangle}{\left\langle \Psi_{FCI} \middle| \Psi_{FCI} \right\rangle}.$$

Equation 3-12

The schematic representation of few single and double excitations from refernce HF configuration is given below. (Figure 3-1)

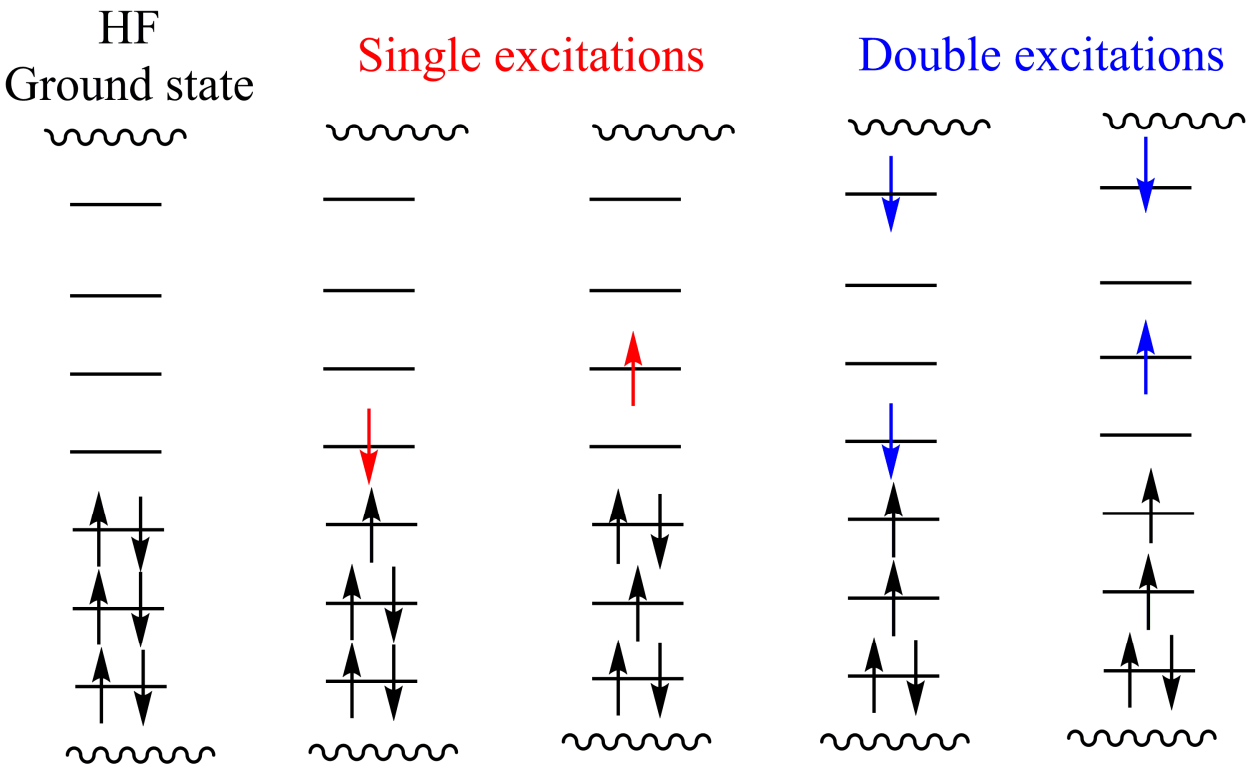

Figure 3-1 The schematic representation of single and double excitations from refernce HF configuration

The FCI solution is the exact solution of the SE (for a given basis set), but it is too computationally demanding and can be used only for systems that have only few electrons. If we limit ourself to only one and two electron excitations we arrive at CISD

$$\left|\Psi_{CISD}\right\rangle = C_0 \underbrace{\Phi_{HF}}_{\substack{HF \\ SD}\ \ \underbrace{reference}} + \sum_{i}^{occ.}\sum_{k}^{vir.} c_i^k \underbrace{\left|\Phi_i^k\right\rangle}_{\substack{single \\ excited \\ SDs}} + \sum_{i}^{occ.}\sum_{k}^{vir.}\sum_{i<j}^{occ.}\sum_{k<l}^{vir.} c_{ij}^{kl} \underbrace{\left|\Phi_{ij}^{kl}\right\rangle}_{\substack{double \\ excited \\ SDs}}$$

Equation 3-13

where Φ_i^k and Φ_{ij}^{kl} are Slater determinants with single and double excitations.

The computational cost of these methods is greatly reduced if we use only the most important SDs in the CI procedure by selecting the appropriate active space and restricting the number and type of some additional excitations, complete active space (CAS) and restricted active space (RAS) methodologies. They can be additionally improved by perturbative treatment in order to include more dynamical correlation (CASPT2 and NEVPT2).

In coupled cluster, the wavefunction is expressed in a form

$$\left|\mathrm{CC}\right\rangle = e^{\hat{T}} \left|\Psi_{ref}\right\rangle$$

Equation 3-14

where $\left|\Psi_{ref}\right\rangle$ is usually Hartree Fock reference. $\hat{T}$ is called the cluster operator and is a sum of excitation operators with their associated coefficients.

$$\hat{T} = \hat{T}_1 + \hat{T}_2 + \cdots$$

Equation 3-15

Thus, $\hat{T}_1$ includes all single excitations $\hat{T}_1 = \sum_i^{occ.} \sum_k^{vir.} t_i^k a_k^\dagger a_i$ where t_i^k are the associated coefficients, and $a_k^\dagger$ and a_i denote creation and annihilation operators, $\hat{T}_2$ includes all double excitations $\hat{T}_2 = \sum_i^{occ.} \sum_k^{vir.} \sum_{i<j}^{occ.} \sum_{k<l}^{vir.} t_{ij}^{lk} a_k^\dagger a_l^\dagger a_j a_i$ and so on. If we only take into account the single and double excitations, we get CCSD. It is important to understand that even in the truncated CCSD approach, contributions from higher excitations are partially included as the product of a single and a double excitation yields a triple excitation. Since it is not a variation method, the convergence towards the exact result is not necessarily from above. CCSD can be perturbationaly corrected for

the contribution of triple excitations, labeled CCSD(T), and a much smaller computational cost compared to exact CCSDT and excellent performance (which is partially a consequence of some favorable error cancelation) made this method a gold standard for the accurate *ab initio* single reference calculation.

The coupled cluster energy is given by

$$\left\langle \Psi_{ref} \left| \hat{H} e^{\hat{T}} \right| \Psi_{ref} \right\rangle = E_{CC} \underbrace{\left\langle \Psi_{ref} \left| e^{\hat{T}} \right| \Psi_{ref} \right\rangle}_{=\left\langle \Psi_{ref} | 1 | \Psi_{ref} \right\rangle + 0 + 0 + \cdots = 1} \Rightarrow E_{CC} = \left\langle \Psi_{ref} \left| \hat{H} e^{\hat{T}} \right| \Psi_{ref} \right\rangle$$

Equation 3-16

The coefficients of the excitation operators are found by

$$\left\langle \Phi_e \left| (\hat{H} - E_{CC}) \exp(\hat{T}) \right| \Psi_{ref} \right\rangle = 0$$

Equation 3-17

with configurations $\left\langle \Phi_e \right|$ from the appropriate excitation space.

3.4. Density Functional Theory

The wavefunction of an N-electron system depends on 3N spatial- and N spin-coordinates, and in order to obtained physical observables, integrals over all these coordinates need to be calculated. Deeper analysis reveals the simple conclusion that since the Hamiltonian contains only one- and two-electron terms, any observable can be expressed in terms of integrals involving only three and six spatial coordinates. Following the beginings of quantum chemistry, in which wavefunction was considered indispensable for proper description of micro particle dynamics, maturity of the field bought the recognition that the wawefunction contains much more information than we actually need. Electron density is not only much simpler than the wavefunction, but also it can be experimentally determined.

Utilizing the wavefunction, the electronic density distribution of i-th electron can be simply obtained by integrating over all other electrons (with total *n* electrons)

$$n\int\int\ldots\int\psi^{*}\psi d^{3}r_{1}d^{3}r_{2}\ldots d^{3}r_{n}\xrightarrow[\substack{d^{3}r_{i}\ is\ not\ one\ of\ the\\ integration\ variables}]{\substack{integrate\ over\ all\\ exept\ i-th\ electron}}\rho_{i}$$

Equation 3-18

The corner stone of the interest in DFT as a tool for the molecular electronic structure calculations and the point that gave the initial momentum in it's incorporation in the language and routines of vast scientific community are two theorems by Hohenberg and Kohn developed in the 1960s:

1. There exists a functional E[ρ] from which the exact energy (and other observables) can be calculated using just the ground state density ρ.

2. The energy computed from any provided density is higher[vi] than the one obtained from the correct ground state density of the system under consideration

For it's simplicity, the qualitative proof of the above theorems can be found in almost any book/chapter/thesis at least partially concerning with DFT.[34,35] These two theorems provide a conceptual framework for first principle quantum mechanical description of system dynamics utilizing different central concept as a way of bypassing wavefunctions. Unfortunately, despite it's exactness, the Hohenberg–Kohn theorem does not provide any prescription on how to obtain ground state energy from ρ nor does it tell us how to find ρ if we first don't have a wavefunction. The exact formulation of this relationship is still unknown, and, although it is often used as an argument that if it would be discovered, and DFT becomes exact quantum mechanical description, there is no guarantee that it would be easier to evaluate observables and densities from it than from the equally exact wavefunction approach.

To follow one attempt[vii] to express the energy as a functional of electron density we first need to introduce the concept of external potential, υ. Since the electron density is

[vi] Or equal, if provided density is identical to the ground state density of the system

[vii] Kohn-Sham aproach

purely electronic quantity, the electron electron interaction is described separately and everything except the interelectronic interaction is labeled as external potential (it is produced by charges or fields external to the system of electrons).

First step is to note that expectation value of sum of external potential contributions, $V = \sum_i \upsilon_i$, $\langle V \rangle = \langle \psi | V | \psi \rangle$ can be expressed using density distribution ρ instead of ψ.

If we focus our attention of the i-th electron,

$$\langle \psi | \upsilon_i | \psi \rangle = \int\int ... \int ... \int \psi^* \upsilon_i \psi d^3 r_1 d^3 r_2 ... d^3 r_i ... d^3 r_n \xrightarrow{\substack{integrate\ over\ all \\ exept\ i-th\ electron}} \frac{1}{n} \int \upsilon_i(\rho) \rho_i d^3 r_i$$

Equation 3-19

We will consider the electron subjected to the external potential (attraction with the N nuclei with charge Z_α and position R_α) $\upsilon = \sum_\alpha \frac{-Z_\alpha}{|r_i - R_\alpha|}$. The next step is to imagine the fictitious Kohn-Sham (KS) system in which there is an external potential υ_0 that is completely identical to one that would be produced by the nuclei, and without electron electron interaction. Since we have the expression for the external potential, and there is no electron electron interaction, we only have to solve one-electron equation (exactly solvable) and generate so called KS spinorbitals. In order to formulate some attempt to calculate the electronic ground state energy we need to describe the kinetic energy of the electrons, the electron nuclear interaction, the interelectronic repulsion and correct all the terms so they could describe the real system instead fictitious one (with noninteracting electrones):

$$E[\rho] = T_0[\rho] + \int \upsilon(\rho) \rho d^3 r + \frac{1}{2} \int\int \frac{\rho_i \rho_j}{|r_i - r_j|} d^3 r_i d^3 r_j + E_{XC}[\rho]$$

Equation 3-20

Corresponding respectively to the electronic kinetic energy of the fictitious KS system, the correct Columbic interaction of the electron distribution with external potential, the classical Columbic interactions, and the "exchange-correlation" contribution which

corrects the former three terms for their neglect of various effects. To get a better understanding of the scope and limitations of this expression, we will discuss each term in some more detail.[4,36]

The first term, representing kinetic energy, is very difficult to accurately calculate directly from the density, and that is one of the main reasons that the above mentioned KS orbitals are introduced (i.e. instead of varying ρ, we are varying the KS orbitals which determine ρ), although that represents the clear deviation in attempt to represent the energy in terms of the density only. This approach strongly resembles the one incorporated in HF theory, and the variationaly obtained occupied KS orbitals resemble molecular orbitals calculated by the HF method, and they can be utilized in qualitative MO considerations.

Of course, the obtained kinetic energy is by no means exact, since it originates from fictitious KS system of non interacting electrons, and it requires additional corrections. The term, describing the interaction of the electron density distribution with the external potential (nuclei) is exact. The third term is the classical expression for the electrostatic interelectronic repulsion energy if the electrons were smeared out into a continuous distribution of charge with electron density ρ . It is essentially identical to the Coulombs interaction term in HF theory. The final term, or exchange-correlation functional, should, in principle, contain the correction to all the previous contributions. Although the exact exchange-correlation functional should incorporate the effect of electronic interactions on kinetic energy, in practice, such a term is not explicitly present in most DFAs. It is common practice to further separate this XC corrective term to the part corresponding to "exchange", E_X, and other corresponding to "correlation", $E_{C.}$ Naturally, the purpose of E_X term is to correct neglect of exchange in DFT and E_c should take into account the existence of Coulomb hole. The different form of the Coulombic and Exchange expressions in DFT, as opposed to HF, prevents the perfect cancelation of the fictitious self-interaction contributions, and thus, requiring that E_X contribution take into account this problem as well.

Since the exact form of XC term is unknown, in the rest of the discussion, we will call the model Hamiltonians the exchange-correlation (XC) approximations, reserving the term exchange-correlation functional for the unknown, exact, formulation of this

expression. By analogy, various approximations to the Hamiltonian in DFT will be called density functional approximations (DFAs). Although, some of them are developed on a basis of constrains emerging from the physical considerations, the more successful ones, do contain empirical parameters that must be determined by some means. This is usually done by fitting a functional to a few *ab initio* or experimental atomic properties, although it is definitely preferable to include some molecular observables and reactivity patterns. For example, the low quality performance of many early functionals for spin state energetics of transition metal complexes is partially a consequence of the fact that in the fitting procedure during their development, the spin state energetics was never used in a data set. The important consequence of the fitted parameters beside the unwanted premise of semiempirical character, is that these DFAs cannot be improved in a systematic manner (which is a major drawback compared with standard wavefunction theory). Before we start discussing the specific DFAs, by using the acronyms under which they are most familiar, we mention, that these approximations are often labeled by the initials of the quantum chemists who have proposed them.

3.4.1. Jacob's ladder

Many proposals have been made for the functional form of the E_X and E_C, and there is an enormous list of DFAs arranged into a number of classes with varying levels of complexity. We adopt here an order of presentation of exchange–correlation DFAs hierarchy, proposed by Perdew, which is most often called a ''Jacob's ladder'' of increasing accuracy and sophistication in DFAs design and construction. The steps start at the simplest LDA (*vide infra*) expression and should end up in the hypothetical exact functional. (Figure 3-2)

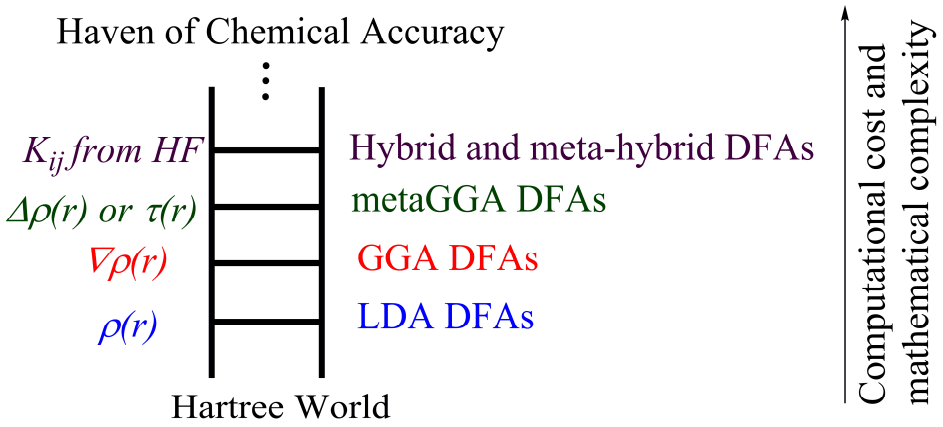

Figure 3-2 Jacobs's ladder of density functional approximations.

3.4.2. Local Spin Density Approximation (LDA)

LDA[37] depends solely upon the value of the electron density at each point in space. In the framework of this approximation, the energy is obtained from a purely local integral over only the simple, point value of the electron density, with separate local exchange $\varepsilon_x\left(\rho(r)\right)$ and correlation terms $\varepsilon_c\left(\rho(r)\right)$.

$$E_{xc}^{\mathrm{LDA}}\left[\rho(r)\right]=\int\left(\varepsilon_x\left(\rho(r)\right)+\varepsilon_c\left(\rho(r)\right)\right)\rho(r)\,d^3r$$

Equation 3-21

This relatively simple description emerged from the electrically neutral system of homogeneous electron gas over the uniformly smeared out positive charge in a box. This model was extensively studied in theoretical physics, has the exact solutions for some properties and bears very important similarities with problem of electrons in molecules (where electron density is smeared around positive nuclear charge). Of course, the electronic density distribution in a molecule is certainly not homogeneous, but to a good approximation, locally, we may assume its homogeneity. Within this approximation, the analytical expressions for the exchange contribution are available, for example the Slater proposed:

$$\varepsilon_x\left(\rho(r)\right) = -\frac{3}{4}\left(\frac{3}{\pi}\right)^{\frac{1}{3}} \rho^{\frac{1}{3}}(r)$$

Equation 3-22

$$E_x^{\mathrm{LDA}}\left[\rho(r)\right] = \int \varepsilon_x\left(\rho(r)\right)\rho(r)\,d^3r = -\frac{3}{4}\left(\frac{3}{\pi}\right)^{1/3} \int \rho^{4/3}(r)\,d^3r$$

Equation 3-23

From which we see that exchange energy will be higher (more negative) in the regions of higher density. The contribution of the E_c is not that simple and only limiting expressions for the density dependence are known exactly. In the limits situations (high- and low-density that generate infinitely-weak and infinitely-strong correlation), correlation energy as a functional of density can be written as[34]:

$$\varepsilon_c = \frac{1}{3} A \ln\left(\frac{3}{4\pi\rho}\right) + B + \left(\frac{3}{4\pi\rho}\right)^{\frac{1}{3}} \left(\frac{1}{3} C \ln\left(\frac{3}{4\pi\rho}\right) + D\right)$$

Equation 3-24

$$\varepsilon_c = \frac{1}{2}\left(\frac{g_0}{\left(\frac{3}{4\pi\rho}\right)^{\frac{1}{3}}} + \frac{g_1}{\left(\frac{3}{4\pi\rho}\right)^{\frac{1}{2}}} + \ldots\right)$$

Equation 3-25

The most common of these correlation DFAs have been parameterized to reproduce the highly accurate Monte Carlo results obtained for the simulations of the homogeneous electron gas for several intermediate values of the density, while reproducing the exactly known limiting behavior. So, for this system with constant density, this functional is exact. The combination of the Slater local exchange DFA with the correlation contribution obtained by the described manner is often reported to as the

SVWN (Slater-Vosko-Wilk-Nusair)[37] or just as (simple and a little misleading) LDA DFA. As is more sophisticated DFAs, the electron–electron interactions effectively includes the electron self-repulsion, because the exchange and correlations contribution don't exactly cancel out as in HF theory. As a simple demonstration, for a H atom analyzed with SVWN functional, the Coulomb energy (of one electron with itself) is 0.298 atomic units (au) while the Slater exchange term is -0.278 au and they almost (but not completely) cancel out.

Generally, LDA methodology is remarkably accurate when we consider the relative simplicity of the energy expression.[24,36] For example, it provides good geometries, with bond lengths being usually underestimated, which makes it superior to many higher levels of theory when considering the geometrical parameters obtained from crystal diffraction methods (where bond lengths are contracted by the compact crystal packing). The simple properties that crucially depend on the quality of the optimized geometry, like vibrational frequencies, charge densities and the Jahn Teller(JT) stabilization parameters are also described accurately with LDA. However, the LDA is not a good approximation for systems with weak bonds or, generally, the systems with complicated electronic structure, like transition metal systems with close lying electronic states of different spin multiplicity. The various variants of LDA methodology have been utilized in a broad variety of applications for calculations on solid state as well as discrete molecular properties.[38]

Since density in molecular systems is non-local, and a purely local description is obviously insufficient, the further development include also functions of the gradient ($\nabla\rho$), GGA DFAs, and Laplacian ($\nabla^2\rho$) of the density, metaGGA DFAs. Qualitatively, the incorporation of the derivatives can be justified by the fact that energy is different in regions where density varies rapidly (close to nuclei) compared to those where there are no abrupt changes (far away from the nuclei).

3.4.3. Generalized Gradient Approximation (GGA)

There is a great diversity of GGA exchange and correlation DFAs. They differ among each other by various design considerations such as number of parameters, the

theoretical and experimental data to which the parameters have been adjusted and the form of constraints that have been applied to the nature of the solutions.[4,36,38] The typical expression for the GGA exchange can be written using the Slater's LDA exchange contribution, Equation 3-22, by utilizing the enhancement factor, $F(s)$, that is a function of reduced density gradient, s:[39]

$$E_{x,GGA} = \int \varepsilon_x F(s) d^3 r$$

Equation 3-26

$$s = \frac{|\nabla \rho|}{2\rho^{\frac{4}{3}} \left(3\pi^2\right)^{\frac{1}{3}}}$$

Equation 3-27

The reduced density gradient, s, can be understood as a local inhomogeneity parameter.[24] Since it is a quotient of $\nabla\rho$ and $\rho^{\frac{4}{3}}$ it will have large values in the region where ether $\nabla\rho$ is large or the ρ is small (far away from the nuclei). The $\rho^{\frac{4}{3}}$ is used so the s would be dimensionless quantity.[24] One of the more important variations in GGA DFAs is PBE. It represents a starting point in development of specialized DFAs, crucial for the subject of this thesis, so it will be considered in more details. The exact form of the $F_{XPBE}(s)$ can be written as

$$F_{PBE,X}(s) = 1 + K_{PBE}\left[1 - \frac{1}{1 + L_{PBE} s^2}\right]; \qquad \mathrm{L}_{PBE} = \mu_{PBE} / \mathrm{K}_{PBE}$$

Equation 3-28

The expression for the GGA correlation in the same functional can be expressed as

$$E_{c,PBE} = \int \rho \cdot \left[\varepsilon_C(\rho,\zeta) + H(\rho,\zeta,\mathrm{t}) \right] d^3r$$

Equation 3-29

Where ζ is relative spin polarization $\zeta = \frac{\rho_\uparrow - \rho_\downarrow}{\rho_{total}}$, and *H* is the gradient contribution to the correlation part, which is a function of another dimensionless density gradient, *t*. Gradient contribution to the correlation part can be written in the following form

$$H_{PBE,\mathrm{C}}(t) = W_{PBEc} \cdot \ln\left(1 + U_c \cdot \left[1 - \frac{1}{1 + Gt^2 + G^2t^4}\right]\right)$$

Equation 3-30

And the equations for *t* and scaling factor $\phi(\zeta)$ are

$$t = \frac{|\nabla\rho|}{4\phi(\zeta)\rho^{\frac{7}{6}}\left(3\pi^{-1}\right)^{\frac{1}{6}}}$$

Equation 3-31

$$\phi(\zeta) = \frac{(1+\zeta)^{2/3} + (1-\zeta)^{2/3}}{2}$$

Equation 3-32

We can see that the exchange part contains only s^2 term in the denominator while correlation contribution contains both t^4 and t^2.

3.4.4. The metaGGA aproximations

The expression for the E_{XC} in meta-GGA or MGGA DFAs additionaly incorporate the Laplacian $\Delta\rho$ and/or the kinetic-energy density τ .[4,36,38]

$$E_{XC}^{MGGA}[\rho] = \int f\left(\rho, \nabla\rho, \nabla^2\rho, \tau\right) d^3r$$

Equation 3-33

Just for the sake of demonstration, total density can be easily separated into contributions from α and β spin (as with all other DFAs).

$$E_{XC}^{MGGA}\left[\rho_\alpha,\rho_\beta\right]=\int f\left(\rho_\alpha,\rho_\beta,\nabla\rho_\alpha,\nabla\rho_\beta,\nabla^2\rho_\alpha,\nabla^2\rho_\beta,\tau_\alpha,\tau_\beta\right)d^3r$$

Equation 3-34

It has been demonstrated that these two ingredients carry essentially the same extension to the GGA approach. Considering the additional complexity of these DFAs, it is a bit surprising that they do not have significantly improve accuracy compared to GGA level of theory.

3.4.5. The Hybrid DFAs

LDA and many GGA DFAs as an artifact of design give the overbinding and somewhat short bond lengths (this is one of the reasons that the results for atomization energies are poor). [4,36,38] Since HF have completely opposite trends it is natural to assume that some form of combined treatment might bring improved results. The hybrid DFAs are obtained by linear combination of the exact exchange interaction calculated from the HF theory and E_x and E_c from standard DFAs. The exchange contribution from Eq. 3-4 have the following form

$$E_x^{\mathrm{HF}}=-K_{ij}=-\sum_{i,j}\int\phi_j^*\left(r_1\right)K_i\left(r_1\right)\phi_j\left(r_1\right)d^3r_2=-\sum_{i,j}\int\int\phi_j^*(r_1)\phi_i^*\left(r_2\right)\frac{1}{r_{12}}\phi_i\left(r_1\right)\phi_j\left(r_2\right)d^3r_1d^3r_2$$

Equation 3-35

One of the most popular flavors of hybrid DFAs is B3LYP,[40] which is acronim for for Becke, 3-parameter, and Lee-Yang-Parr.

Although the computational cost of hybrids is higher compared to GGA DFAs (but this strongly depends of the way that some functionalities are implemented and of general characteristics of a particular DFT software), hybrid DFAs, and especially

B3LYP are widely accepted as a DFT "gold standard" for accurate property calculation. As a consequence, concerning all DFT metodologies, they are by far the most cited and utilized among chemist's comunity. It should be mentioned that B3LYP is not "golden standard" for systems that contain transition metals.[38] HF exchange can be included also in a range-separated fashion, where long-range interactions are treated with HF while short range interactions are modeled with GGA DFA.

3.4.6. The importance of DFT in modern computational chemistry and physics

After covering the basics in the previous sections of this chapter, we can understand why state of the art wavefunction based methods are oftenly regarded as methodology of choise for accurate calculations of chemical interest, but that they need to be handled by experts in the field and come at great computational expense. Thus, they are limited to relatively small systems, if drastic simplifications in basis set or the method itself are not introduced. As a consequence, from a broad palette of electronic structure methods, Density Functional Theory (DFT) emerged into the mainstream of quantum chemical methods, because of its good compromise between the accuracy of the results and the computational efficiency. DFT expirienced an explosive growth since the 1990s following the development of hardware and software capabilities, see Figure 3-3. In the last decade, DFT have become not only a important tool for researchers all over the world, but also a inescapable tool in many undergraduate curiculums, as verry accessible, simple to use and valuable insight into the electronic, structural, spectroscopic, magnetic and mechanistic properties of various chemical proceses and phenomena.[viii] (Figure 3-3)

[viii] For example, there are 192 papers in the Journal of Chemical Education that are in various ways utilizing and refering to the Density Functional Theory, but only 10 before 1998 (results are obtained by searching the exact phrase "density functional")

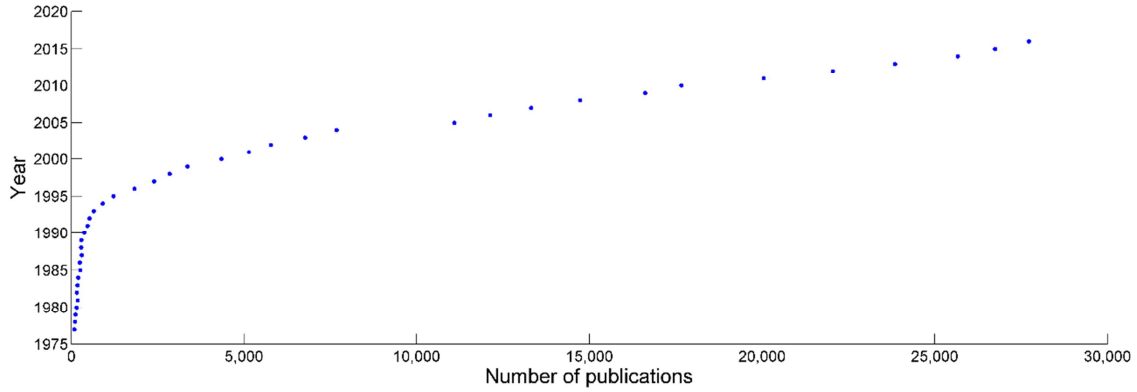

Figure 3-3 The number of publications where the phrase "density functional theory" appear in the title or abstract from a Chemical Abstracts search covering the years from 1977 to 2017.

3.5. Basis sets

Since Schrodinger equation can not be solved analyticaly for anything but trivial systems, for virtualy all molecules the trial wavefunction have to be constructed as Slater determinant consistring of one-electron functions, molecular orbitals, MOs. These MOs are in turn most oftenly expressed as variationaly optimized linear combination of atomic orbitals from constituting atoms. This is very reasonable approach, since at large internuclear separations, MOs became pure AOs, but have a serious set back in fact that we do not know how atomic orbitals look like. Even worse, it was soon discovered that unless the continuum was included[ix], the only starting point, hydrogen-like orbitals do not form a complete set. Among alternatives, the most useful for chemistry are Gaussian type basis functions (GTO) and Slater type basis functions (STO).[41] Slater type orbitrals have the cusp at r=0, i.e. they show correct behaviour, that we expect from atomic orbital. They also demonstrate correct behaviour at large values of r (Gaussians don't capture the exponential decay (e^{-r}) naturally, sice they have e^{-r^2} form). Thus, as a consequence, Slater basis functions are closer to the actual solution, and therefore fewer of them are needed for accurate resuls. Linear combination of Gaussian basis functions can be used to reproduce correct behaviour by curve-fitting to a Slater orbital, but any orbital made froom Gaussians have a slope of zero at the origin (Figure 3-4). These discrepancies turn out to be very significant in molecular calculations (*vide supra*).

The biggest advantage of Gaussian functions is that their integrals can be evaluated analytically, and, even more importantly, that a products of Gaussians at different centers can be expressed as a one Gaussian function. This enable us to reduce all multi-centered integrals to two-centered integrals, which then can be evaluated analytically. Unfortunatly, distinct to the wavefunction based methods, matrix elements that incorporate exchange correlation potential can not be evaluated analyticaly. As a consequence, DFT specialized software (e.g. ADF)[42] that utilizes the fact that numerical integration can not be avoided have emerged. They produced the code that utilizes STO as basis functions since they are intrinsically the most suitable for electronic structure calculations. This makes ADF specially convenient and accurate for the systems where complicated electronic effects and significant contributions from electron correlation are pressent, important example being transition metals and their compounds. (Figure 3-4)

[ix] continuum demonstrated to be prohibitively challenging to utilize in real life calculation

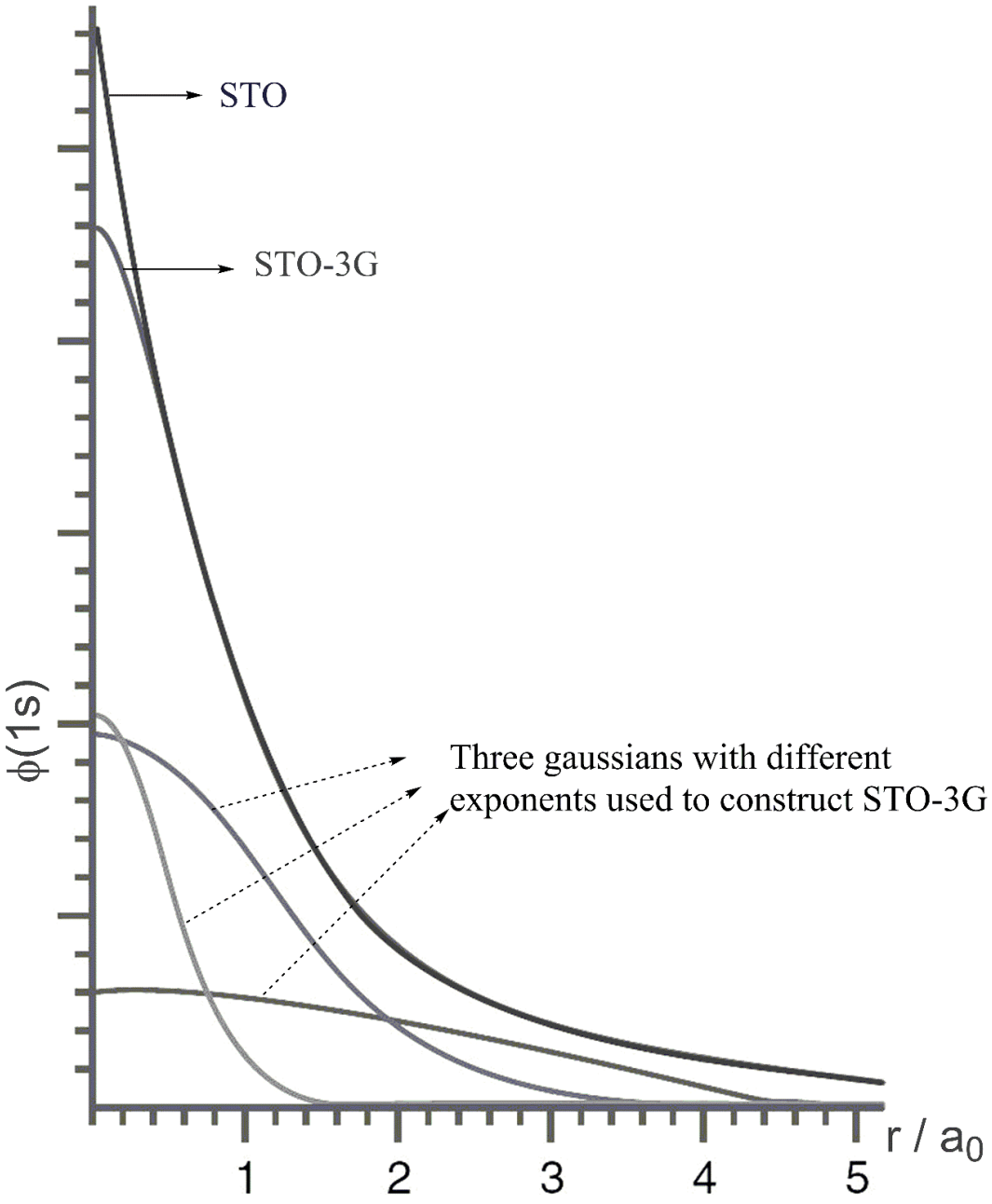

Figure 3-4 A hydrogen atom 1s STO can be fit with the three Gaussian functions (that is the origin of the STO-3G label). Both the values and the coefficients multiplying the Gaussian functions are optimized in the best method.

3.6. Spin states and Density Functional Theory

The problem in application of DFT for spin states was first noted in 2001,[43] and it was concluded that early Generalized Gradient Approximation (GGA) DFAs favored low-spin states, while hybrid DFAs including HF exchange favored high-spin states. In the following years, many DFAs showed partial success, but mainly failures in attempt to tackle the problem of close lying spin states in TM complexes.[4,12,44] In 2004, the combination of relatively new, OPTX exchange functional,[101] with the PBE correlation part gave excellent results for the spin states of iron complexes, and hence a new DFA was born (OPBE).[45,46]

Since correlation part of OPBE (OPTX) indicated excelent performance of for spin states, and later as well SN2 reaction barriers, it was combined with PBE that gives good results for week interactions. After incorporation of Grimme's D2 dispersion energy, the SSB-D functional was created.[39] It should be noted that in the new SSB-D DFA, beside exchange term with s^2, the simplified correlation term that contains only t^2 was used

$$H_{sPBE,\mathrm{C}}\left(t\right)=W_{PBEc}\cdot\ln\left(1+U_c\cdot\left[1-\frac{1}{1+Gt^2}\right]\right)$$

Equation 3-36

Future developement led to the S12g DFA,[47] in which instead of reducing the correlation term to t^2, exchange term is extended to include s^4 term in F_X expression.[47] The equations look simpler if we introduce the new variable

$$x=\frac{\left|\nabla\rho\right|}{\rho^{\frac{4}{3}}}\Rightarrow s=\frac{x}{2\left(3\pi^2\right)^{\frac{1}{3}}}$$

Equation 3-37

In order to achieve a flat profile for low values of x the somewhat rearranged expression is given, with the A, B, C, D and E being parameters:

$$F_{s12g,X}\left(x_i\right)=A+B\cdot\left[1-\frac{1}{1+Cx_i^2+Dx_i^4}\right]\cdot\left[1-\frac{1}{1+Ex_i^2}\right]$$

Equation 3-38

$$F_{s12g,X} = \sum_{i=\alpha,\beta} C_{LDA,X} \cdot \rho_i^{4/3} \cdot F_{s12g}\left(x_i\right)$$

Equation 3-39

To sumarize, initial sucsess[45,46,48] and some failures[44] with OPBE led to the SSB-D DFA in which there is Grimme's D2 dispersion contribution and exchange part containes expressions for O and PBE in order to capture the complementary good sides of both GGAs. Further refinements to make the DFA numerically more stable and inclusion of Grimme's D3 dispersion energy, finaly led to the improved SSB-D successor, S12g DFA.

Both SSB-D and S12g kept good performance for both structural parameters and electronic structure from OPBE, but also have certain adventages, most notably with weak interactions. OPBE is still better choise for geometry optimization that SSB-D because of some numerical discrepancies. Demand for simple and accurate treatemant of complicated electronic states of TM systems led to many validation studies of different DFAs, on various systems that proved to be chalanging for spin state energetics. The three above mentioned DFAs that are specifically designed for spin states (e.g. OPBE, SSB-D and S12g), shown to be excelent starting point for vast diversity of interesting coordination compounds. The thorough examination of available theoretical methods was one of the aims of this PhD thesis, and, in a final step, it directed us toward the best theoretical methodology for the study of the effect of different close lying spin states on a complicated catalytic mechanism of catechol dioxygenase mimic complexes.

Some systematic influences of the different calculation types on the spin states are well documented, naming just few: dispersion,[49] scalar relativistic effects,[49] zero point energy and enthropic contributions,[49] implicit solvation[49] and basis set.[44,50]

4. Our calculations

4.1. P450 mimics and chalanging complexes for spin state calculation

4.1.1. Short introduction

Metalloenzymatic reactions are a great challenge for accurate theoretical methods, not only because of the size of such systems, but also because of the different electronic spin states that the active center has at the various catalytic steps. Illustrative example is the well-studied oxidation by cytochrome P450[51,52], that has an iron in the active site. The low spin (LS) (doublet) ground state of the enzyme's substrate free resting state changes to a high spin (HS) sextet as the substrate expels the stabilizing water cluster from the active site.[52-54] The change from iron six- to five-coordination enables the first electron reduction, so that molecular oxygen can bind on which the system returns to a LS (singlet) state.[51,54] A second electron reduction and protonation of the distal oxygen occurs next, [54,55] but the following steps are less well established. [54,56] Most probable mechanism[10] presumes that a second protonation leads to loss of a water molecule and formation of the elusive compound I, which abstracts a hydrogen from the substrate, followed by a rebound reaction[57,58] to give the hydroxylated product (see Scheme 4-1). [54,56] One of the alternative mechanistic pathways would be that, the protonated dioxygen compound leads directly to product via a cationic pathway. The recent characterization of compound I, a key intermediate in the oxidation of carbon-hydrogen bonds by cytochrome P450,[59] together with various other theoretical and experimental results[60-63] have opened many doors that will lead to a better insight in mechanism for controlling reactivity of O_2 by metalloproteins. An accurate theoretical description of the spin ground states of the various intermediates of cytochrome P450 is vital to elucidate the mechanism of the catalytic cycle. [54,64,65]

In this chaper, we will present a detailed DFT study on OPBE optimized geometries of iron complexes (**1-7**), Figure 4-1, with experimentally established spin ground states, ranging from singlet to sextet, and extended it with two iron porphyrinato complexes (**8**, **9**, Figure 4-1, that have been reported to have different electronic ground state in spite of their similarity[64,66,67].

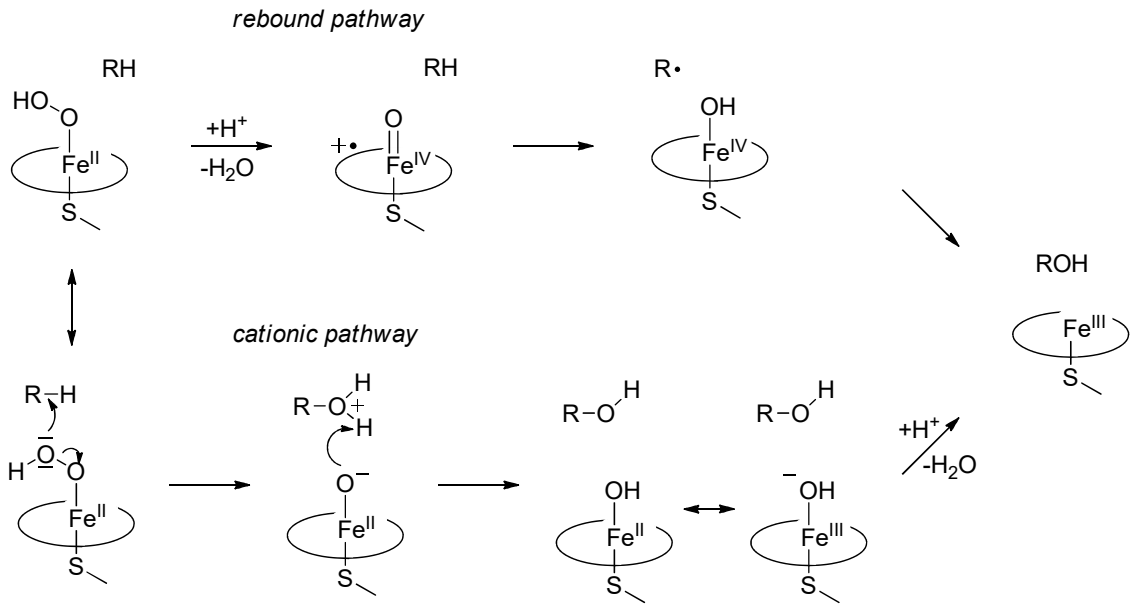

Scheme 4-1 Schematic representation of "rebound" and "cationic" mechanistic pathways, in the catalytic cycle of cytochrome P450 enzymes

The implications of obtained results on the future studies and exploration of spin states in the catalytic cycle of P450, in order to unambiguously determine the exact mechanism, are thoroughly discussed. In addition, spin ground states of few iron complexes, that Yoshizawa and co-workers[68] have studied with B3LYP using three different basis sets, were reexamined in order to choose the proper level of theory in determination of P450 catalytic cycle.

The total set of molecules consists both of Fe(III) (**1–3**, **8–9**) and Fe(II) (**4–7**) complexes, Figure 4-1, and show a diversity of experimentally observed spin ground states. After the thorough examination with versatile set of DFAs, on OPBE optimized geometries, validation study of the new S12g functional is performed. We will start our discussion focusing on the influence of structure relaxation on the spin states of the Fe(III)-complexes **1-3**.[69] Experimentally, Fe-$(PyPepS)_2$ (**1**, $PyPepSH_2$=N-2-mercaptophenyl-2'-pyridine-carboxamide) has a LS doublet ground state,[70] Fe(tsalen)Cl (**2**, tsalen = N,N'-ethylenebis-(thio-salicylideneiminato)) an intermediate spin (IS), quartet ground state[71] and Fe(N(CH2-o-C6H4S)3)(1-Me-imidazole) (**3**) a HS sextet ground state.[72] Then we will discuss the Fe(II)-complexes ($(Fe(NH)S_4)L$, $(NH)S_4$=bis(2-((2-mercaptophenyl)thio)ethyl)amine, L=CO (**4**), PMe_3 (**5**), NH_3 (**6**) and N_2H_4 (**7**)). Compounds **4–5** have a LS (singlet) state and compounds **6–7** reportedly a HS (quintet)

ground state. [73-75] Futher, we will focus on Fe^{III}(porphyrinato)Cl, FePCl (**8**) and, Fe^{III}(porphyrazinato)Cl, FePzCl (**9**), which have a sextet and a quartet ground state, respectively. Finally, we will address the implications of the choice of DFT functional on the catalytic cycle of cytochrome P450.

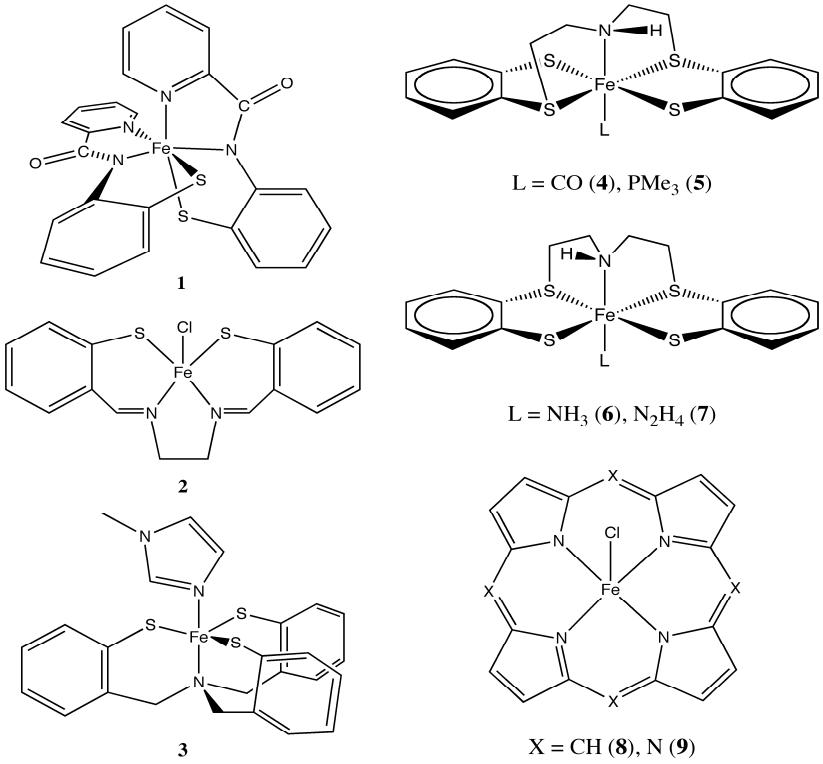

*Figure 4-1 Fe-(PyPepS)$_2$ **1** (PyPepSH$_2$ = N-2-mercaptophenyl-2'-pyridine-carboxamide); Fe(tsalen)Cl **2** (tsalen =N,N'-ethylenebis-(thio-salicylideneiminato)); Fe(N(CH$_2$-o-C$_6$H$_4$S)$_3$)(1-Me-imidazole) **3**; (Fe(NH)S$_4$)L **4** (L=CO), **5** (PMe$_3$), **6** (NH$_3$), **7** (N$_2$H$_4$) ((NH)S$_4$ = bis(2-((2-mercaptophenyl)thio)ethyl)amine); Iron porphyrin chloride (**8**, FePCl) and iron porphyrazine chloride (**9**, FePzCl)*

4.1.1.1. Structure relaxation of Fe(III) compounds **1-3**

The optimization of the three Fe(III) molecules (**1-3**) leads in all cases to the expected structural changes for the different spin states. Comparison of optimized structures of **1-3** indicates to an expansion of the ligand sphere, when we go from low to high spin state. Going from the doublet to the quartet state, first the equatorial ligands move away from iron while the axial ligands stay almost at the same position. In the

sextet state, the equatorial ligands remain virtually at the same position, but the axial ligands (have to) move out.

4.1.1.2. Spin state energies for compounds 1-3

Comparing the spin state energies, calculated on the experimental structure,[46] with results from optimized geometries, Table 4-1, it is evident that the energy gap between different spin states decreases. In the case of compound **1**, the doublet ground state has the closer lying quartet and the sextet state after geometry optimization. Molecule **2** has the quartet ground state. The relative energies of the doublet and sextet states are also reduced after structure relaxation. Same trends apply for the sextet ground state of complex **3**. For all complexes, after the spin state relaxation, OPBE continues to give the correct spin ground state. Its recently developed successor, S12g, also predicts all spin ground states correctly. Spin contamination is small for these complexes, and therefore shall not be attributed any further. From the Table 4-1, it is clear that after optimizing the structures for each spin state separately, also a number of the s^4 term containing DFAs(see Equation 3-27 and discussion from the introduction), that were successful on experimental geometry,[46] failed to reproduce the ground state of molecules **1** and **2**. The hybrid DFAs, τ-HCTHh, B97, O3LYP and M06, some of the MGGA (τ-HCTH, OLAP3, VS98), as well as HCTH/407 tend to overestimate the stability of the HS state, Table 4-1. The hybrid DFAs without s^4 term show the same trend, which remarkably holds true for B3LYP, which gave at least the right trend using the experimental geometries. The only hybrid DFAs that give reasonable results are TPSSh and B3LYP*, where the correct spin ground state for all three molecules is observed, Table 4-1. TPSSh predicts for molecule **3** the LS and IS state at almost the same energy level as the sextet state, while B3LYP* places the HS state of **1** at almost the same energy as the doublet ground state. The standard GGAs, including XLYP fuctional, tend to predict LS ground state for the HS molecule **3**, instead.

Table 4-1 Spin state energies (kcal/mol) for Fe(III) molecules 1-3 using TZP basis set

	Fe-(PyPepS)$_2$ **1**			Fe(tsalen)Cl **2**			Fe(N(CH$_2$-o-		
xc	*LS*	*IS*	*HS*	*LS*	*IS*	*HS*	*LS*	*IS*	*HS*
DFAs that containe s^4 term									
OPBE	0	17.1	10.2	6.5	0	3.9	6.6	7.9	0
S12g	0	15.8	8.7	7.6	0	3.8	6.8	7.2	0
OPerdew	0	15.7	10.2	7.3	0	3.8	5.6	6.8	0
OLYP	0	11.9	5.1	8.9	0	1.6	10.1	9.9	0
HCTH/4	0	7.1	–5.7	12.9	0	–3.4	19.6	15.8	0
VS98	0	11.5	–6.6	14.1	0	–2.8	8.4	2.5	0
OLAP3	0	6.6	–6.6	13.2	0	–4.9	22.2	18.0	0
KCIS	0	19.8	19.4	3.7	0	8.2	–3.9	0.9	0
τ-HCTH	0	10.4	0.1	10.9	0	–0.2	12.8	10.8	0
τ-	0	10.3	–0.8	15.3	0	1.6	9.4	5.9	0
B97	0	6.6	–8.0	19.0	0	–1.5	16.3	9.2	0
TPSSh	0	15.5	9.8	10.4	0	5.8	1.1	0.9	0
O3LYP	0	7.9	–6.5	16.6	0	–2.3	17.6	12.1	0
M06-L	0	8.3	-8.7	14.9	0	-7.2	16.2	11.7	0
M06	0	2.1	-19.3	26.1	0	-6.9	25.5	13.5	0
M06-2X	0	-13.9	-52.2	44.2	0	-19.0	54.4	25.0	0
DFAs that do not containe s^4 term									
LDA	0	35.2	44.9	–5.6	0	21.8	–31.1	–15.5	0
XLYP	0	15.9	15.9	5.0	0	8.5	–3.2	1.2	0
BLYP	0	16.9	17.5	4.5	0	9.2	–4.7	0.3	0
PBE	0	21.0	22.5	2.6	0	11.2	–8.8	–2.5	0
Becke00	0	8.1	–4.6	13.2	0	–3.4	15.8	12.7	0
FT97	0	18.2	21.2	4.5	0	11.2	–13.9	–3.5	0
B3LYP	0	6.5	–7.3	19.1	0	–0.6	15.1	8.3	0
PBE0	0	6.7	–10.2	21.6	0	–1.9	17.6	8.4	0
B1LYP	0	2.7	–15.3	23.4	0	–3.9	21.7	11.2	0
B3LYP*	0	10.5	1.0	14.7	0	2.8	8.1	5.1	0
X3LYP	0	5.9	–9.1	20.2	0	–1.3	16.4	8.7	0
OPBE0	0	2.5	–19.6	25.1	0	–7.6	28.9	15.8	0

Table 4-2 Spin state energies (kcal/mol) for Fe(III) molecules 1-3 using TZP basis set, with OPBE and S12g DFAs, in vacuum and COSMO

Geo.[x]	SP[xi]	Fe-(PyPepS)$_2$ **1**			Fe(tsalen)Cl **2**			Fe(N(CH$_2$-o-C$_6$H$_4$S)$_3$)(1MIm[b]) **3**		
		LS	*IS*	*HS*	*LS*	*IS*	*HS*	*LS*	*IS*	*HS*
OPBE	**OPBE**	0	17.1	10.2	6.5	0	3.9	6.6	7.9	0
	OPBE	0	19.4	13.0	9.3	0	6.9	7.9	7.4	0
	S12g	0	15.8	8.7	7.6	0	3.8	6.8	7.2	0
	S12g	0	18.2	11.6	10.2	0	6.4	8.2	6.8	0
OPBE cosmo	**OPBE**	0	18.8	13.1	5.2	0	2.9	6.2	7.5	0
	OPBE	0	17.4	10.2	9.7	0	7.7	8.0	7.2	0
	S12g	0	18.4	13.3	6.0	0	3.0	6.5	6.8	0
	S12g	0	17.1	10.6	10.2	0	7.4	8.3	6.5	0
S12g	**OPBE**	0	18.3	10.5	7.4	0	6.2	7.6	8.1	0
	OPBE	0	22.7	14.7	10	0	9.2	8.6	7.1	0
	S12g	0	15.4	8.7	7.5	0	6.6	6.5	7.0	0
	S12g	0	19.9	13.1	9.9	0	9.3	7.7	6.1	0
S12g cosmo	**OPBE**	0	17.5	10.6	7.0	0	4.7	7.5	8.4	0
	OPBE	0	20.5	14.9	11.2	0	6.7	8.8	7.2	0
	S12g	0	15.7	9.2	6.6	0	4.7	6.1	6.8	0
	S12g	0	18.8	13.7	10.4	0	6.5	7.6	5.9	0

The choice of exchange correlation functional has an obvious influence on geometry, with tendency of S12g to give somewhat longer bond lengths than OPBE. Unlike the choice of functional, influence of environment on geometrical parameters during the structural relaxation was not very significant, and it depends on system under consideration. In most cases, optimizations with COSMO gave slightly longer bonds, but without consequences on spin-state order, Table 4-2.

4.1.1.3. Structure relaxation of compounds 4-7

The spin state dependent structure relaxation (full geometry optimization) for the Fe(II) compounds results in the similar differences of Fe-ligand distances as for the Fe(III) compounds. In the case of compound **4**, the Fe-N, Fe-S and Fe-C distances are slightly elongated in comparison to the distances in Fe(III) complexes due to the additional *d*-electron in Fe(II) systems. Interestingly, the hydrazine group in molecule **7**

[x] Geometry optimization with frozen core electrones
[xi] Subsequent single point calculations with full electron basis sets

is found at 2.025 Å in the singlet, and at 2.338 Å in the quintet state, but dissociates to 2.668 Å in the triplet state (in OPBE optimized structures). This dissociation occurs also with the "trans" form of $(Fe(NH)S_4)L$ (*vide infra*). Therefore, triplet energies for **7** are not discussed in the next section.

4.1.1.4. Spin state energies of compounds 4-7

The spin ground state of the Fe(II) complexes **4** and **5** is correctly predicted using OPBE and S12g levels of theory (see Table 4-3), i.e. the singlet is the lowest in energy for both molecules, in agreement with experimental data. For compound **4**, the triplet and quintet states are significantly higher in energy. The energy differences between the different states are smaller for compound **5**. As a result, the relative stability of the HS (quintet) state of **5** is overestimated by almost all hybrid levels of theory due to the inclusion of a portion of HF exchange in these DFAs. The HF part leads to an erroneous overstabilization of the exchange interactions between electrons having the same spin. In accordance with the explanations from the methodology chapter, the larger the amount of HF exchange, the more the HS state is stabilized. For instance for the series B3LYP*, B3LYP, X3LYP, B1LYP, the relative energy of the quintet state of **5** is respectively -0.7, -11.0, -12.7, -20.8 kcal/mol, which correlates very well with the amount of HF exchange in these DFAs of respectively 15, 20, 21.8 and 25%. The only hybrid functional that does not seem to suffer from this is the TPSSh hybrid functional, which includes only 10% HF exchange. Similar to the compounds **4** and **5**, we found after spin state structure relaxation a LS ground state for iron complexes **6** and **7**, with the IS and HS higher in energy by 3-10 kcal/mol (see Table 4-4). Unfortunately, the experimental determination of the spin states of compounds **6** and **7** is inconclusive, since anomalous high μ_{eff} values of 10-13 μ_B have been measured that indicate impurities, e.g. by metallic iron. For compound **7** in solution, a HS state was observed,[75] but a compound similar to **7** showed a diamagnetic LS Fe center.[76] Moreover, indications of dimer formation of the ligand-free $[(Fe(NH)S_4)]$-complex were observed. [74,75] Since the different forms of the $(Fe(NH)S_4)L$ complex in these studies were obtained, we have checked both forms for compounds **4**-**7**, i.e. with the "trans" and "meso" form (see Figure 4-2 Different forms of compounds 4-7). For both forms of

each of compounds **4-7** we found a LS ground state, albeit with smaller spin-state splitting for compounds **6** and **7.**

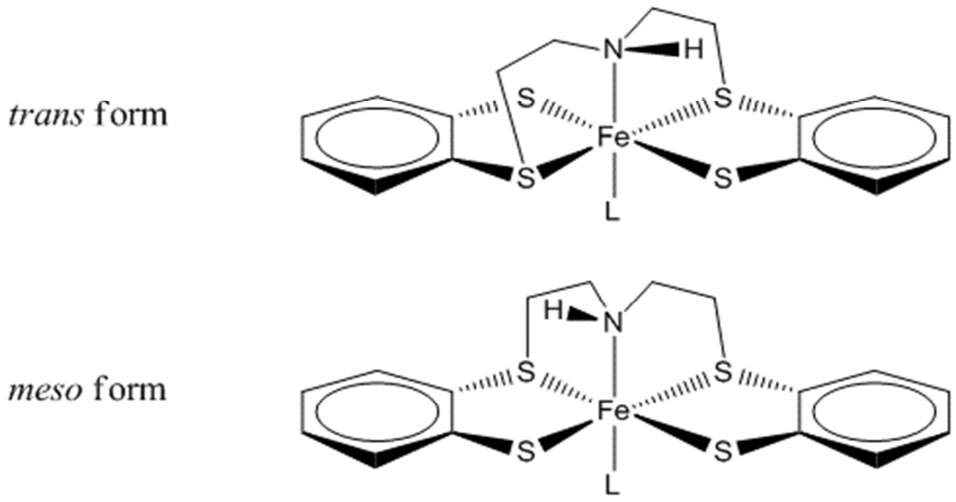

Figure 4-2 Different forms of compounds 4-7

These findings can be traced back to the strength of the iron-ligand bond, which seems to be much weaker for compounds **6**/**7** than for compounds **4**/**5**. The weakly bounded NH_3 and N_2H_4 ligands are easily exchanged with CH_3OH, solvent (THF) or CO. [75] These experimental data corroborate the computed ligand-binding energies, which indicate strong and favorable binding of CO and $P(Me)_3$ to form the singlet ground state, but less favorable binding of the other ligands or spin states.[77] Interestingly, the monomeric $Fe(NH)S_4$ complex without a ligand is predicted to have a triplet spin ground state in the trans form, while the other spin states or the meso form lying higher in energy by at least 7 kcal/mol. The ligand-free complex may dimerize to give the experimentally observed HS state through ferromagnetic coupling. The latter process has not been studied due to the complexity involved with ferromagnetic versus anti-ferromagnetic coupling of the many spin states that need to be considered. This is confirmed by a recent study using high-level *ab initio* methods that indeed found a singlet ground-state for these molecules.[78] In a detailed study, "accurate" spin ground state for molecules **6** and **7** was found with double hybrid B2PLYP functional, and also authors obtained the HS state for molecule **6** with OPBE.[79] Since the last result is in disagreement with our study, we optimized the structures of molecules **6** and **7** using OPBE functional. The obtained results were in accordance with the previous study,[79]

but the structures were highly distorted representing only the local minima on the potential energy surface.

Comparing the different DFAs for prediction of spin ground states of compound **6** and **7** (Table 4-4), it gets clear that the only DFAs that give good results are OPBE, S12g, OPerdew and TPSSh. Hybrid DFAs were not able to capture correct ground state and predict the quintet state as the ground state.

Table 4-3 Spin state energies (kcal/mol) for "trans" complexes 4 and 5 using TZP basis

	trans-(Fe(NH)S_4)CO **4**			(Fe(NH)S_4)PMe_3 **5**		
xc	*singlet*	*triplet*	*quintet*	*singlet*	*triplet*	*quintet*
DFAs that containe s^4 term						
OPBE	0	23.4	34.8	0	16.3	20.1
S12g	0	19.1	28.0	0	14.5	17.7
OPerdew	0	22.8	33.7	0	16.7	20.2
OLYP	0	17.7	24.4	0	10.2	8.9
HCTH/407	0	13.1	14.6	0	5.7	-2.1
VS98	0	10.5	6.4	0	20.7	9.7
OLAP3	0	15.0	13.4	0	5.0	-6.7
KCIS	0	22.3	36.4	0	19.4	26.2
τ-HCTH	0	15.7	20.1	0	9.4	4.8
τ-HCTHh	0	14.3	14.8	0	10.2	2.0
B97	0	11.1	5.9	0	6.6	-8.0
TPSSh	0	17.6	22.7	0	15.0	11.4
O3LYP	0	14.8	13.5	0	8.2	-2.8
M06-L	0	15.9	11.0	0	16.7	6.8
M06	0	11.3	-0.9	0	8.2	-8.8
M06-2X	0	-8.3	-44.6	0	-14.5	-63.2
DFAs that do not containe s^4 term						
LDA	0	36.1	67.8	0	36.4	62.7
XLYP	0	15.5	26.5	0	10.6	13.7
BLYP	0	16.7	28.8	0	11.9	16.4
PBE	0	22.7	39.4	0	19.6	29.5
Becke00	0	10.8	8.7	0	6.5	-4.7
FT97	0	21.7	37.4	0	17.7	28.2
B3LYP	0	9.2	4.1	0	4.7	-11.0
PBE0	0	11.9	5.7	0	8.6	-8.1
B1LYP	0	6.0	-4.8	0	1.3	-20.8
B3LYP*	0	12.5	13.2	0	8.3	-0.7
X3LYP	0	8.7		0	4.4	-12.7

Table 4-4 Spin state energies (kcal/mol) for labile ("meso") complexes 6 and 7 using TZP basis

	$(Fe(NH)S_4)NH_3$ **6**			$(Fe(NH)S_4)N_2H_4$ **7**		
xc	*singlet*	*triplet*	*quintet*	*singlet*	*triplet*	*quintet*
DFAs that containe s^4 term						
OPBE	0	10.3	6.6	0	- [a]	6.6
S12g	0	7.7	2.6	0	- [a]	2.5
OPerdew	0	11.0	7.0	0	- [a]	8.0
OLYP	0	5.1	-1.4	0	- [a]	-0.7
HCTH/407	0	-1.3	-13.2	0	- [a]	-12.4
VS98	0	11.0	-7.4	0	- [a]	-3.1
OLAP3	0	-1.0	-14.4	0	- [a]	-14.3
KCIS	0	13.2	13.2	0	- [a]	14.8
τ-HCTH	0	4.3	-6.2	0	- [a]	-5.2
τ-HCTHh	0	5.9	-7.1	0	- [a]	-5.6
B97	0	2.1	-15.1	0	- [a]	-13.9
TPSSh	0	11.5	3.4	0	- [a]	4.9
O3LYP	0	2.5	-12.0	0	- [a]	-11.2
M06-L	0	9.1	-3.9	0	- [a]	-3.2
M06	0	4.5	-18.6	0	- [a]	-16.7
M06-2X	0	-15.4	-70.7	0	- [a]	-63.0
DFAs that do not containe s^4 term						
LDA	0	33.9	45.9	0	- [a]	48.3
XLYP	0	7.3	5.4	0	- [a]	6.7
BLYP	0	8.8	7.6	0	- [a]	9.0
PBE	0	15.3	17.0	0	- [a]	18.6
Becke00	0	1.5	-12.2	0	- [a]	-11.0
FT97	0	13.6	16.9	0	- [a]	18.3
B3LYP	0	0.6	-16.8	0	- [a]	-15.5
PBE0	0	3.3	-16.2	0	- [a]	-14.8
B1LYP	0	-3.0	-25.3	0	- [a]	-24.1
B3LYP*	0	4.5	-7.8	0	- [a]	-6.4
X3LYP	0	0.3	-18.3	0	- [a]	-17.0

a) ligand dissociated (see text)

As in the case of previous investigated molecules **1-3**, after optimization with S12g, somewhat longer bond lengths have been obtained. In contrast to the Fe(II) complexes (**1-3**), the Fe(III) P450 model systems (**4-7**) are prone to the influence of environment (COSMO calculations) on spin state ordering, Table 4-5 and Table 4-6. Calculations with COSMO solvation model revealed a tendency to favor the HS state in almost all complexes. The fact that inclusion of COSMO can affect the energy separation of states does not make much difference in complexes **4** and **5** where

there is large LS-HS barrier, but can produce considerable effect with molecules **6** and **7** that have close laying HS-LS states. Examination of the results given in Table 4-5 and Table 4-6 shows that, for all systems, S12g gives the values in a good agreement with OPBE.

*Table 4-5 Spin state energies (kcal/mol) for labile ("trans") complexes **4** and **5** using TZP basis, with OPBE and S12g DFAs, in vacuum and COSMO*

Geo.[xii]	SP[xiii]	*trans*-(Fe(NH)S_4)CO **4**			*trans*-(Fe(NH)S_4)PMe_3 **5**		
		singlet	*triplet*	*quintet*	*singlet*	*triplet*	*quintet*
OPBE	**OPBE**	0	23.4	34.8	0	16.3	20.1
	OPBE	0	24.5	36.6	0	17.3	18.6
	S12g	0	19.1	28.0	0	14.5	17.7
	S12g	0	20.2	29.7	0	15.4	16.3
OPBE cosmo	**OPBE**	0	23.5	35.3	0	16.4	20.4
	OPBE	0	24.5	36.5	0	17.3	18.3
	S12g	0	19.4	29.1	0	15.1	19.1
	S12g	0	20.3	30.3	0	15.9	17.1
S12g	**OPBE**	0	23.4	34.2	0	19.6	19.4
	OPBE	0	24.3	36.4	0	20.3	19.2
	S12g	0	18.7	29.3	0	15.6	16.8
	S12g	0	19.6	31.4	0	16.3	16.6
S12g cosmo	**OPBE**	0	24.6	35.0	0	19.9	19.2
	OPBE	0	24.8	36.5	0	20.6	18.2
	S12g	0	20.4	30.8	0	15.8	17.1

[xii] Geometry optimization with frozen core electrones
[xiii] Subsequent single point calculations with full electron basis sets

	S12g	0	20.5	32.2	0	16.4	16.2

*Table 4-6 Spin state energies (kcal/mol) for labile ("meso") complexes **6** and **7** using TZP basis, with OPBE and S12g DFAs, in vacuum and COSMO*

Geo.[xiv]	SP[xv]	*meso*-(Fe(NH)S_4)NH_3 **6**			*meso*-(Fe(NH)S_4)N_2H_4 **7**		
		singlet	*triplet*	*quintet*	*singlet*	*triplet*	*quintet*
OPBE	**OPBE**	0	10.3	6.6	0	-[xvi]	6.6
	OPBE	0	10.1	3.9	0	-[xiv]	4.4
	S12g	0	7.7	2.6	0	-[xiv]	2.5
	S12g	0	7.4	-0.1	0	-[xiv]	0.3
OPBE cosmo	**OPBE**	0	10.6	7.2	0	-[xiv]	7.1
	OPBE	0	9.9	3.5	0	-[xiv]	3.8
	S12g	0	7.9	3.5	0	-[xiv]	3.6
	S12g	0	7.0	-0.2	0	-[xiv]	0.5
S12g	**OPBE**	0	10.1	7.5	0	-[xiv]	7.6
	OPBE	0	10.7	5.7	0	-[xiv]	6.8
	S12g	0	8.4	5.3	0	-[xiv]	5.3
	S12g	0	8.7	3.4	0	-[xiv]	4.6
S12g cosmo	**OPBE**	0	10.1	6.8	0	-[xiv]	6.6
	OPBE	0	10.5	4.4	0	-[xiv]	5.2
	S12g	0	8.7	4.9	0	-[xiv]	4.6
	S12g	0	8.8	2.4	0	-[xiv]	3.2

4.1.1.5. Iron porphyrin chloride and the porphyrazine analogue

The structures of FePCl (**8**) and FePzCl (**9**) were optimized within C_{4v} symmetry, separately for each spin state. Similarly as in previous results,[64,65,80] it was found that porphyrin core size increases when going from the low to the HS state, and that the Fe-Cl distance increases in going from the LS to IS state, and then slightly decreases in the HS state.

OPBE predicts the correct spin ground state for both, FePCl and FePzCl (see Table 4-7). In the case of FePCl a sextet ground state was predicted with the quartet higher in energy by 4 kcal/mol and for FePzCl a quartet ground state with the sextet 4 kcal/mol higher. In both cases the LS state is considerably higher in energy. Similar

[xiv] Geometry optimization with frozen core electrones
[xv] Subsequent single point calculations with full electron basis sets
[xvi] ligand dissociated (see text)

results are found with the S12g, OPerdew and OLYP DFAs. The hybrid DFAs B3LYP, X3LYP, τ-HCTHh and B97 (as well as B97-1[81] that gives results almost indistinguishable from B97 results) predict the correct spin ground states, but place the LS doublet state at considerable higher energy than the pure DFAs. This might be caused by the inclusion of HF exchange (known to favor HS states), and could therefore be an indication of a cancellation of errors.

Table 4-7 Spin state energy differences (kcal/mol, TZP basis) for FePCl (8) and FePzCl (9)

		FePCl			*FePzCl*		
		doublet[b]	*quartet*[b]	*sextet*[b]	*doublet*[c]	*quartet*[c]	*sextet*[c]
containing s^4 term or higher							
OPBE	*gga*	18.4	3.9	0	12.5	0	3.7
S12g	*gga*	15.7	1.5	0	12.8	0	4.9
OPerdew	*gga*	17.9	3.5	0	12.7	0	4.1
OLYP	*gga*	18.2	3.3	0	13.6	0	3.4
HCTH/407	*gga*	25.9	8.1	0	16.6	0	-2.3
VS98	*meta*	26.4	7.1	0	19.4	0	-1.8
OLAP3	*meta*	28.2	9.8	0	17.4	0	-2.8
KCIS	*meta*	6.2	-4.2	0	9.4	0	11.1
τ-HCTH	*meta*	23.0	6.4	0	15.4	0	0.6
τ-HCTHh	*hybr*	31.8	3.1	0	28.0	0	4.1
B97	*hybr*	40.3	5.8	0	33.6	0	1.2
TPSSh	*hybr*	20.9	-1.6	0	21.6	0	8.4
O3LYP	*hybr*	37.2	8.3	0	27.5	0	-1.1
M06-L	*meta*	30.3	11.6	0	20.1	0	-4.9
M06	*hybr*	54.5	13.4	0	41.6	0	-5.6
M06-2X	*hybr*	101.3	22.3	0	76.7	0	-16.2
containing no s^4 term							
LDA	*lda*	-14.8	-16.6	0	0.5	0	24.2
XLYP	*gga*	2.2	-7.8	0	9.8	0	13.3
BLYP	*gga*	1.5	-8.1	0	9.3	0	13.8
PBE	*gga*	1.6	-7.5	0	8.1	0	14.1
Becke00	*meta*	24.0	5.7	0	18.3	0	-0.2
FT97	*meta*	-0.8	-7.9	0	8.8	0	14.0
B3LYP	*hybr*	38.4	3.5	0	34.1	0	3.0
PBE0	*hybr*	48.8	7.5	0	39.8	0	0
B1LYP	*hybr*	48.7	6.9	0	41.0	0	-0.3
B3LYP*	*hybr*	27.9	-0.1	0	27.3	0	6.5
X3LYP	*hybr*	41.4	4.3	0	36.2	0	2.3

S^2 values in parenthesis. a) obtained post-SCF using OPBE densities/orbitals; b) relative to FePCl sextet spin state; c) relative to FePzCl quartet spin state

In accordance to previous studies, [64,65,46,80] standard DFAs like LDA,[37] BLYP[40,82] and PBE[83] disfavor the HS state of FePCl (see Table 4-7). From the group of DFAs containing s[4], HCTH, VS98, OLAP3, KCIS and O3LYP do not give the expected result for either FePCl (TPSSh) or FePzCl.

Hybrid DFAs, O3LYP, B1LYP and PBE0, predict correctly the HS ground state for FePCl, but place the quartet and sextet state at equal level for FePzCl. Likewise, M06 predicts the HS state for FePCl correctly, but fails for FePzCl. On the other hand, the B3LYP* functional predicts the spin state for FePzCl correctly, but fails for FePCl. XLYP functional also predicted wrong ground state for FePCl.[84]

*Table 4-8 Spin state energy differences (kcal/mol, TZP basis) for FePCl (**8**) and FePzCl (**9**), with OPBE and S12g DFAs, in vacuum and COSMO*

Geo.[xvii]	SP[xviii]	*FePCl*			*FePzCl*		
		doublet	*quartet*	*sextet*	*doublet*	*quartet*	*sextet*
OPBE	**OPBE**	18.4	3.9	0	12.5	0	3.7
	OPBE	16.3	-1.0	0	15.6	0	7.6
	S12g	15.7	1.5	0	12.8	0	4.9
	S12g	13.8	-2.9	0	15.8	0	8.6
OPBE cosmo	**OPBE**	18.0	4.8	0	11.6	0	2.9
	OPBE	16.9	-1.7	0	16.6	0	8.2
	S12g	15.0	2.3	0	11.8	0	4.2
	S12g	14.1	-3.6	0	16.5	0	9.2
S12g	**OPBE**	18.6	4.0	0	12.7	0	3.7
	OPBE	16.3	-0.7	0	15.7	0	7.5
	S12g	15.4	1.5	0	12.6	0	5.0
	S12g	13.4	-2.8	0	15.4	0	8.6
S12g cosmo	**OPBE**	18.3	4.5	0	12.0	0	3.2
	OPBE	17.1	-1.6	0	16.8	0	8.1
	S12g	15.0	2.0	0	11.8	0	4.6
	S12g	14.0	-3.5	0	16.3	0	9.2

COSMO calculations revealed clear and unambiguous effect on electronic structure, Table 4-8. Introduction of the solvent favor the LS state, and as such have small effect on a spin ground state of molecule **9** that has quartet ground state and a

[xvii] Geometry optimization with frozen core electrones
[xviii] Subsequent single point calculations with full electron basis sets

close sextet quartet state. As opposed, for molecule **8**, that is in a HS and has low lying quartet state, the quartet state is artificially stabilized to the extent that it becomes the ground state within all COSMO calculations. S12g once again shows excellent agreement with spin state energetics obtained at OPBE level of theory.

4.1.1.6. Implications regarding the catalytic cycle of cytochrome P450

As demonstrated in this chapter, throughout this study, B3LYP continued to fail in providing the correct spin ground state of several iron complexes, as reported also by Reiher and co-workers[85] and Ryde and co-workers. [86] Nevertheless, almost all studies on the catalytic cycle of P450 so far have used the B3LYP functional, [11,51,54,56,63,87-89] which casts doubt on the conclusions drawn from the results obtained in these studies, especially in view of the significance of the spin ground state as evidence for either the "cationic" or "rebound" pathway (*vide supra*). To study the impact of our results on the outcome of previous B3LYP studies on the catalytic cycle, we investigated the spin ground states of few iron complexes (transition states TS1 and TS2 from ref. [68]; see Figure 4-3) that Yoshizawa and co-workers have studied with B3LYP using three different basis sets. The results with the smaller basis sets (CEP-121G, LanL2DZ) differed considerably from the results with the larger (6-311+G**) basis set. [68] Using the TZP basis set, we obtained B3LYP results that are similar to their large basis set results (see

Table 4-9). Having established the similarity between the Yoshizawa and our B3LYP results, it is now instructive to look at the differences between B3LYP, OPBE and S12g functional for these transition states,

Table 4-9.

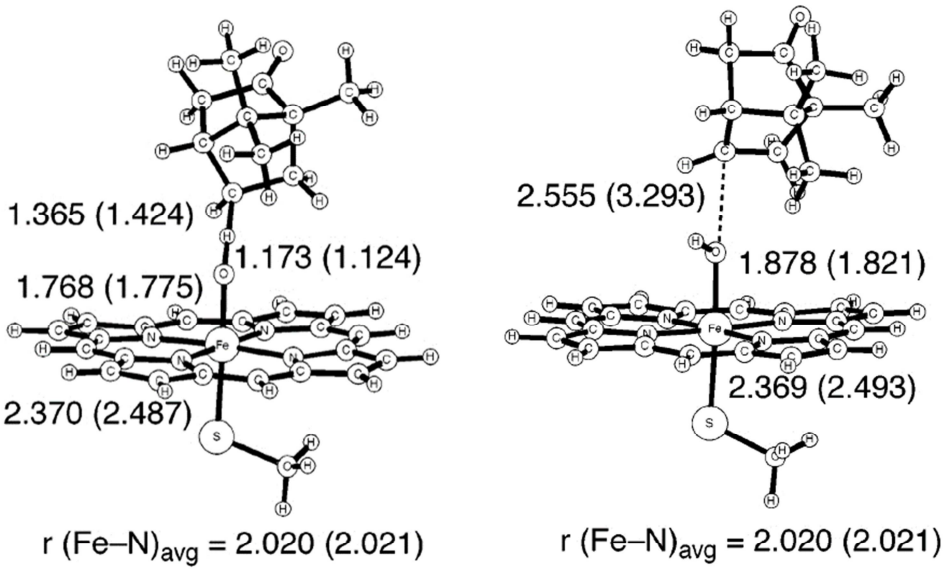

Figure 4-3 TS1 and TS2 structures (taken from Kamachi, Yoshizawa, J. Am. Chem. Soc. 2003, 125, 4652)

Table 4-9 Doublet/quartet energies (kcal/mol) for Yoshizawa complexes (TS1, TS2)

basis set	*TS1 doublet*	*TS1 quartet*	*TS2 doublet*	*TS2 quartet*
B3LYP				
LanL2DZ[a]	4.8	5.4	0	2.5
CEP-121G[a]	6.4	5.2	0.8	0
6-311+G**[a]	10.1	8.3	1.4	0
TZP[b]	10.9[c]	8.4	3.5[c]	0
OPBE				
TZP[b]	3.6[c]	5.5	2.4[c]	0
OPBE COSMO				
TZP[b]	-0.3[c]	3.8	8.4[c]	0
S12g				
TZP[b]	3.2[c]	5.4	9.9[c]	0
S12g COSMO				
TZP[b]	-0.7[c]	3.5	11.1[c]	0
S^2	*1.21*	*3.79*	*1.70*	*3.81*

a) Yoshizawa and co-workers, ref. [68]; b) this work; c) corrected for spin contamination (eq. 2 of ref. [90])

OPBE and S12g agree on the quartet state of TS2 having the lowest overall energy, with the TS1 higher in energy. However, B3LYP predicts a much larger splitting between TS1 and TS2 than OPBE and S12g. Moreover, for TS1 the doublet spin ground state is predicted with OPBE and S12g, which is not in agreement with B3LYP results. This disfavoring of the LS state is a characteristic failure of B3LYP as we have seen throughout this study. It should also be noted that unlike all the other compounds, the LS states of TS1 and TS2 are severely spin contaminated. This may result from the inclusion of a portion of HF exchange, e.g. indicative of the cancellation of errors as discussed above.

Given the evident failure of B3LYP to give a correct description of spin ground states of iron complexes, one should be very cautious when interpreting the outcome of B3LYP studies, especially when arguing in favor of either the "rebound" or "cationic" pathway (see Scheme 4-1) in the catalytic cycle of cytochrome P450 enzymes. Also, recent studies show that it is necessary to include dispersion correction in order to obtain reliable results for reaction barriers in P45O catalytic cycle.[91,92] Based on the excellent performance of S12g for spin states splitting of iron complexes, that contains Grimme D3 dispersion term, previous conclusion seems to be justified.

1.1.1. Conclusion

In this chapter, the extension of our previous validation of DFAs for a correct description of spin states of Fe(II) and Fe(III) complexes was presented. In the present contribution we allow the structure relaxation of the LS, IS and HS states of the iron compounds separately at OPBE and S12g levels of theory, thereby performing a more stringent test on the reliability of DFAs for providing spin ground states of iron complexes. Aditionaly, we find that standard DFAs like LDA, BLYP or PBE, but also XLYP disfavor HS states. The set of reliable DFAs is however drastically reduced: only OPBE, the preferred functional from our previous study, its successor S12g and OPerdew predict the correct spin ground state for all iron complexes under study.

Other DFAs show questionable results for one or more iron complex.

Hybrid DFAs like B3LYP and X3LYP systematically overestimate the stability of higher spin states. Only, the TPSSh functional (with 10% exact exchange) gives reasonable results, e.g. it fails for only two out of the nine compounds.

Questionable veracity of B3LYP results is also shown on transition state models for camphor hydroxylation, TS1 and TS2, that Yoshizawa and co-workers have studied with B3LYP.

4.1.2. Computational detail

All DFT calculations were performed with the Amsterdam Density Functional (ADF) suite of program.[42,93,94] MOs were expanded in an uncontracted set of Slater type orbitals (STOs) of triple-ζ quality containing diffuse functions (TZP)[95] and one set of polarization functions. Core electrons (1s for 2^{nd} period, 1s2s2p for 3^{rd}-4^{th} period) were not treated explicitly during the geometry optimizations (frozen core approximation), as it was shown to have a negligible effect on the obtained geometries.[96] An auxiliary set of s, p, d, f, and g STOs was used to fit the molecular density and to represent the Coulomb and exchange potentials accurately for each SCF cycle.

Energies and gradients were calculated using the OPBE and S12g functional, in vacuum and COSMO[97-99] environment. Geometries were optimized with the QUILD program[100] using adapted delocalized coordinates[101] until the maximum gradient component was less than 10^{-5} a.u. In the first part of the examination, prior to S12g validation, single point energies, on OPBE/vacuum optimized geometries, with all-electron basis sets, were calculated with LDA,[28,37,102] OPBE,[48] S12g,[47] OPerdew,[103,104] XLYP,[84] X3LYP,[84] BLYP,[40,82] PBE,[104] OLYP,[82,103] HCTH/407,[81] τ-HCTH,[81] τ-HCTHh,[81] VS98,[105] OLAP3,[106] KCIS,[107] Becke00,[108] FT97,[109] B97,[110] TPSS,[111] TPSSh,[111] O3LYP,[101] MO6,[112] MO6-L,[113] MO6-2X,[112] PBE0,[114] B3LYP,[115,116] B1LYP,[117] and B3LYP*[85].

4.2. Complexes with 2,6-Diacetylpyridinebis(semioxamazide)

4.2.1. Short introduction

Complexes of polydentate acylhydrazone ligands with d metals are particularly interesting since they have interesting structural features that lead to a diversity of potential applications.[118-120] Among many others, 2,6-diacetylpyridine-bis(semioxamazide) (H_2dapsox), and its mono-anionic (Hdapsox$^-$) and di-anionic (dapsox^{2-}) forms, are conformationally flexible ligands. Moreover, they have a large number of potential donor atoms (see Figure 4-4), and hence display versatile behavior in metal coordination, the exact nature of which depends on the reaction conditions. The mode of coordination is governed by the nature of the central metal atom, the charge of the ligand, as well as the presence of other species capable to compete for coordination pockets.[121] Interestingly, the (H_n)dapsox ligand (n=0,1,2) enables formation of the pentagonal-bipyramidal complexes (PBPY-7) with some 3d elements, although usually seven-coordinate complexes are more common with large d-block metal ions. To date, 3d-block metal PBPY-7 complexes have been isolated and characterized with the H_2dapsox with Mn^{II},[122] Fe^{II},[123] Co^{II},[124] and Zn^{II},[122] and for Hdapsox$^-$ and dapsox^{2-} with Fe^{III}[125,126] and Co^{II}[124,127]. Other geometries are also possible: the octahedral environment is found when Hdapsox$^-$ and dapsox^{2-} are coordinated to Fe^{III},[128] and Ni^{II},[126] respectively, while with dapsox^{2-} Ni^{II} forms a square planar complex.[129] Furthermore, the di- and mono-anionic forms enable formation of square pyramidal (SPY-5) complexes of Cu^{II},[126,130] and Fe^{III}.[128] Therefore these ligands act as ligands of changeable dentation and exhibit a stereochemical diversity, particularly with respect to coordination numbers and/or geometries observed in coordination with various d-block metal ions. In addition, a characteristic feature of open-shell transition metal ions in general is that several electronic configurations are accessible that may give rise to a number of different spin states, where the preferred one is determined by ligand field strength. In the case of the (H_n)dapsox ligand this might be governed by the degree of (de)protonation.[45,131,132]

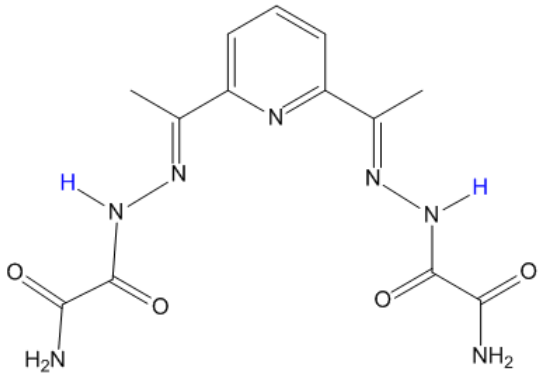

Figure 4-4 Schematic representation of H_2dapsox. Monoanionic and dianionic forms of ligand can be obtained upon dissociation of hydrogens indicated in blue.

To the best of our knowledge, and in spite of many experimental studies,[123,133-135] there are only few theoretical attempts that have tried to rationalize the structure and electronic properties of 3d metal complexes with H_2dapsox and its anionic forms.[119,136-138] Since these compounds represent mimics of superoxide dismutase (SOD) and ditopic receptors for lithium salts, they are of utmost importance, and hence detailed kinetic and mechanistic experimental studies were reported.[123,133-135,138,139] Recently, TDDFT and semi-empirical calculations were performed in order to rationalize the UV-VIS spectra of SOD mimics redox pair $[Fe^{III}(dapsox^{2-})(H_2O)_2]^+$ and $[Fe^{II}(H_ndapsox)(H_2O)_2]^{n+}$, explaining the nature of correctly tuned redox potential in catalytic superoxide disproportionation.[119] However, it is still not clear why the experimentally observed complexes are in particular geometry and what a role of ligand charge and spin state of metal ion is on that geometry. Thus, in order to gain an understanding of any one of these effects, we have performed a systematic DFT study of complexes of some 3d-block metal ions with $H_n$dapsox ligands. In other words, we have tried to elucidate how chelation properties of the ligands through different donor atoms and different orbital occupation patterns of metal ions, influences the stability of different geometries around various metal ions.

4.2.1.1. Stereochemistry of seven coordinate complexes.

The most commonly observed coordination polyhedra in seven-coordinated transition-metal complexes are pentagonal-bipyramidal (PBPY-7), capped octahedron (OCF-7),

and capped trigonal prism (TPRS-7),[121,140] see Figure 4-5. However, the unambiguous experimental assignment of coordination polyhedra in heptacoordinated complexes is often difficult because one structure may resemble more than one reference polyhedral; hence the need for a computational study of these complexes. The H_2dapsox ligand studied here has 11 potential ligator atoms (see Figure 4-4), some of which are mutually exclusive. This, together with the flexibility of both side chains attached to the pyridine ring, creates quite a diversified stereochemistry[130] with respect to the possible coordination modes, which could be summarized as follows: isomer **I** corresponds to the PBPY-7 X-ray determined structures of the investigated complexes (*vide supra*).[123-125] Isomers **II** and **III** might be quoted as rotamers of isomer **I**.

The remaining isomeric structures of PBPY-7 have a different type, or positioning of ligator atoms. In isomers **VII** and **VIII**, the dapsox^{2-} ligand is not planar and its side chains occupy axial positions. When the dapsox^{2-} ligand is in a planar conformation, there are two additional isomers, mutually rotamers, in which terminal NH_2 groups (isomer **XII**) or carbonyl groups (isomer **X**) form six-membered rings upon coordination. Two other isomers, **IX** and **XI**, originate from the asymmetrical combinations of side chain conformations of isomers **I**, **X** and **XII**, and are also rotamers. Of course, combination of isomers **IX** and **XI** is also possible, but the resulting isomer is not shown in the Figure 4-5, since it has an unreasonably high energy and was highly distorted after optimization of its geometry. Finally, isomer **IV** is in a TPRS-7 environment, while isomers **V** and **VI** correspond to OCF-7.

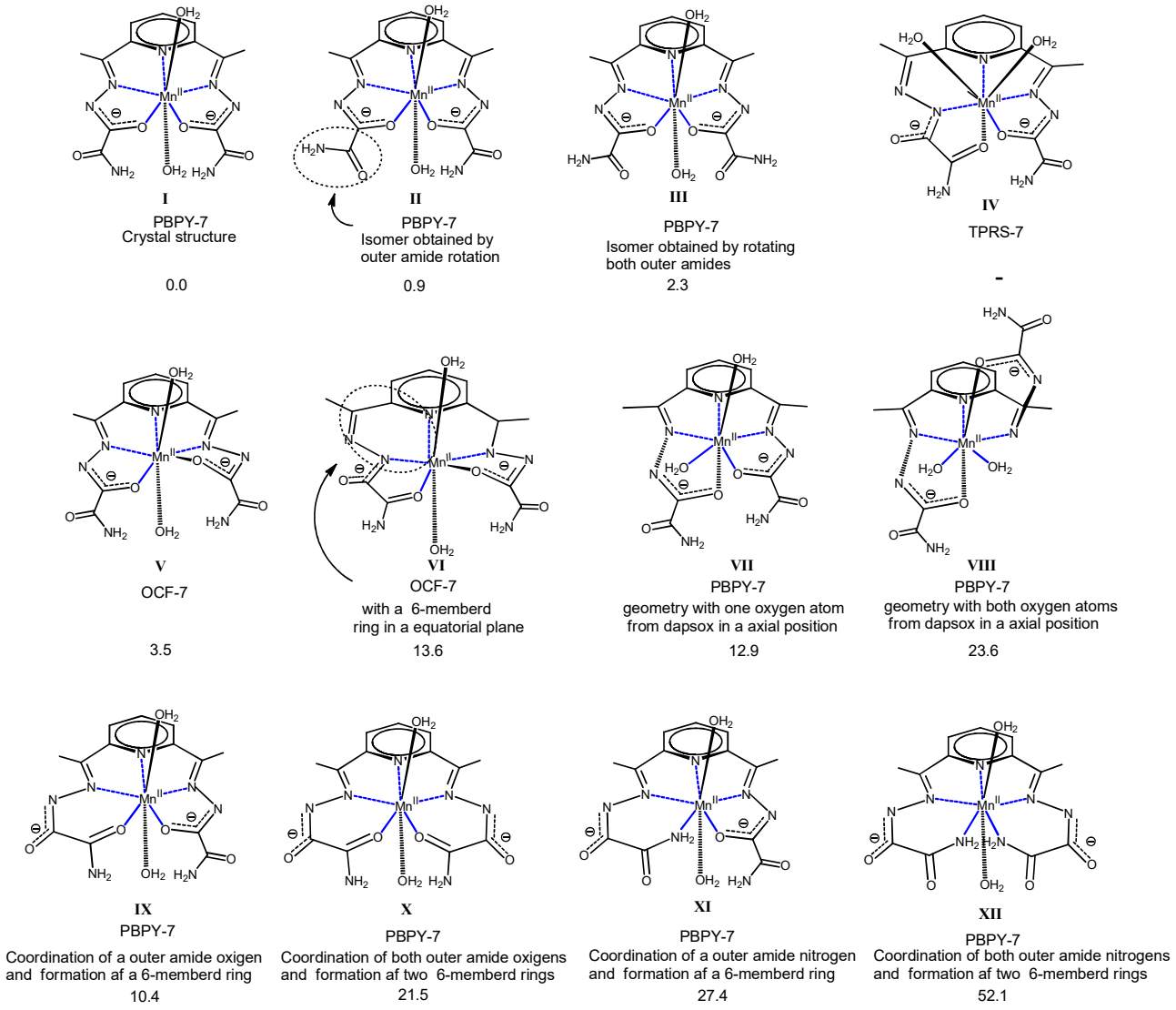

Figure 4-5 Possible general isomeric structures for $[M(H_ndapsox)(H_2O)_2]^q$. For $[Mn^{II}(dapsox^{2-})(H_2O)_2]$ relative energies are compared to the most stable isomer I and are given in kcal/mol; bonds that lie in the equatorial plane are labeled in blue.

Even though there is likelihood of formation of each isomer, it has been experimentally confirmed that $H_n$dapsox form always isomer I - PBPY-7 complexes with Mn^{II}[122], Fe^{III}[125,126], Fe^{II}[123] and Co^{II}[124,127]. Whenever a different ground state is possible, high spin is always observed. In order to elucidate the factors that govern this structural preferences, we performed DFT calculations for all the above mentioned isomers (**I-XII**) of $[M(H_ndapsox)(H_2O)_2]^q$ to examine their relative stability, see Figure 4-5, although some of them cannot be experimentally achieved. The apical position can be

occupied with different molecules, depending on the nature of the solvent,[138] hence for this study we modeled the apical coordination sphere with two molecules of water.

For $[Mn^{II}(dapsox^{2-})(H_2O)_2]$ isomer **I** is the most stable one (see Figure 4-5), in which $dapsox^{2-}$ is coordinated in a symmetrical pentadentate mode through pyridine, two azomethyne (imine) nitrogens, and two α-oxyazine oxygens. The least stable structure corresponds to the isomer **XII** (PBPY-7), due to the coordination of two amide nitrogens and the formation of two six-membered rings. The origin of the different stability for the two OCF-7 isomers (**V**, **VI**) can be found in the distinctive ligator atoms, and the formation of a six-membered ring in isomer **VI**. Isomers **II** and **III**, obtained by outer amide rotation have similar stability as isomer **I**, because the high conjugation in the equatorial plane is preserved. All other isomers are much higher in energy. We were unable to obtain the TPRS-7 coordination (isomer **IV**) due to the structure of the ligand and the presence of strong hydrogen bonds between the two neighboring water molecules. The combination of these two effects made that the TM-complex completely changed conformation, and therefore the relative energy cannot be shown in Figure 4-5. This trend has been observed for all investigated $[M(H_ndapsox)(H_2O)_2]^q$, Table 4-11. It is noteworthy that the geometries of the calculated structures of isomer **I** are in excellent agreement with those of similar structures characterized by X-ray.[123-125] Selected bond lengths and valence angles are collected and compared in original reference[141] for corresponding structures, while the superposition of some of the crystal structures[123-125] and structures computed at LDA level are presented in Figure 4-6. This figure shows the large coherence between the optimized and X-ray structures, which is the confirmation that LDA tends to give good geometries for coordination compounds.[142-145]

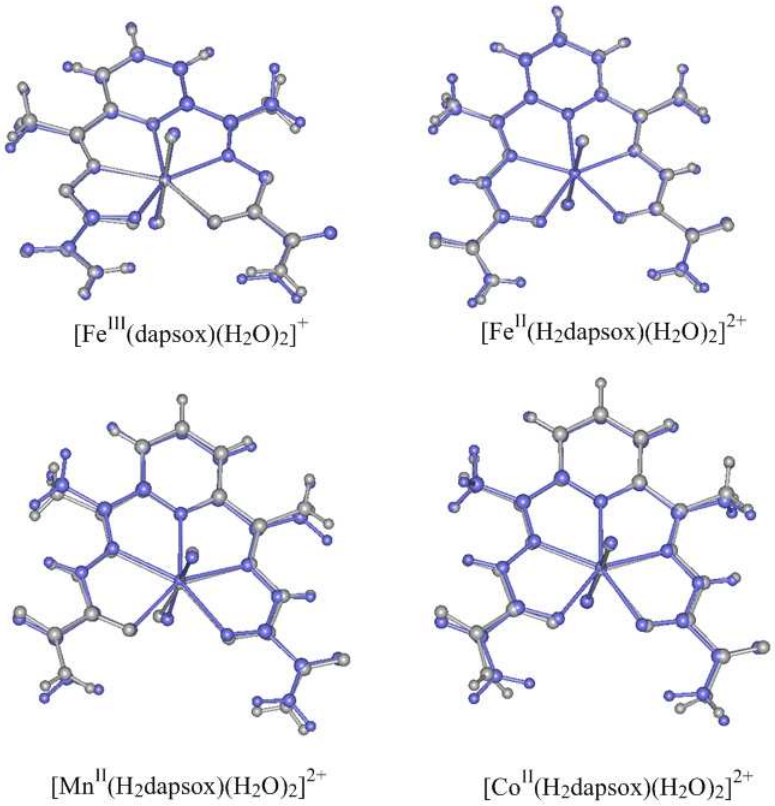

Figure 4-6 Overlays of available experimental X-ray (gray) with LDA optimized (light blue) global minimum structures of $[Fe^{III}(dapsox^{2-})(H_2O)_2]^+$, $[Fe^{II}(H_2dapsox)(H_2O)_2]^{2+}$, $[Mn^{II}(H_2dapsox)(H_2O)_2]^{2+}$ and $[Co^{II}(H_2dapsox)(H_2O)_2]^{2+}$.

The influence of ligand deprotonation and the nature of the central metal ion on the stability of isomers **I** and **V** is presented in Table 4-10 for Mn^{II}, Fe^{III}, Fe^{II}, Co^{II} and Zn^{II}. Additionally, we studied also complexes of the same type with Ni^{II} in order to rationalize experimental findings that reveal another type of coordination with this metal ion.

Table 4-10 Relative energies (kcal·mol^{-1}) of isomers I and V (see Figure 4-5) for different 3d-metal ions in high spin

Metal	Ligand	Exp.	Isomer	LDA	LDA/	LDA/	LDA/
Mn^{II}	dapsox		I	0	0	0	0
			V	1.7	3.5	5.0	5.1
	Hdapsox		I	0	0	0	0
			V	0.1	1.9	4.8	4.0
	H_2dapsox	x[122]	I	0	0	0	0
			V	-0.7	5.4	7.9	7.8
Fe^{III}	dapsox	x[129]	I	0	0	0	0
			V	-2.1	5.2	7.2	6.6
	Hdapsox	x[126]	I	0	0	0	0
			V	2.3	4.9	8.2	6.5
	H_2dapsox		I	0	0	0	0
			V	4.2	8.9	11.2	10.6
Fe^{II}	dapsox		I	0	0	0	0
			V	1.7	0.8	4.4	3.7
	Hdapsox		I	0	0	0	0
			V	0.1	3.6	6.6	5.3
	H_2dapsox	x[123]	I	0	0	0	0
			V	3.1	4.2	7.8	6.9
Co^{II}	dapsox	x[124]	I	0	0	0	0
			V	-0.2	0.2	0.6	0.6
	Hdapsox	x[124]	I	0	0	0	0
			V	-2.3	0.5	3.2	1.8
	H_2dapsox	x[127]	I	0	0	0	0
			V	1.3	4.0	8.1	6.5
Zn^{II}	dapsox		I	0	0	0	0
			V	14.6	4.4	6.4	6.9
	Hdapsox		I	0	0	0	0
			V	3.6	-2.0	3.4	2.1
	H_2dapsox	x[122]	I	0	0	0	0
			V	-0.4	-4.7	1.0	0.5

Table 4-11 Relative energies of isomeric structures depicted in Figure 4-5, compared to the most stable one; Calculations were performed on the LDA, OPBE//LDA, SSB-D//LDA and S12g//LDA level of theory; Relative energies are given in kcal•mol-1.

CM	Ligand	Vxc	I	II	III	V	VI	VII	VIII	IX	X	XI	XII
Fe^{III}	dapsox	LDA	0	-0.3	1.2	-2.1	-1.1	3.1	12.4	6.2	11.5	24.2	61.2
		OPB	0	-1.0	0.8	5.2	6.4	12.1	29.4	12.4	22.4	32.9	76.9
		SSB-	0	-1.0	0.6	7.2	5.3	8.5	22.8	9.2	16.1	26.1	61.9
		S12G	0	-0.8	0.9	6.6	5.8	9.3	22.7	9.2	17.6	25.2	64.7
	Hdapsox	LDA	0	-1.6	11.7	2.3	-2.0	6.4	14.1	3.6	7.4	30.6	71.4
		OPB	0	-2.0	10.1	4.9	3.9	14.1	29.5	8.5	17.7	34.4	87.5
		SSB-	0	-2.3	9.6	8.2	3.6	8.6	22.1	4.9	11.1	26.8	71.5
		S12G	0	-1.4	10.6	6.5	3.2	10.2	22.0	5.4	12.2	28.4	76.1
	H_2dapsox	LDA	0	0.0	2.0	4.2	-	5.5	20.9	3.1	7.1	35.2	87.7
		OPB	0	6.0	13.4	8.9	-	11.1	31.6	7.0	14.9	42.6	102.8
		SSB-	0	3.8	8.7	11.2	-	5.0	19.7	2.2	6.8	35.4	84.8
		S12G	0	4.4	9.8	10.6	-	7.3	22.2	3.4	8.5	35.4	91.0
Fe^{II}	dapsox	LDA	0	9.4	2.4	1.7	6.7	4.2	12.2	6.5	14.5	15.3	46.6
		OPB	0	3.1	2.0	0.8	6.9	13.1	26.9	11.8	22.9	24.5	56.9
		SSB-	0	0.3	1.4	4.4	5.2	6.8	18.8	8.3	15.7	14.9	40.0
		S12G	0	3.1	2.1	3.7	6.0	9.4	19.8	8.5	16.8	16.3	44.3
	Hdapsox	LDA	0	-1.4	14.4	0.1	-0.5	3.0	17.2	3.6	9.6	16.6	59.4
		OPB	0	-1.4	11.6	3.6	1.8	11.8	29.7	8.2	18.4	22.6	68.6
		SSB-	0	-1.8	11	6.6	0.8	7.9	22.2	5.0	12.0	16.4	53.2
		S12G	0	-1.7	12.4	5.3	1.3	8.3	23.2	5.3	12.6	16.8	56.9
	H_2dapsox	LDA	0	4.1	21.2	3.1	-	4.9	11.5	2.1	7.5	22.6	66.4
		OPB	0	16.4	15.8	4.2	-	12.4	17.9	8.5	16.4	31.2	80.2
		SSB-	0	7.5	16.1	7.8	-	7.9	16.8	5.7	9.9	24.7	64.0
		S12G	0	7.5	17.9	6.9	-	8.4	16.6	6.0	10.7	25.4	67.7
Mn^{II}	dapsox	LDA	0	2.8	3.8	1.7	-0.1	1.3	8.6	5.6	13.2	24.0	41.3
		OPB	0	0.9	2.3	3.5	13.6	12.9	23.6	10.4	21.6	27.4	52.1
		SSB-	0	0.2	1.5	5.0	10.5	7.5	14.4	6.4	13.3	18.4	34.4
		S12G	0	0.8	2.3	5.1	9.8	8.9	16.0	7.8	15.7	21.1	39.5
	Hdapsox	LDA	0	0.5	14.5	0.1	-4.3	4.0	13.1	6.2	8.0	24.1	52.6
		OPB	0	2.1	11.7	1.9	8.4	12.4	25.6	9.1	15.5	24.8	62.4
		SSB-	0	1.9	11.3	4.8	6.7	7.1	17.0	6.1	8.7	18.2	46.0
		S12G	0	1.9	12.2	4.0	5.1	8.6	18.2	6.4	10.2	19.5	50.6
	H_2dapsox	LDA	0	4.1	23.8	-0.7	-	5.4	12.0	2.1	6.5	22.0	61.6
		OPB	0	11.0	19.3	5.4	-	13.3	28.7	9.4	16.1	30.6	77.0
		SSB-	0	7.5	18.7	7.9	-	7.4	19.8	5.0	9.1	23.4	59.5
		S12G	0	8.4	19.7	7.8	-	8.8	20.9	6.1	10.1	24.7	64.7
Co^{II}	dapsox	LDA	0	0.4	3.4	-0.2	-1.1	3.6	25.7	8.2	14.0	25.2	44.0
		OPB	0	0.5	2.6	0.2	14.0	13.2	30.4	13.0	24.5	28.5	55.2
		SSB-	0	0.9	2.2	0.6	16.5	10.4	22.5	10.4	16.5	19.2	39.4
		S12G	0	1.0	2.7	0.6	13.8	10.5	23.6	10.3	17.5	21.6	42.8
	Hdapso	LDA	0	-3.7	11.8	-2.3	-	1.3	18.5	2.4	6.6	19.8	50.6

	x	OPB	0	-3.0	9.5	0.5	2.4	12.6	33.2	8.5	17.2	24.2	63.5
		SSB-	0	-4.2	8.4	3.2	3.9	7.9	23.9	4.4	9.9	15.6	46.7
		S12G	0	-3.5	9.7	1.8	2.1	8.3	25.6	5.0	10.8	17.7	51.5
	H_2daps ox	LDA	0	10.4	22.6	1.3	-	5.2	25.1	-2.4	8.3	23.8	61.3
		OPB	0	9.8	17.7	4.0	-	13.2	39.0	6.3	17.9	31.4	76.6
		SSB-	0	7.6	17.4	8.1	-	9.2	28.3	5.3	10.8	24.5	59.1
		S12G	0	7.8	18.4	6.5	-	9.3	30.5	5.9	11.6	25.5	64.1
Zn^{II}	dapsox	LDA	0	0.8	2.7	14.6	16.0	15.1	27.9	17.2	23.1	32.4	53.9
		OPB	0	0.8	2.5	4.4	7.0	13.0	30.0	11.3	19.0	24.9	53.2
		SSB-	0	0.5	1.7	6.4	5.4	9.7	22.4	11.3	16.0	19.6	38.1
		S12G	0	0.7	2.1	6.9	6.9	10.8	22.4	11.6	16.6	21.2	41.8
	Hdapso x	LDA	0	-0.5	16.1	3.6	5.9	13.5	28.6	15.1	19.8	30.5	56.9
		OPB	0	-0.6	12.0	-2.0	27.1	1.2	29.4	9.5	14.2	24.7	57.4
		SSB-	0	-1.4	10.8	3.4	25.6	9.3	20.4	8.8	12.4	19.7	42.5
		S12G	0	-0.9	12.1	2.1	26.0	10.6	23.2	9.4	12.8	21.1	46.3
	H_2daps ox	LDA	0	14.9	5.3	-0.4	-	15.3	28.1	8.4	19.3	36.8	63.6
		OPB	0	10.7	3.4	-4.7	-	12.2	23.0	2.5	14.2	28.3	63.4
		SSB-	0	9.9	3.5	1.0	-	8.3	19.5	2.2	8.3	24.3	49.3
		S12G	0	11.4	3.5	0.5	-	10.3	20.5	3.3	10.6	26.0	53.8

The differences in energy for the isomers **I** and **V** are observed within range of a few kcal/mol (see Table 4-10), and in some isolated cases the order of stability depends on the choice of XC functional. The largest differences are found between LDA on one hand, and OPBE//LDA, SSB-D//LDA and S12g//LDA on the other. However, it is well known that LDA has a very poor performance considering energies of d-block metal (TM) complexes,[146] in contrast to the geometries and vibrational frequencies of coordination compounds for which it does give accurate results.[142-145] Therefore, the relative energies obtained at LDA will not be further discussed. With the LDA/GGA DFAs isomer **I** is always found to be the most stable one, irrespective of the charge on the ligand and the nature of the central metal ion, except in the case of $[Zn^{II}(Hdapsox^{-})(H_2O)_2]^{+}$ and $[Zn^{II}(H_2dapsox)(H_2O)_2]^{+2}$. For these two cases OPBE//LDA predicts OCF-7 (isomer **V**) to be the most stable isomeric structure, while the differences obtained with SSB-D//LDA and S12g//LDA are also quite smaller than for the other d-block metal systems. To be assured about results we performed OPBE geometry optimization and the same conclusions have been drawn (Table 4-12).

Table 4-12 Relative energies (kcal•mol-1) of isomers I and V for different 3d-metal ions in high spin; Calculations were performed on the OPBE, OPBE/SSB-D and OPBE/S12G level of theory

3d-metal	Ligand	Isomer	OPBE	OPBE/SSB-	OPBE/S12g
Mn^{II}	H_2dapsox	I	0	0	0
		V	8.99	12.06	10.9
	Hdapsox	I	0	0	0
		V	6.30	8.55	7.68
	dapsox	I	0	0	0
		V	6.29	9.16	8.09
Fe^{III}	H_2dapsox	I	0	0	0
		V	11.42	12.49	11.75
	Hdapsox	I	0	0	0
		V	4.00	4.72	4.04
	dapsox	I	0	0	0
		V	0.60	1.19	0.02
Fe^{II}	H_2dapsox	I	0	0	0
		V^{xix}	-	-	-
	Hdapsox	I	0	0	0
		V	7.03	9.04	7.99
	dapsox	I	0	0	0
		V	0.88	3.48	2.55
Co^{II}	H_2dapsox	I	0	0	0
		V	4.63	5.81	5.58
	Hdapsox	I	0	0	0
		V	1.22	2.73	2.31
	dapsox	I	0	0	0
		V	1.23	3.96	3.2
Zn^{II}	H_2dapsox	I	0	0	0
		V	-1.64	2.65	1.56
	Hdapsox	I	0	0	0
		V	1.31	5.88	3.88
	dapsox	I	0	0	0
		V	1.87	3.97	5.38

While with Mn^{II}, Fe^{III}, Fe^{II}, Co^{II} and Zn^{II} hepta-coordination is always found to be the stable one, attempts to model hepta-coordinated structures with Ni^{II} and $H_n$dapsox ligands failed, resulting in an OC-6 geometry, even if we started from PBPY-7 environment. The calculated geometry resembles the OCF-7 coordination, but one oxygen that lies on the face of the octahedron is sufficiently far away from Ni^{II} (3.16 Å)

that it cannot be considered as a bond. This is in agreement with experimental findings, which hinted at the infeasibility of obtaining PBPY-7 structures for Ni^{II} with the any for of the dapsox ligand. In fact, the octahedral geometry (OC-6) in the Ni^{II} complex can be explained as the result of a pseudo Jahn-Teller effect operating in on the PBPY-7 environment, which leads to a structural distortion.[121] The results obtained for the two isomers of Ni^{II} are shown in Table 4-13; they differ in the size of chelate ring upon coordination and resemble isomers **V** and **VI** of the hepta-coordinated environment from Figure 4-5 (differing from these because of the hexa-coordination, *vide supra*), respectively. Isomer **VI*** is the most stable one with both $Hdapsox^-$ and $dapsox^{2-}$, while isomer **VI*** cannot be formed with H_2dapsox.

Table 4-13 Relative energies (kcal·mol^{-1}) of isomers V and VI* for Ni^{II} complexes*[a]

TM ion	Ligand	Isomer	LDA	OPBE//LDA	SSB-	LDA/S21G
Ni^{II}	dapsox	V*	0	0	0	0
		VI*	-4.9	-0.4	-6.4	-4.5
	Hdapsox	V*	0	0	0	0
		VI*	-9.1	-3.2	-7.7	-6.6

a) the coordinations V* and VI* resemble those of isomer V and VI shown in Figure 4-5(see text)

As expected, structures with the H_2dapsox ligand are less distorted in comparison with its mono- and dianionic analogues, because of weaker intermolecular H-bonds, Figure 4-7. In all $[M(dapsox^{2-})(H_2O)_2]^q$ complexes water molecules are oriented in order to form strong intermolecular H-bonds, while in the complexes with H_2dapsox H-bonds are much weaker due to the different orientation of water ligands.

4.2.1.2. Spin state energies of seven coordinate complexes

The effect of (de)protonation of the coordinated acylhydrazone polydentate ligands on the ligand field strength and spin state of 3d-block metal ions, and thus on the stability of the PBPY-7 geometry, was only empirically approached in the literature,[121] although

[xix] OPBE failed to optimize this isomer; Starting from different initial geometries, the optimization always resulted in Isomer I

the high-spin state was experimentally found to be the ground state in all investigated complexes.[122-127] As a result of our interest in both the coordination chemistry of 2,6-diacetylpyridine hydrazones and 3d-metal hepta-coordinate complexes,[121-130] and an accurate theoretical description of spin state energetics,[45,131,142,147] here we performed DFT calculations for a systematic investigation of the spin state splitting in these complexes. We studied $[MH_ndapsox(H_2O)_2]^q$ (n=0, 1, 2) and M= Mn^{II}, Fe^{III}, Fe^{II}, Co^{II} and Ni^{II} with the aim to examine how the degree of (de)protonation and the nature of central metal ion affects spin state preferences.

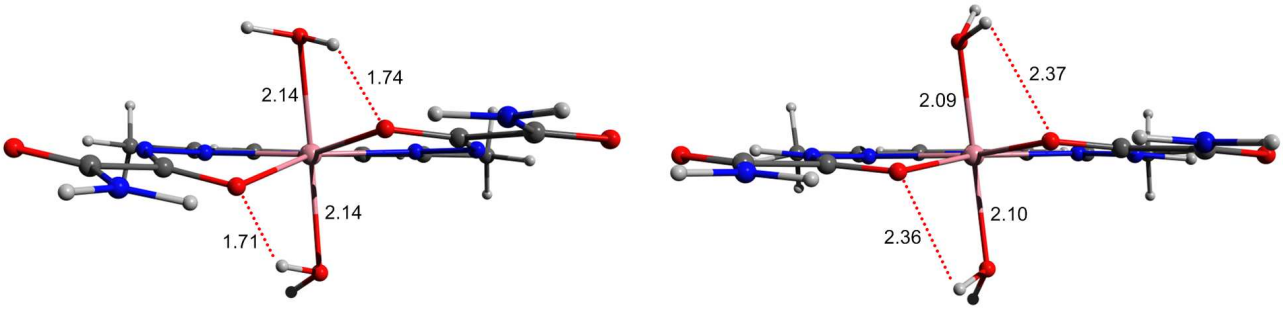

Figure 4-7 Structures of $[Co^{II}(dapsox^{2-})(H_2O)_2]$ (left) and $[Co^{II}(H_2dapsox)(H_2O)_2]^{2+}$ (right) with depicted bonds. Bond lenghts are given in Å.

For the accurate description of spin states in these complicated systems, we decided to use our favorites OPBE, SSB-D and S12g.[45,47,131,142] Our theoretical findings, which is in accordance with experimental data, suggest that the high spin configuration is favored for all investigated complexes in PBPY-7 environment with OPBE//LDA, SSB-D//LDA and S12g//LDA, except for $[Co^{II}(Hdapsox^{-})(H_2O)_2]^{+}$ and $[Co^{II}(dapsox^{2-})(H_2O)_2]$, where OPBE//LDA and S12g//LDA predict low spin, while SSB-D//LDA functional was able to capture high spin as the ground state (see Table 4-14 and Table 4-15). Note that these are electronic energies, without zero-point energies or entropy effects, both of which favor high-spin states.[49] The same results are obtained when we performed OPBE geometry optimizations (Table 4-15).

Table 4-14 Relative spin-state energies (kcal·mol^{-1}) for some metal complexes with $H_n$dapsox ligands

V_{XC}		OPBE//LDA			SSB-D//LDA			S12G//LDA		
Complex		HS	IS	LS	HS	IS	LS	HS	IS	LS
Mn^{II}	H_2dapsox	0	33.1	45.2	0	37.7	52.7	0	30.2	42.3
	Hdapsox	0	12.6	25.9	0	16.9	33.5	0	10.7	23.6
	dapsox	0	12.9	21.1	0	19.3	28.9	0	12.9	19.0
Fe^{III}	H_2dapsox	0	23.8	17.4	0	23.7	29.3	0	22.3	20.8
	Hdapsox	0	13.4	14.4	0	20.5	25.6	0	15.8	17.5
	dapsox	0	12.0	12.4	0	18.9	23.8	0	14.1	15.5
Fe^{II}	H_2dapsox	0	32.7	17.8	0	34.8	29.5	0	32.0	22.2
	Hdapsox	0	8.6	12.0	0	16.6	24.8	0	12.1	17.4
	dapsox	0	9.6	7.5	0	16.9	17.7	0	12.5	11.4
Co^{II}	H_2dapsox	0	-	2.1	0	-	15.1	0	-	8.4
	Hdapsox	0	-	-8.1	0	-	1.9	0	-	-3.8
	dapsox	0	-	-7.8	0	-	2.5	0	-	-3.1

Table 4-15 Relative spin-state energies (kcal•mol-1) for some metal complexes with Hndapsox ligands; Single point calculations were performed using OPBE optimized geometries with SSB-D, and S12G functional

V_{XC}		OPBE			OPBE/SSB-D			OPBE/S12g		
Spin State		H	IS	LS	H	IS	LS	H	IS	LS
Mn^{II}	$[Mn^{II}(H_2dapsox)(H_2O)_2]^{2}$	0	31.0	48.8	0	34.	50.	0	27.	41.
	$[Mn^{II}(Hdapsox)\ (H_2O)_2]^{+}$	0	16.7	32.6	0	18.	34.	0	11.	25.
	$[Mn^{II}(dapsox)\ (H_2O)_2]$	0	12.7	26.5	0	15.	31.	0	7.6	21.
Fe^{III}	$[Fe^{III}(H_2dapsox)(H_2O)_2]^{3}$	0	28.2	19.2	0	27.	30.	0	17.	22.
	$[Fe^{III}(Hdapsox)$	0	11.0	16.7	0	18.	25.	0	13.	17.
	$[Fe^{III}\ (dapsox)\ (H_2O)_2]^{+}$	0	9.7	14.6	0	18.	25.	0	12.	16.
Fe^{II}	$[Fe^{II}(H_2dapsox)(H_2O)_2]^{2+}$	0	32.8	21.6	0	32.	30.	0	29.	22.
	$[Fe^{II}(Hdapsox)\ (H_2O)_2]^{+}$	0	11.7	18.4	0	19.	29.	0	10.	20.
	$[Fe^{II}(dapsox)\ (H_2O)_2]$	0	9.4	9.0	0	17.	20.	0	8.8	11.
Co^{II}	$[Co^{II}(H_2dapsox)(H_2O)_2]^{2}$	0	-	5.9	0	-	15.	0	-	7.7
	$[Co^{II}(Hdapsox)(H_2O)_2]^{+}$	0	-	-	0	-	5.2	0	-	-2.7
	$[Co^{II}(dapsox)\ (H_2O)_2]$	0	-	-	0	-	4.4	0	-	-3.0

[xx] These structures could not be optimized with OPBE, because apical water tends to dissociate. We obtained reasonable geometries with PBE-D, that can take dispersion interactions into account more adequately, and subsequently performed single point OPBE, SSB-D and S12g calculations.

If the nature of the central metal ions and the degree of deprotonation do not affect the order of the isomers, this cannot be said for the spin states. Interestingly, during the optimization of low spin states, structures distort from a PBPY-7 geometry toward the isomeric structure OCF-7 (or in some cases even to OC-6) which becomes the global minimum on the potential energy surface (PES). This is an interesting example that spin state can change the relative stability of the isomers, since a change of spin state is usually accompanied only with changes in bond lengths.[148-151] Again, Ni^{II} is a special case, where the triplet state is in an octahedral environment, while the singlet state distorts toward square pyramidal geometry, corroborating experimental observations.[129]

A closer look at the molecular orbitals (see Figure 4-8 and Figure 4-9), helps to explain our findings for the different coordination modes. In all heptacoordinated molecules, molecular orbitals that originated from d atomic orbitals are quite similar (see Figure 4-8). The lowest two molecular orbitals are π-antibonding with respect to the oxygen atom of the $dapsox^{2-}$ ligand. The third MO is clearly σ-antibonding, with significant contribution of oxygen *p* orbitals, while the highest two MOs are non-bonding with respect to the oxygen atoms. According to the obtained results, the high spin configuration will always favor the formation of a bond between the central metal and the oxygen atom in the equatorial plane, except for Ni^{II} complexes. Complexes with a d^5 high spin electronic configuration, i.e. $[Fe^{III}(H_2dapsox)(H_2O)_2]^{3+}$ and $[Mn^{II}(H_2dapsox)(H_2O)_2]^{2+}$, possess one unpaired electron in each MO. In contrast, in the low spin state one unpaired electron is placed in the σ-antibonding MO, but the π-antibonding orbitals are now fully occupied, which leads to the rupture of the $M\text{-}O_{eq}$ bond. Something similar happens for the $[Fe^{II}(H_2dapsox)(H_2O)_2]^{2+}$ complex with a d^6 electronic configuration which has four unpaired electrons in the high spin state. These unpaired electrons are placed in the highest-lying π-antibonding, in a σ-antibonding and two non-bonding MOs. Instead in the low spin state two π-antibonding and the σ-antibonding MO are doubly occupied, hence the breaking of $M\text{-}O_{eq}$ bond is a consequence of both π-antibonding and σ-antibonding unfavorable interactions. In the case of $[Co^{II}(H_2dapsox)(H_2O)_2]^{2+}$ both high spin and low spin states have doubly occupied π-antibonding MOs (Figure 4-9), hence the difference in geometry between the two states results almost completely from σ-antibonding interactions. Finally, $[Ni^{II}(H_2dapsox)(H_2O)_2]^{2+}$ has doubly occupied π-antibonding and σ-antibonding MOs in

high spin and low spin states, thus, in both cases, PBPY-7 cannot be preferred geometry (as is indeed observed in our calculations and in previous experiments).

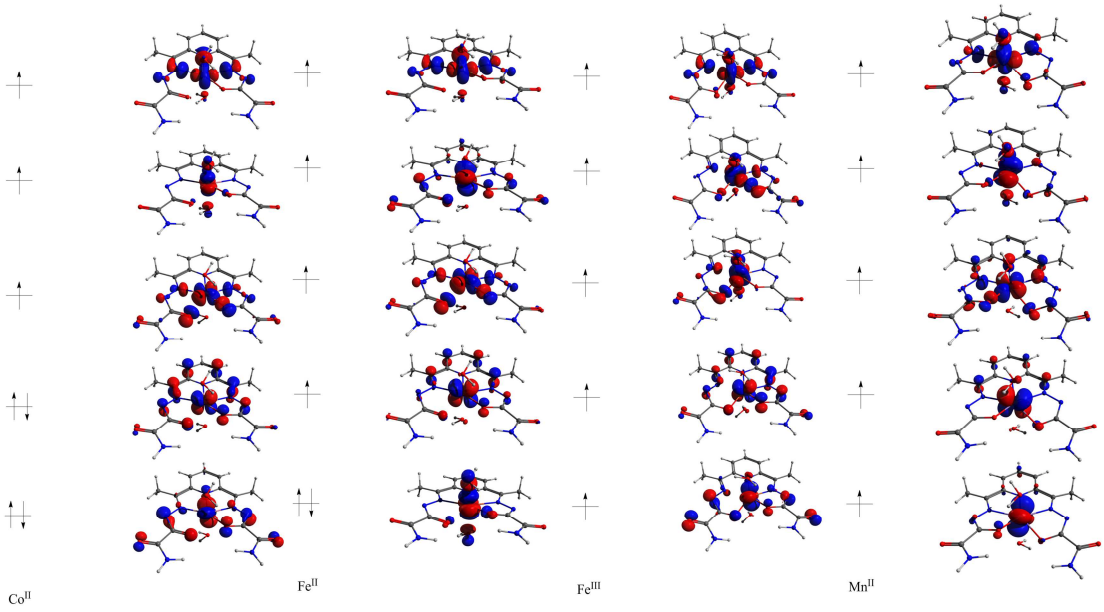

Figure 4-8 Molecular orbitals for [M(dapsox)(H$_2$O)$_2$]q, where q=0,1 and M = Fe^{II}, Fe^{III}, Mn^{II} and Co^{II}.

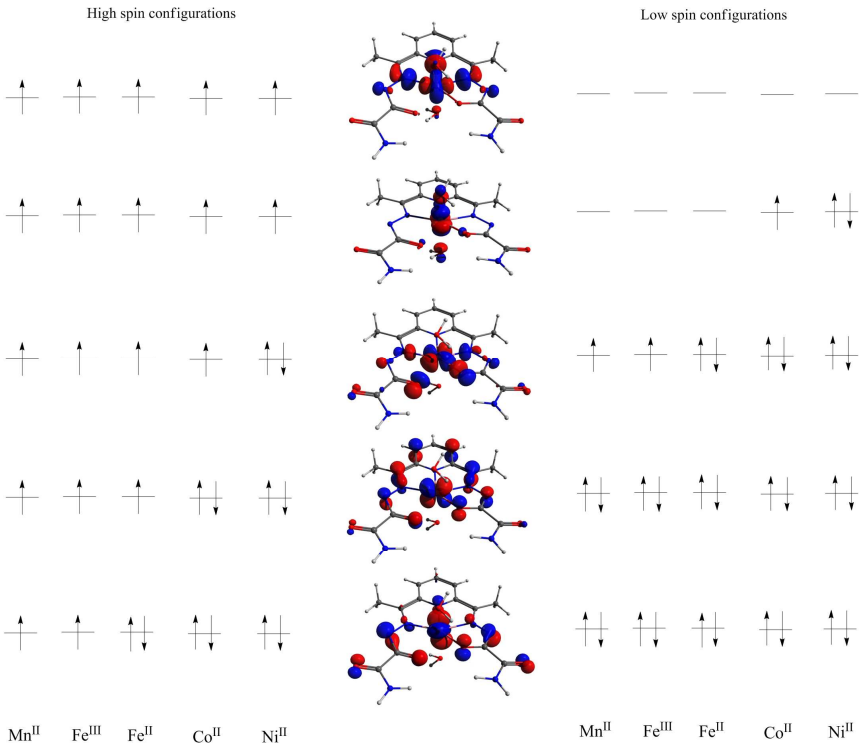

Figure 4-9 Representation of molecular orbitals for [Co^{II}(dapsox)(H$_2$O)$_2$].

4.2.1.3. Five coordinate complexes

Since $H_n$dapsox has many potential ligator atoms, it can be coordinated not only as pentadentate, but also as tetradentate ligand, forming complexes with coordination number five. It is well known that complexes with coordination number five can form trigonal bipyramidal (TBPY-5) and SPY-5 geometries. Bearing in mind the rigidity of the mono- and dianionic form of the ligand upon coordination in the equatorial plane, the formation of the TBPY-5 isomer is not possible and our discussion will be limited to SPY-5 complexes. Furthermore, because of the presence of the two additional protons at the nitrogens, SPY-5 cannot be formed with H_2dapsox. To the best of our knowledge, only $[Cu^{II}(dapsox^{2-})H_2O]$ and $[Cu^{II}(Hdapsox^{-})H_2O]^+$ complexes were crystallographically determined,[126,130] while $[Fe^{III}(dapsox^{2-})Cl]$ was synthesized but not characterized crystallographically.[128] The two crystal structures of the copper complexes have different conformations, i.e. the uncoordinated pending arm of the ligand lays respectively above and below the equatorial plane in $[Cu^{II}(dapsox^{2-})H_2O]$ and $[Cu^{II}(Hdapsox^{-})H_2O]^+$. Interestingly, previous experimental work had shown that the intermediate spin state (S=3/2) is the electronic ground state for the SPY-5 complex of $[Fe^{III}(dapsox^{2-})Cl]$.[128] In order to study this intriguing spin ground-state in more detail, we performed DFT calculations for $[M(H_n dapsox)L]^q$, where M = Fe^{III}, Cu^{II}, and L=H_2O, Cl^-. The DFT optimized geometries of $[Cu^{II}(dapsox^{2-})H_2O]$ and $[Cu^{II}(Hdapsox^{-})H_2O]^+$ are in excellent agreement with the X-ray structures (see Figure 4-10). Selected average bond lengths and valence angles for DFT optimized and X-ray structures are tabulated in original reference.[141]

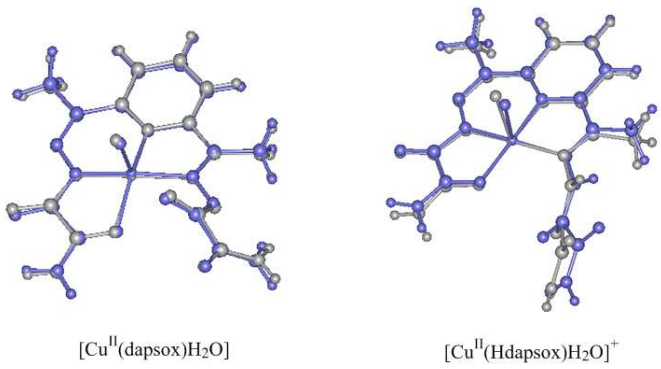

Figure 4-10 Superposition of available experimental X-ray (gray) with LDA optimized (light blue) structures of $[Cu^{II}(dapsox^{2-})H_2O]$ and $[Cu^{II}(Hdapsox^{-})H_2O]^+$.

4.2.1.4. Spin state energies of five coordinate complexes

The only synthesized penta-coordinated complex with $H_n$dapsox ligands that has the possibility of multiple spin states is [Fe^{III}($dapsox^{2-}$)Cl]. As already mentioned above, this complex has been well characterized, and the measurement of its magnetic momentum with EPR spectra at different temperatures clearly indicated a rarely observed intermediate spin state.[128] Motivated by this interesting result, we have performed DFT calculations for obtaining the spin state splitting in [Fe^{III}($H_n$dapsox)L] with n=0,1, L=H_2O,Cl^-, with the aim to examine how the degree of deprotonation and the nature of apical ligand affects spin state preferences. The results are shown in Table 4-16.

In the case of [Fe^{III}($dapsox^{2-}$)Cl], all three DFAs (OPBE, SSB-D and S12g) indicated correctly the intermediate spin ground-state, with a substantial spin-state splitting to either the low or high spin state. These results are in excellent agreement with the intriguing experimental results.[128] In contrast, for the $Hdapsox^-$ ligand (not isolated experimentally) a high-spin state is predicted by all methods, but the splitting with the intermediate spin is greatly reduced (to ca. 1-6 kcal·mol^{-1}, depending on the functional and whether solvent effects have been taken into account). Hence, in the continuous compromise between larger orbital splittings (preferring low-spin) and enhanced exchange interactions[152] (favoring high-spin), in this latter case the exchange interactions are more important.

Examination of complexes with water in the apical position, [Fe^{III}($dapsox^{2-}$)H_2O]$^+$ and [Fe^{III}($Hdapsox^-$)H_2O]$^{2+}$, showed that the intermediate spin is favored by OPBE//LDA and S12g//LDA, while SSB-D//LDA predicts a high spin configuration with Hdapsox but intermediate spin with $dapsox^{2-}$ (see Table 4-16). It is worth mentioning that in the case of [Fe^{III}($dapsox^{2-}$)H_2O]$^+$ all three methods predict that the high and intermediate spin state are very close in energy, thereby indicating that it can be considered a potential candidate for spin-crossover systems. Neither including the perturbation of environment with COSMO (

Table 4-17), nor optimization of geometry at OPBE level of theory (Table 4-18), did not affect previous conclusions.

Table 4-16 Relative spin-state energies (kcal·mol^{-1}) for penta-coordinated Fe^{III} with Hdapsox and dapsox ligands

M=Fe^{III}	OPBE//LDA			SSB-D//LDA			S12G//LDA		
Ligands	HS	IS	HS	HS	IS	LS	HS	IS	LS
(dapsox)	0	-9.7	7.6	0	-6.6	11.1	0	-11.9	3.3
(Hdapsox)	0	2.6	13.6	0	5.6	19.8	0	2.2	14.0
(dapsox)	0	-2.2	3.7	0	1.8	11.9	0	-3.4	5.1
(Hdapsox)	0	-6.3	8.4	0	-4.9	12.3	0	-7.8	6.2

Table 4-17 Relative energetics of available spin states for penta-coordinated Fe^{III} complexes with mono- and di-anionic forms of H_2dapsox. Single point calculations were performed using optimized geometries with SSB-D, OPBE and S12G functional, as well as with included solvent. The energy is given in kcal•mol^{-1}

V_{XC}	LDA/ OPBE /			SSB-D//LDA /			S12G//LDA /		
Spin State	**HS**	**IS**	**LS**	**HS**	**IS**	**LS**	**HS**	**IS**	**LS**
[Fe^{III}(dapsox)Cl]	0	-10.5	8.1	0	-7.4	11.3	0	-12.7	3.5
[Fe^{III}(Hdapsox)Cl]$^{+}$	0	0.6	11.7	0	2.7	18.2	0	-0.4	12.6
[Fe^{III}(dapsox)H_2O]$^{+}$	0	-1.5	4.8	0	1.5	10.7	0	-3.8	3.9
[Fe^{III}(Hdapsox)H_2O]$^{2+}$	0	-6.4	8.8	0	-4.9	12.9	0	-7.9	6.6

Table 4-18 Relative spin-state energies (kcal•mol^{-1}) for penta-coordinated Fe^{III} with Hdapsox and dapsox ligands; Calculations were performed on the OPBE, OPBE/SSB-D and OPBE/S12G level of theory

V_{XC}	OPBE			SSB-D//LDA			S12G//LDA		
Spin State	HS	IS	LS	HS	IS	LS	HS	IS	LS
[Fe^{III}(dapsox)Cl]	0	-	8.4	0	-	15.3	0	-	8.2
[Fe^{III}(Hdapsox)Cl]$^{+}$	0	0.6	13.3	0	5.9	22.3	0	0.6	14.8
[Fe^{III}(dapsox)H_2O]$^{+}$	0	-	4.1	0	-	10.3	0	-	4.2
[Fe^{III}(Hdapsox)H_2O]$^{2+}$	0	-	9.5	0	-	15.9	0	-	9.2

4.2.2. Conclusion

Electronic structure and stereochemistry of acylhydrazone complexes with Mn^{II}, Fe^{III}, Fe^{II}, Co^{II}, Ni^{II}, Cu^{II} and Zn^{II} were studied by means of density functional theory. Our theoretical investigations have shown that the geometry of isomer **I**, in the high spin configuration, is in excellent agreement with X-ray determined structures; moreover, this isomer is found to be the most stable one, irrespective of the nature of the central metal or charge of the ligand. The energy ordering for the other isomers was found to be clearly influenced by the type of donor atoms and the size of chelate rings formed upon coordination.

A different situation is observed when we consider low spin configurations of the central metal ions. Due to the different population of bonding/anti-bonding orbitals, geometry optimization of an initial PBPY-7 coordination distorts toward an OCF-7 geometry, which explains why only high-spin states are detected in a PBPY-7 environment. Furthermore, our calculations explain why Ni^{II} is not forming hepta-coordinated complexes with these ligands: an octahedral polyhedral environment is found to be the most stable one, for high spin, even though optimization was started from different coordination number. However, Ni^{II} complexes in a singlet state distort towards a SPY-5 geometry, corroborating experimental observations. This is an interesting example that the spin state can change completely the geometry of the stable species, even though usually the change of spin state is accompanied only with change of bond lengths.

The intriguing experimental observation that $[Fe^{III}(dapsox^{2-})Cl]$ is in intermediate spin, has been confirmed by our DFT calculations, with the OPBE, SSB-D or S12g DFAs. This proves that DFT calculation with either one of these DFAs is the method of choice for studying spin state diversity.

4.2.3. Computational details

The calculations using the unrestricted formalism have been performed with the ADF program package,[42,93,94] versions 2012.01/2013.01. Molecular orbitals were expanded in an uncontracted set of Slater type orbitals (STOs),[95] of triple-ζ quality containing diffuse

functions plus one set of polarization functions (TZP). Geometry optimizations of all investigated structures were performed with the local density approximation (LDA).[28,37,102] Geometry optimization has also been performed using non-local gradient (GGA) corrections consisting of OPTX[103] for the exchange and PBE[83] functional for correlation (OPBE[48]) on a carefully selected subset of investigated compounds. Default integration and gradient convergence criterions were used. Subsequently, single-point energy calculations were performed on the LDA and OPBE optimized geometries using OPBE (for LDA) and dispersion corrected functional by Swart-Solà-Bickelhaupt, SSB-D[39,153], and S12g.[47] In order to check the possible influence of an environment, we also performed single point calculations with a dielectric continuum model (COSMO)[97-99] (using water as a solvent) as implemented in ADF,[154,155] with the OPBE//LDA, SSB-D//LDA and S12g//LDA DFAs. The examined heptacoordinated complexes are described by the general formula $[M(H_ndapsox)(H_2O)_2]^q$, where q=0,1,2,3, n=0,1,2 and M=Mn^{II}, Fe^{II}/Fe^{III}, Co^{II}, Ni^{II} and Zn^{II}, while penta-coordinated complexes are denoted by $[M(H_ndapsox)L]^q$, q=-1,0,1,2, n=0,1 , L=H_2O,Cl and M=Fe^{III} and Cu^{II}. For all d-block metal complexes the geometry optimization is carried out for all accessible spin states separately: S=1/2,3/2,5/2 for Mn^{II}, S=1/2,3/2,5/2 for Fe^{III}, S=0,1,2 for Fe^{II}, S=1/2, 3/2 for Co^{II}, S=0,1 for Ni^{II}, S=1/2 for Cu^{II} and S=0 for Zn^{II}.

4.3. Polypyrazolylborato (scorpionate) complexes

4.3.1. Short introduction

Polypyrazolylborate anions with general formula $[R_nB(pz)_{4-n}]^-$ (*n*=0, 1 or 2; pz is pyrazol-1-yl group and R is H, alkyl or aryl) represent a very important and versatile class of ligands.[156-158] In the case of R=H and *n*=1, the ligand has the formula $[HB(pz)_3]^-$ and is usually abbreviated as Tp^-. Popularly those ligands are called *scorpionates*, which suggests how the ligand binds to metal ions (see Figure 4-11).[156] *Scorpionate* complexes are very interesting from a fundamental point of view and practically applicable in technology and medicine.[132,159-165]

The Tp^- ligands are suitable to bind a variety of metals,[132,159-165] although most

of the research has been focused on the first-row transition metals[161,166-169], and can generally act as bidentate or tridentate ligands.[161] In the latter coordination mode they are particulary interesting since it is possible to synthesize simple models for active sites of bio-organic macromolecules such as enzymes.[170-172]

The N_3 donor set of the *scorpionate* ligand mimics the tris-histidine motif found in several metalloenzymes.[173,174] Furthermore, complexes formed with two Tp^- ligands[161,175-178] have been recognized as spin-crossover (SCO) molecules.[132,159-165] Substituents placed at pyrazolyl rings have significant impact on SCO behaviour, since they can change electronic and steric features, but this area of research has not been explored enough.[132,159]

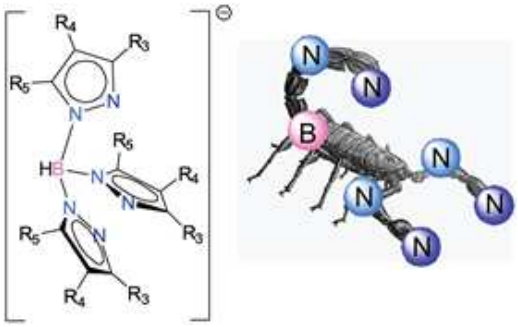

Figure 4-11 General structure of the substituated $[HB(pz)_3]^-$ chelate ligand (left) and analogy to the scorpion pincers (right).

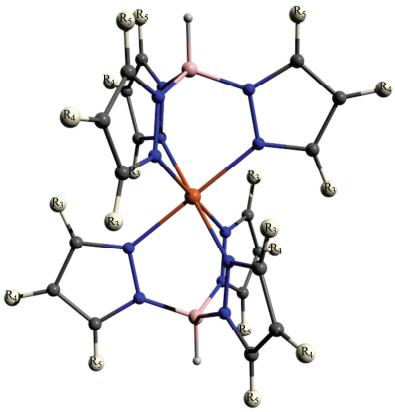

Figure 4-12 Coordination by two $[HB(pz)_3]^-$ ligands.

In this sub-chapter we report a systematic investigation of the spin state splittings for several $[M^x(Tp)_2]^q$ complexes (M^x=Mn^{II}, Fe^{II}, Co^{II}; Cr^{III}, Mn^{III}, Fe^{III}, Co^{III}; Mn^{IV}; q=0,

1+, 2+) (see Figure 4-12). For this we used DFT, with the OPBE, SSB-D and S12g DFAs, and compare the results with experimental values available in the literature. For these complexes, two tridentately coordinated Tp^- ligands in general, form a trigonally distorted octahedron, belonging to the D_{3d} point group. However, due to the electronic configuration, and depending on the spin state, some of the complexes exhibit Jahn-Teller (JT) distortions.[142,167] Therefore, the distortion from D_{3d} to C_{2h}, the consequences of this distortion on spin state preferences, and the JT parameters (describing the Adiabatic Potential Energy Surface (APES) of JT active species), were determined by means of the Multi-Determinant-DFT (MD-DFT) method. Furthermore, we have also examined the impact of different substituents at the pyrazolyl rings on spin-state splittings in order to establish (and in particular: obtain a deeper understanding of) the factors that enable Tp^- ligands to modulate spin states preferences, which is of the utmost importance for its practical application.

4.3.1.1. Spin-state energies of scorpionate transition-metal complexes

Let us start by analyzing the spin state splittings for the non-substituted $[M^x(Tp)_2]^q$ complexes in the highest possible symmetry (D_{3d}), in a pseudo-octahedral environment. The influence of the JT distortion on spin state energetic will be discussed afterwards.

The results obtained with different DFAs are summarized in Table 4-19, which shows the spin-state energies relative to the high spin state. They are overall consistent and in excellent agreement with experimental data. This good behaviour reinforces the notion that these DFAs (OPBE, SSB-D, S12g) can be trusted for providing reliable spin-state energies.[45,47,142,179] As noted before, LDA functional is very poor for spin state energies.[142] Nevertheless, if single point OPBE, SSB-D and S12g DFT calculations were performed on LDA geometries, the results are very satisfactory (compare the OPBE/OPBE and OPBE/LDA results in Table 4-19). In comparison with OPBE and SSB-D functional, S12g slightly favours low spin states, although this does not affect the prediction of ground-states for the *scorpionate* complexes.

Table 4-19 Spin state energies (TZP basis, kcal·mol^{-1}) relative to the high-spin state for $[M^x(Tp)_2]^q$ complexes using D_{3d} symmetry

	spin	OPBE	OPBE/LDA	SSB-D/LDA	S12g/LDA	Exp.
M^{II} complexes (q=0)						
Mn (d^5)	1/2	28.08	25.43	24.24	17.96	S=5/2 [169,180]
	3/2	36.95	36.98	33.75	30.85	
	5/2	0	0	0	0	
Fe (d^6)	0	-5.78	-9.18	-3.98	-11.37	S=0
	1	17.94	16.90	17.11	13.73	[132,169,181]
	2	0	0	0	0	
Co (d^7)	1/2	6.26	4.52	8.47	4.37	S=3/2 [169,176]
	3/2	0	0	0	0	
M^{III} complexes (q=1)						
Cr (d^3)	1/2	27.76	26.74	25.93	24.27	S=3/2 [169,182,183]
	3/2	0	0	0	0	
Mn (d^4)	0	5.98	2.62	4.75	-2.98	S=1
	1	-7.34	-8.80	-6.47	-11.42	[169,184]
	2	0	0	0	0	
Fe (d^5)	1/2	-7.91	-8.76	-3.62	-11.58	S=1/2
	3/2	9.23	9.52	11.48	6.85	[169,178,185]
	5/2	0	0	0	0	
Co (d^6)	0	-31.96	-33.15	-26.89	-32.61	S=0
	1	-1.91	-1.94	0.95	-2.60	[169,183,186]
	2	0	0	0	0	
M^{IV} complexes (q=2)						
Mn (d^3)	1/2	17.72	20.82	18.87	16.62	S=3/2
	3/2	0	0	0	0	[187]

The complexes with a d^3 electronic configuration, i.e. $[Cr^{III}(Tp)_2]^+$ and $[Mn^{IV}(Tp)_2]^{2+}$, possess a quartet ground state, as was to be expected. The energy difference between the ground state and the lowest doublet is nearly two times smaller for $[Mn^{IV}(Tp)_2]^{2+}$ than

for $[Cr^{III}(Tp)_2]^+$, due to the higher oxidation state of the former. our calculations for $[Mn^{III}(Tp)_2]^+$ (d^4 configuration) clearly indicate $^3A_{2g}$ as the spin ground-state.

Regardless of the fact that both Mn^{II} and Fe^{III} have a d^5 electronic configuration, different ground-states for $[Mn^{II}(Tp)_2]$ and $[Fe^{III}(Tp)_2]^+$ were found in the D_{3d} environment, i.e. a $^6A_{1g}$ for the former and ^2E_g for the latter (both of which are in perfect agreement with experimental findings). Clearly, the higher oxidation state of Fe^{III} causes a larger splitting of the d-orbitals, which results in the low-spin ground state. Unfortunately, it should be pointed out that the energy differences in $[Fe(Tp)_2]^+$ are still large enough to prevent SCO behaviour. The could be circumvented by a careful modification of the Tp^- ligands (*vide infra*).

Complexes with a d^6 electronic configuration, i.e. $[Fe^{II}(Tp)_2]$ and $[Co^{III}(Tp)_2]^+$, have a low-spin $^1A_{1g}$ state as the most stable one. The energy separation between the low-spin ground-state and the high-spin state is much larger in $[Co^{III}(Tp)_2]^+$, due to higher charge of cobalt ion, hence only $[Fe^{II}(Tp)_2]$ might possess SCO properties. Earlier theoretical and experimental investigations[142,188] on similar molecules have confirmed that complexes with a d^7 configuration prefer the high-spin over the low-spin state. Indeed, our calculations revealed that $[Co^{II}(Tp)_2]$ has ^4E_g as the ground state. However, the energy difference between the high-spin and low-spin states is of the order of 1–4 kcal mol^{-1}, which reproduces nicely the well established spin-flexibility of Co^{II} compounds and the related spin-crossover behaviour of $[Co^{II}(Tp)_2]$.[142]

Since the results are consistent with each other at all levels of theory, our discussion will from here on be focused only on the OPBE results (on OPBE geometries).

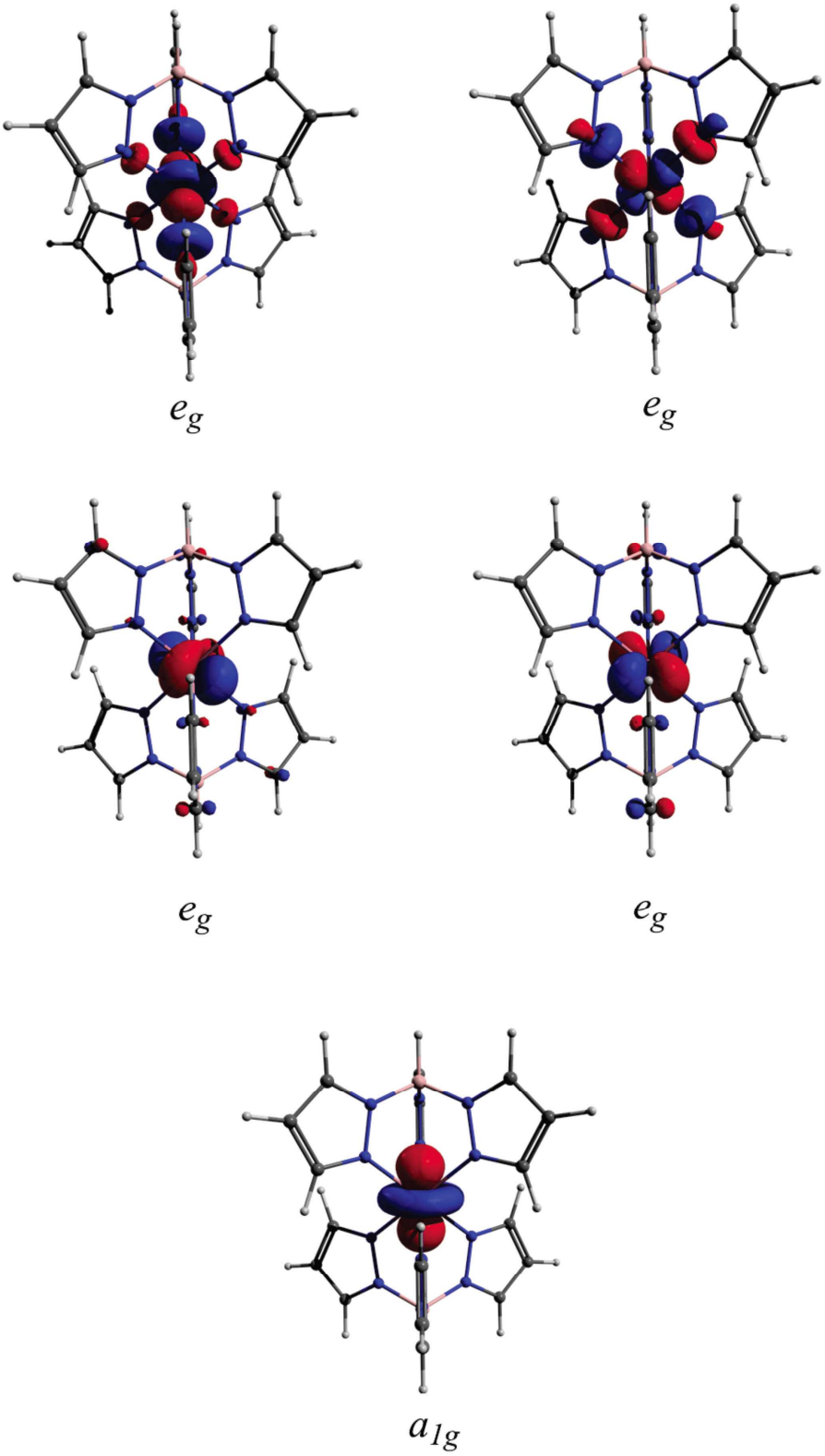

Figure 4-13 Schematic representation of molecular orbitals with dominant d-character, from top to bottom: anti-bonding e_g, non-bonding e_g and non-bonding a_{1g} orbitals (shown here are orbitals for high-spin $[Co^{II}(Tp)_2]$)

4.3.1.2. The influence of Jahn-Teller distortions

When we have a degenerate state, there exist a non-symetric normal mode that reduces the symmetry, removes the degeneration and lowers the energy (JT effect). Since in our systems, with every complex, there is allways at least one degenerate spin state, those structures are prone to JT distortion and therefore the analysis of spin state energetic demands a more comprehensive exploration.

In the D_{3d} point group, the degeneracy of the t_{2g} orbital set as present in the O_h point group is partially removed. Therefore the frontier orbitals, dominated by *d*-orbitals of the metal cation, are of type: a_{1g}, e_{1g} and e_{1g} (Figure 4-13). As result, all complexes studied here which are prone to JT distortion possess a E_g ground-state in the high symmetry (D_{3d}) configuration. This nuclear arrangement is not a stationary point on the potential energy surface, and hence the systems distort along the e_g vibrations to go from D_{3d} to C_{2h} symmetric structures ($E\otimes e$ problem in the JT terminology). There are two types of distortions, depending on the electronic configuration and occupations of d-orbitals. If the non-bonding e_g orbitals (Figure 4-13) are partially occupied the distortion is less prominent. However, when anti-bonding e_g orbitals (Figure 4-13) are partially filled, the distortion will result in an elongated or compressed octahedron. Regardless of the type of distortion, a deformation towards lower symmetry removes the degeneracy, which leads to two distorted structures, corresponding to the minimum and transition state on the adiabatic PES (APES).

Table 4-20 Spin state energies (kcal·mol^{-1}), relative to the high-spin state and JT stabilization energies (kcal·mol^{-1}) obtained with MD-DFT calculations[a]

M	Spin[b]	D_{3d} state	D_{3d} energy	C_{2h} state	C_{2h} energy	E_{JT}
M^{II} complexes (q=0)						
Mn (d^5)	1/2	^2E_g	28.08	^2A_g	27.94	0.14
				^2B_g	28.11	0.15
	3/2	^4E_g	36.95	^4A_g	33.23	5.29
				^4B_g	27.61	9.34
	5/2	$^6A_{1g}$	0	-[c]	-[c]	-[c]
Fe (d^6)	0	$^1A_{1g}$	-5.78	-[c]	-[c]	-[c]
	1	^3E_g	17.94	^3A_g	13.47	8.52
				^3B_g	12.37	5.57
	2	$^5A_{1g}$	0	-[c]	-[c]	-[c]
Co (d^7)	1/2	^2E_g	6.26	^2A_g	-1.11	7.65
				^2B_g	1.39	4.87
	3/2	^4E_g	0	^4A_g	-0.07	0.07
				^4B_g	-0.10	0.10
M^{III} complexes (q=1)						
Mn (d^4)	0	^1E_g	5.98	^1A_g	14.38	0.29
				^1B_g	5.87	0.05
	1	$^3A_{2g}$	-7.34	-[c]	-[c]	-[c]
	2	^5E_g	0	^5A_g	-4.60	4.50
				^5B_g	-5.89	5.96
Fe (d^5)	1/2	^2E_g	-7.91	^2A_g	-8.12	0.21
				^2B_g	-8.01	0.18
	3/2	^4E_g	9.23	^4A_g	4.64	5.05
				^4B_g	3.20	6.03
	5/2	$^6A_{1g}$	0	-[c]	-[c]	-[c]
Co (d^6)	0	$^1A_{1g}$	-31.96	-[c]	-[c]	-[c]
	1	^3E_g	-1.91	^3A_g	-4.78	7.88
				^3B_g	-5.05	3.14
	2	$^5A_{1g}$	0	-[c]	-[c]	-[c]
M^{IV} complexes (q=2)						
Mn (d^3)	1/2	^2E_g	17.72	^2A_g	21.13	0.15
				^2B_g	17.43	0.29
	3/2	$^4A_{2g}$	0	-[c]	-[c]	-[c]

a) at OPBE/TZP//OPBE/TZP; b) total S values; c) not Jahn-Teller active

The results of the MD-DFT calculations performed to analyze the JT effect in the scorpionate complexes are given in Table 4-20. Of all complexes with a d^3 electronic configuration, only $[Mn^{IV}(Tp)_2]^{2+}$ in the low spin state is prone to the JT distortion (Cr^{III} is JT inactive). The high-symmetry D_{3d} configuration is ^2E_g which splits

into ^2A_g (transition state) and ^2B_g (minimum) upon distortion. Bearing in the mind that only non-bonding e_g orbitals are partially occupied, it is understandable that E_{JT} is small. For this complex, the quartet $^4A_{2g}$-state still represents the ground state for $[Mn^{IV}(Tp)_2]^{2+}$, but the energy separation is slightly reduced due to the distortion.

Contrary to the complex with a d^3 configuration, the d^4-complex $[Mn^{III}(Tp)_2]^+$ is JT active only in the high spin state. Due to the partially occupied anti-bonding orbitals, the distortion is significant, which is confirmed by the calculated E_{JT} energy, which is substantial (4.5-6.0 kcal·mol^{-1}). Nevertheless, the distortion is insufficient to change the spin state in this case; hence $^2A_{2g}$ is still the ground state.

In the case of the d^5-complexes $[Mn^{II}(Tp)_2]$ and $[Fe^{III}(Tp)_2]^+$, JT-distortions may occur in both the intermediate and low spin-state. In the intermediate spin state at the high symmetry (D_{3d}) geometry, the ^4E_g state shows partially occupied anti-bonding orbitals. In contrast, the low-spin ^2E_g structures show partially occupied non-bonding orbitals. Hence, strong distortions in the intermediate spin state cause significant stabilization, while the stabilization of the low spin state is less prominent upon distortion. In both cases spin ground-state switching due to JT does not occur.

The d^6-complexes $[Fe^{II}(Tp)_2]$ and $[Co^{III}(Tp)_2]^+$ are prone to JT only in the intermediate spin state. In this particular case both sets of e_g orbitals are unequally populated giving rise to strong distortions. Nevertheless, the distortion has insignificant impact on spin related properties of these complexes.

Finally, for the d^7-complex $[Co^{II}(Tp)_2]$ both the high-spin and low-spin state are susceptible to the JT distortions. The lowest energy electronic state for the high-spin (S=3/2) D_{3d} structure is ^4E_g, while the low-spin structure has ^2E_g as the lowest-energy state. The distortion in the high spin state is very poor as evidenced by a small E_{JT} energy, Table 4-20. A much stronger distortion in the low-spin structure causes a significant stabilization with respect to the high-spin state, which leads to the switching of the spin ground-state. These findings are seemingly inconsistent with experimental results.[169,176,189] This seems to indicate that the spin ground-state for this complex is not determined by the electronic energies (ΔE), but instead a significant effect is to be expected from solvation, enthalpy and entropy corrections. Indeed, when we include those terms we do find the high-spin (S=3/2) to be lower in (free) energy than the low-spin states (see Table 4-21), in accordance with experimental findings.

Table 4-21 Free energy and solvation contributions to the ΔE_{LH} (=$E_{low\text{-}spin} - E_{high\text{-}spin}$) for $[Co(Tb)_2]$ in C_{2h} symmetry. Energies are calculated at OPBE level of theory, and are given in kcal/mol.

Electronic state	^{2}Ag	^{2}Bg	^{4}Ag	^{4}Bg	
ΔE_{cosmo}[xxi]	-8220.25	-8217.69	-8219.82	-8220.07	-0.18
ΔG	-7992.50	-7989.14	-7993.58	-7993.93	1.43

4.3.1.3. Spin-state energies in mono-substituted Tp complexes

The substitution of hydrogen atoms at the positions 3 and 5 of pyrazolyl rings is known to lead to significant changes in SCO properties of the complexes studied here.[159] Some earlier studies on mainly the iron(II) complex revealed that substituents at position 4 do not influence much the spin state energetics, which is also confirmed by our current explorations (Table 4-22). Hence, although we examined substitutions at all three positions, we will discuss here only those at positions 3 and 5. For these substitutions we used both electron withdrawing groups, NO_2 and CF_3, and electron donating groups such as NH_2 and CH_3.

[xxi] Dichloroethane

Table 4-22 Spin state energies (kcal mol^{-1}) relative to the high spin electronic state, at OPBE level of theory, for substituted $[M^x(Tp^{4\text{-}R})_2]^q$ complexes.

					OPBE		
M^{n+}	d^n	Symm.	Spin state	Electronic state	$H(Pz)_3$	4-NH2	4-NO2
Cr^{3+}	d^3	D_{3d}	HS	$^4A_{2g}$	0	0	0
			LS	$^2A_{2g}$	43.57	28.75	30.21
Mn^{4+}	d^3	D_{3d}	HS	$^4A_{2g}$	0	0	0
			LS	^2E_g	21.03	3.2	7.5
Mn^{3+}	d^4	D_{3d}	HS	^5E_g	0	0	0
			IS	$^3A_{2g}$	-5.75	-6.7	-3.44
			LS	^1E_g	20.01	13.69	22.48
Mn^{2+}	d^5	D_{3d}	HS	$^6A_{1g}$	0	0	0
			IS	^4E_g	41.3	40.92	41.03
			LS	^2E_g	29.93	29.41	29.08
Fe^{3+}	d^5	D_{3d}	HS	$^6A_{1g}$	0	0	0
			IS	^4E_g	23.43	12.62	8.93
			LS	^2E_g	-6.82	-4.24	-6.23
Fe^{2+}	d^6	D_{3d}	HS	$^5A_{1g}$	0	0	0
			IS	^3E_g	35.47	23.85	23.31
			LS	$^1A_{1g}$	-5.78	-4.99	-6.8
Co^{3+}	d^6	D_{3d}	HS	$^5A_{1g}$	0	0	0
			IS	^3E_g	1.01	6.31	-0.22
			LS	$^1A_{1g}$	-31.96	-16.68	-32.2
Co^{2+}	d^7	D_{3d}	HS	^4E_g	0	0	0
			LS	^2E_g	2	1.13	1.44

The calculated values for the spin-state splittings of the substituted complexes $[M^x(Tp^{3\text{-}R})_2]^q$ and $[M^x(Tp^{5\text{-}R})_2]^q$ are given in Table 4-23 and Table 4-24, respectively.

Table 4-23 Spin state energies for 3-substituted $[M^{x}(Tp^{3\text{-}R})_2]^{q}$ D_{3d} complexes (at OPBE/TZP, kcal·mol^{-1}) relative to the high-spin state

	spin[a]	R=H	R=NH_2	R=CH_3	R=CF_3	R=NO_2
M^{II} complexes (q=0)						
Mn (d^5)	1/2	28.08	38.97	43.14	51.34	58.89
	3/2	36.95	39.93	42.41	46.03	51.38
	5/2	0	0	0	0	0
Fe (d^6)	0	-5.78	10.77	11.00	21.92	23.56
	1	17.94	24.05	24.97	31.43	31.75
	2	0	0	0	0	0
Co (d^7)	1/2	6.26	13.69	13.43	14.95	17.99
	3/2	0	0	0	0	0
M^{III} complexes (q=1)						
Cr (d^3)	1/2	27.76	28.93	44.65	30.49	31.06
	3/2	0	0	0	0	0
Mn (d^4)	0	5.98	7.98	13.8	20.87	24.37
	1	-7.34	-4.02	-0.07	6.65	10.47
	2	0	0	0	0	0
Fe (d^5)	1/2	-7.91	4.29	4.27	15.10	17.62
	3/2	9.23	13.90	13.47	17.25	19.88
	5/2	0	0	0	0	0
Co (d^6)	0	-31.96	-8.43	-19.51	-6.94	-5.85
	1	-1.91	9.27	3.64	8.72	12.12
	2	0	0	0	0	0
M^{IV} complexes (q=2)						
Mn (d^3)	1/2	17.72	0.73	21.05	21.61	14.27
	3/2	0	0	0	0	0

Our results indicate that substituents at position 3 (see Figure 4-11) for atom numbers) tend to stabilize in general high-spin states over the low-spin state, regardless of the type of substituent we put at this position. In most cases, electron withdrawing and donating substituents have no impact on the spin ground-state; however, this is not the case for $[Fe^{II}(Tp^{3\text{-}R})_2]$ and $[Fe^{III}(Tp^{3\text{-}R})_2]$, which change from low-spin with R=H to high-spin with all four substituents at position 3 (see Table 4-23). A similar thing occurs for $[Mn^{III}(Tp^{3\text{-}R})_2]^{+}$, which changes from intermediate-spin (S=1) to high-spin (S=2) for two of the four substituents (CF_3, NO_2). This spin-state switching is resulting from inter-ligand steric repulsions, i.e. repulsions between substituents that elongate M-N bonds with respect to the non-substituted complexes (see Figure 4-14).[159] This elongation leads to a decrease of

unfavourable anti-bonding interactions, i.e. the energy of the upper set of e_g orbitals is lowered. This effect is most noticeable for NO_2 substituents, due to the strong repulsions between the negatively charged oxygen atoms of this group, and the least for the NH_2 substituents, in the following order: $NH_2 < CH_3 < CF_3 < NO_2$.

The $[Cr^{III}(Tp^{3\text{-}R})_2]^+$ and $[Mn^{IV}(Tp^{3\text{-}R})_2]^{2+}$ complexes stand out from the others in the sense that there does not seem to be a clear pattern in the trend for the different substituents. I.e., in both cases is a substantial reduction of the ΔE_{LH} ($=E_{low\text{-}spin} - E_{high\text{-}spin}$) observed for R=$NH_2$, but no such an effect for R=CH_3. The origin of behaviour remains unclear.

Table 4-24 Spin state energies for 5-substituted $[M^x(Tp^{5\text{-}R})_2]^q$ D_{3d} complexes (at OPBE/TZP, kcal·mol^{-1}) relative to the high-spin state

	spin[a]	R=H	R=NH_2	R=CH_3	R=CF_3	R=NO_2
M^{II} complexes (q=0)						
Mn	1/2	28.08	27.99	25.08	20.42	15.42
	3/2	36.95	37.86	35.45	33.11	29.45
	5/2	0	0	0	0	0
Fe	0	-5.78	-2.65	-8.18	-13.35	-18.28
	1	17.94	19.16	16.57	13.79	16.31
	2	0	0	0	0	0
Co	1/2	6.26	8.46	5.6	3.33	0.42
	3/2	0	0	0	0	0
M^{III} complexes (q=1)						
Cr	1/2	27.76	28.36	41.94	29.89	29.79
	3/2	0	0	0	0	0
Mn	0	5.98	1.15	4.2	3.96	4.98
	1	-7.34	-10.06	-8.54	-9.19	-8.29
	2	0	0	0	0	0
Fe	1/2	-7.91	-4.11	-9.09	-11.58	-12.65
	3/2	9.23	13.38	8.71	7.57	6.53
	5/2	0	0	0	0	0
Co	0	-	-16.92	-31.36	-35.67	-37.31
	1	-1.91	6.23	-1.64	-3.91	-0.70
	2	0	0	0	0	0
M^{IV} complexes (q=2)						
Mn	1/2	17.72	6.55	15.55	17.57	8.72
	3/2	0	0	0	0	0

Since the $[Co^{III}(Tp)_2]^+$ complex exhibits a very large energy separation between the low- and high-spin state, the substitutions can only reduce the energy splitting. Indeed, our calculations are consistent with this assumption, revealing that $^1A_{1g}$ remains the ground state. On the other hand, by replacing hydrogen atoms at pyrazolyl rings in the high-spin complexes $[Mn^{II}(Tp)_2]$ and $[Co^{II}(Tp)_2]$, the energy separation is significantly enhanced (see Table 4-23).

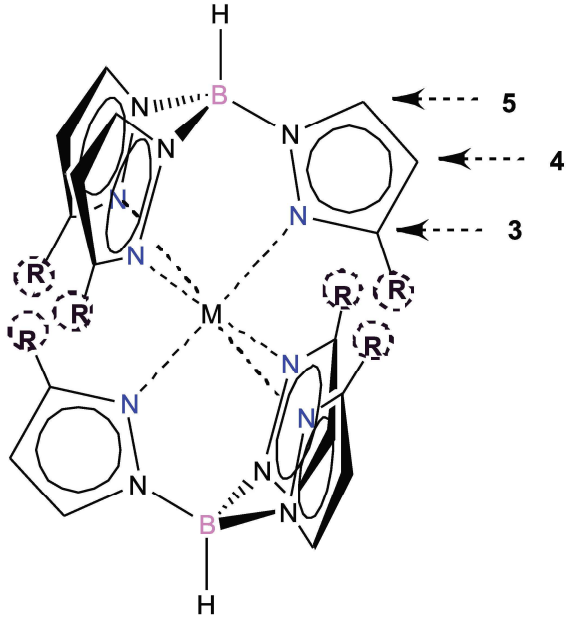

Figure 4-14 Schematic representation of steric repulsions in $[M^x(Tp^{3\text{-}R})_2]^q$ complexes. The positions 3, 4 and 5 are indicated in the picture

The substituents at position 5 (see Table 4-24) influence the SCO properties mainly through electron-withdrawing and electron-donating effects. Withdrawing groups such as NO_2 and CF_3 generally tend to enhance π-acceptor properties of the ligands. In contrast, electron-donating groups enhance π-donor properties of the investigated ligands. This implies that the withdrawing NO_2 and CF_3 groups at position 5 tend to stabilize the low-spin state, while the NH_2 group tends to stabilize the high-spin state. At the same time, it is well known that the methyl group has a very weak electronic effect, hence it is understandable that results obtained for $[M^x(Tp^{5\text{-}CH_3})_2]^q$ complexes do not follow the general trend. In fact, the calculations have shown that the energy gap between two sets of e_g orbitals increases in the case of $[M^x(Tp^{5\text{-}NO_2})_2]^q$ and $[M^x(Tp^{5\text{-}CF_3})_2]^q$ complexes, and significantly decreases in the case of $[M^x(Tp^{5\text{-}NH_2})_2]^q$ complexes (Table 4-12). These findings are schematically shown in Figure 4-15

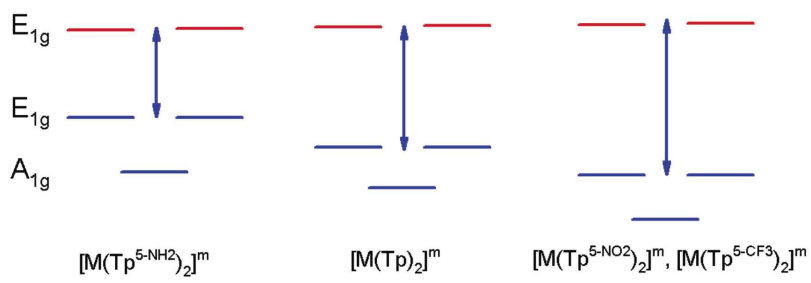

Figure 4-15 Schematic representation of orbitals in $[M^{x}(Tp^{5\text{-}R})_2]^{q}$ complexes

Let us now consider the spin state preferences of the low-spin complexes, i.e. $[Mn^{III}(Tp)_2]^{+}$, $[Fe^{II}(Tp)_2]$, $[Fe^{III}(Tp)_2]^{+}$ and $[Co^{III}(Tp)_2]^{+}$ after the substitution has taken place. In all cases the electron donating NH_2 group does not change the spin state, but only reduces the energy separation. For obvious reasons (see Table 4-24), only $[Fe^{II}(Tp^{5\text{-}NH_2})_2]$ and $[Fe^{III}(Tp^{5\text{-}NH_2})_2]^{+}$ complexes can be considered as SCO compounds. In $[Co^{III}(Tp^{5\text{-}NH_2})_2]^{+}$ the $^{1}A_{1g}$ ground state is well separated from the intermediate and high-spin states, thus preventing any SCO behaviour.

Due to the very large spin-state splitting in the $[Mn^{II}(Tp)_2]$ complex, none of the substituents leads to any significant change. Interestingly, for $[Co^{II}(Tp)_2]$ the replacement with the NO_2 group causes stabilization of the low spin state in $[Co^{II}(Tp^{5\text{-}NO_2})_2]$ with respect to the high-spin state with an energy difference of only 0.42 kcal·mol^{-1}. Based on these results, $[Co^{II}(Tp^{5\text{-}NO_2})_2]$ and $[Co^{II}(Tp^{5\text{-}CF_3})_2]$ should be considered as possible SCO compounds.

4.3.1.4. Spin-state energies of disubstituted Tp complexes

The calculated values for the spin-state energy splitting for di-substituted $[M^{x}(Tp^{3,5\text{-}R})_2]^{q}$ complexes, along with the experimental findings for them, are presented in Table 4-25. Since the substituents are now on both positions, the splitting of spin states is governed by a combination of steric and electronic effects, which makes a detailed analysis more difficult. Still, it is evident that steric effects, due to the substitution at position 3 are dominant. Spin state switching was observed in $[Mn^{III}(Tp^{3,5\text{-}CF_3})_2]^{+}$, $[Mn^{III}(Tp^{3,5\text{-}NO_2})_2]^{+}$ and in all substituted complexes of Fe^{II} and Fe^{III}. The possible SCO properties of $[Co^{II}(Tp)_2]$ compound are significantly disabled upon substitution, owing to the dominant effect of groups in position 3. Very small energy separations indicating possible SCO properties were obtained for $[Co^{III}(Tp^{3,5\text{-}NH_2})_2]^{+}$ and $[Fe^{III}(Tp^{3,5\text{-}CH_3})_2]^{+}$. Although the small spin state splitting of 0.33 kcal·mol^{-1} is somewhat surprising for the $[Co^{III}(Tp^{3,5\text{-}NH_2})_2]^{+}$ complex, it is understandable because of the combined synergistic effects of two NH_2 groups.

Table 4-25 Spin state energies for di-substituted $[M^x(Tp^{3,5\text{-}R})_2]^q$ D_{3d} complexes (at OPBE/TZP, kcal·mol^{-1}) relative to the high-spin state

	spin[a]	R=H	R=NH_2	R=CH_3	R=CF_3	R=NO_2
M^{II} complexes (q=0)						
Mn (d^5)	1/2	28.08	39.01	39.93	42.14	55.86
	3/2	36.95	39.79	40.98	39.48	51.78
	5/2[b]	0	0	0	0	0
Fe (d^6)	0	-5.78	13.95	8.31	13.99	16.48
	1	17.94	25.23	25.90	25.05	29.06
	2[c]	0	0	0	0	0
Co (d^7)	1/2	6.26	14.85	12.43	13.34	16.26
	3/2[d]	0	0	0	0	0
M^{III} complexes (q=1)						
Cr (d^3)	1/2	27.76	27.85	44.12	30.33	31.05
	3/2	0	0	0	0	0
Mn (d^4)	0	5.98	4.44	25.50	17.82	41.83
	1[e]	-7.34	-6.53	-1.62	3.57	27.34
	2	0	0	0	0	0
Fe (d^5)	1/2	-7.91	7.13	2.82	10.51	17.42
	3/2	9.23	14.79	13.00	14.93	12.63
	5/2[f]	0	0	0	0	0
Co (d^6)	0	-31.96	-0.33	-19.35	-11.54	-10.37
	1	-1.91	13.19	8.90	6.60	4.04
	2	0	0	0	0	0
M^{IV} complexes (q=2)						
Mn (d^3)	1/2	17.72	1.81	17.23	21.81	21.32
	3/2	0	0	0	0	0

a) given are the total S values; b) exp. spin state (S=5/2)[169,187]; c) exp. spin state (S=2)[132,169,181]; d) exp. spin state (S=3/2)[169]; e) exp. spin state (S=1)[169,184]; f) exp. spin state (S=5/2)[169]

4.3.2. Conclusion

In this work we have shown relative energies among possible spin states in polypyrazolylborate metal complexes by means of DFT, with the OPBE functional, which has been proven to be accurate for spin state energies. Calculations performed on non-substituted complexes perfectly match with experimental data. Depending on the electronic configuration and occupation of the *d* levels of the metal ion, some of the investigated complexes are prone to the distortions from D_{3d} to C_{2h} due to the JT effect. Our calculations reveal that

energy stabilization upon descent in symmetry were generally not enough to overcome initial spin-state splittings.

A second objective of this reseach was to establish and to analyse factors that enable Tp^- ligands to modulate spin state preferences. Modification of investigated complexes leads to very interesting phenomena and qualities. Our exhaustive calculations revealed that $[Co(Tp)_2]$ complex and some of their substituted analogues, i.e. $[Co(Tp^{5\text{-}CF_3})_2]$, show potential SCO behaviour. Furthermore, the calculated energy separations for $[Mn(Tp^{3,5\text{-}CH_3})_2]^+$ and $[Co(Tp^{3,5\text{-}NH_2})_2]^+$ are also very small, which is especially interesting in the case of $[Co(Tp^{3,5\text{-}NH_2})_2]^+$ compound.

Generally speaking high spin complexes with large spin state splitting can be adjusted for technological application by replacing hydrogen atom in position 5 with strong electron withdrawing groups. Contrary to that, low spin complexes, with large ligand field splitting, can be modified by placing electron donating groups in position 5 or any voluminous group in position 3 of pyrazolyl rings.
These findings pave the way towards rational design of transition-metal compounds with spin crossover properties.

4.3.3. Computational details

The calculations using the unrestricted formalism have been performed with the ADF program package, version 2013.01.[42,93,94] MOs were expanded in an uncontracted set of Slater type orbitals (STOs),[95] of triple-ζ quality containing diffuse functions plus one set of polarization functions (TZP). Geometry optimizations and frequency calculations were performed using a generalized gradient (GGA) functional, consisting of OPTX[103] for exchange and PBEc[83] for correlation (OPBE[48]). Geometry optimizations have also been performed using the local density approximation (LDA)[28,37,102] on non-substituted $[M(Tp)_2]^m$ complexes. Geometries were optimized, either in D_{3d} or C_{2h} symmetry, with the QUILD[100] program (provided in the ADF program package), using adapted delocalized coordinates[101] with the standard Becke grid[190,191] until the maximum gradient component was less than $1.0 \cdot 10^{-5}$ a.u. Subsequently, single-point energy

calculations were performed on the OPBE//LDA optimized geometries using OPBE, the dispersion corrected functional by Swart-Solà-Bickelhaupt, SSB-D,[39] which has so far shown to be very accurate for spin states, and its recently reported successor S12g.[47]

In order to tackle the degenerate states, Multi-Determinant DFT (MD-DFT),[192,193] proven to be accurate for determination of Jahn-Teller parameters,[143,145,193-195] has been performed. This procedure consists of the following steps: (i) average of configuration (AOC) calculation in the D_{3d} point group, which gives the high-symmetry (HighSym) geometry. (ii) a single-point calculation with the HighSym geometry (D_{3d}) and a low symmetry (LowSym) for the electron density (C_{2h}); this is achieved by introducing an adequate irrep occupation scheme of the molecular orbitals (MOs), and using the *symrot* procedure in the QUILD[100] program. (iii) A geometry optimization constraining the structure to the (LowSym) C_{2h} point group, with an *appropriate* occupancy of the irreps. In the end, this leads to E_{JT} which is the difference between the energies obtained in steps (ii) and (iii) with the same electron distribution.

4.4. Small molecule mimics for catechol dioxygenase class of enzymes

4.4.1. Short introduction

The microbial aerobic degradation of aromatic pollutants, which are widespread contaminants in soils and groundwaters, obviously represents the intensive research area in the scientific community.[196,197] A key step in the biodegradation of aromatic compounds is an oxidative cleavage of catechol derivatives and is facilitated by a class of enzymes known as catechol dioxygenase.[198,199] Two different groups of enzymes play an essential role in the ring cleavage of catechol derivatives: the extradiol- and intradiol-cleaving dioxygenases.[200] These two enzyme groups have different active sites, and thus catalyze different metabolic transformations, Figure 4-16.[201] In the case of extradiol enzymes, the oxygen in the product is next to one of hydroxyl groups. Regarding the intradiol-cleaving dioxygenases, the first step represents insertion of oxygen between two hydroxyl groups of catechol.

Extradiol-cleaving dioxygenases utilize Fe^{II} in their active site, coordinated by a 2-His-1-carboxylate facial triad in octahedral environment. Vacant sites are occupied by solvent molecules that can be easily replaced by a substrate and oxygen in the catalytic process, Figure 4-16. In the subsequent step the formation of alkyl peroxide is followed by a hemolytic cleavage of the O-O bond and the insertion of oxygen into catechol ring occurs.

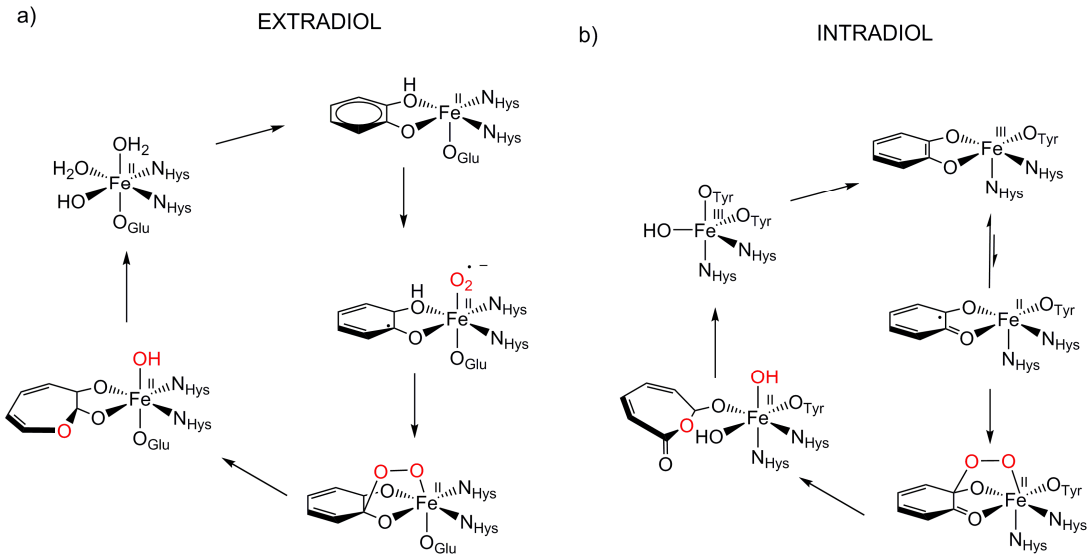

Figure 4-16 Proposed catalytic cycle in the active site for a) extradiol-, and b) intradiol-cleaving catechol dioxygenases.

Active site of intradiol-cleaving dioxygenases consists of Fe^{III} coordinated with two histidines and two tyrosines, and one hydroxide anion, Figure 4-16. One of proposed mechanistic pathways suggests that Fe^{III} firstly has to oxidise the aromatic ring to catechol radical, enabling coordination of oxygen and the formation of alkyl peroxide. It has been believed that the incorporation of the oxygen atom into the catechol ring proceeds via a concerted process, so-called Criegee rearrangement.[201-203]

Yet, a lot of questions still remain unknown concerning reaction mechanisms of these enzymes along with the factors that determine intra- versus extradiol specificity.[201] Since small molecule analogues, that mimic the enzymatic function, can be easily modified and characterized, their careful inspection by the means of quantum mechanical modeling represents guideline into the investigation of complicated

enzymatic systems.[112,201,204,205] There is a wide variety of QM levels that can be applied on the simple models of enzymatic active sites, ranging from semiempirical methods to high level *ab initio* approaches, passing through all the derivations of Hartree-Fock and Density Functional Theory (DFT) methods.[206] As explained in methodology part of introduction, DFT offers fast and easy way to calculate properties of medium-to-large sized molecules, but the choice of DFA for the analysis of the close lying spin states is a very demanding task.[45,46,50,79,131,141,165,207,208] However, so far, almost all studies on the both, enzyme active sites and their small molecule mimics, have used hybrid DFAs.[10,54,63,88,89,202,203,206] Unfortunately, doubts arise on the conclusions drawn from the obtained results, due to the difficulties for predicting of the correct spin ground state among the several possibilities (as a consequence of their tendency to favor the high spin (HS) state).[45,46] It is important to stress that the hybrid DFAs give accurate energy values of the reaction barriers. Encouridged with our previous validation studies and good performance, we strongly belived that SSB-D, S12g, and S12h represent methodology of choise, both for spin state energetics and reaction barriers.

Earlier experimental investigations on iron complexes with rigid L-N_2H_2 (2,11-diaza[3.3](2,6)pyridinophane) and L-N_2Me_2 (N,N′-dimethyl-2,11-diaza[3.3](2,6)pyridinophane) ligands, Figure 4-17, have shown that the complex with L-N_2Me_2 mainly follow intradiol pathway,[209] while for the complex with L-N_2H_2 both pathways are equally pursued.[210] Previous experimental and theoretical DFT studies indicated that the formation of alkyl peroxide is a rate determining step in both cases.[203] Since, several spin states can differently determine the reaction course of these interesting enzymes, in this chapter we present the thorough DFT examination of the spin-state energetics and the mechanism of these functional mimetic iron complexes in order to analyze possible pathways of catechol cleavage.

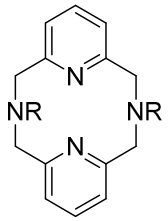

R=H **L-N_2H_2**

R=Me **L-N_2Me_2**

Figure 4-17 Schematic representation of the ligands used to model the reactivity of extradiol- and intradiol-cleaving catechol dioxygenases, L-N_2H_2 (2,11-diaza[3.3](2,6)pyridinophane) and L-N_2Me_2 (N,N'-dimethyl-2,11-diaza[3.3](2,6)pyridinophane).

4.4.1.1. General mechanism

Proposed mechanism of both, extra- and intradiol cleavage of iron catechol complex coordinated by chelating L-N_2H_2 ligand, is presented in Figure 4-18. The mechanism for compound with L-N_2Me_2 is analogus. As it will be demonstrated, it represents stepwise progression via multiple local minima, on a potential energy surfaces (PESs) with close lying spin states. In the examined biomimetics, iron^{III} is coordinated by four nitrogen atoms from the chelate ligand, having two adjacent sights accessible for the coordination of the catechol which donates two oxygen atoms to the iron, specie (0) presented in Figure 4-18.

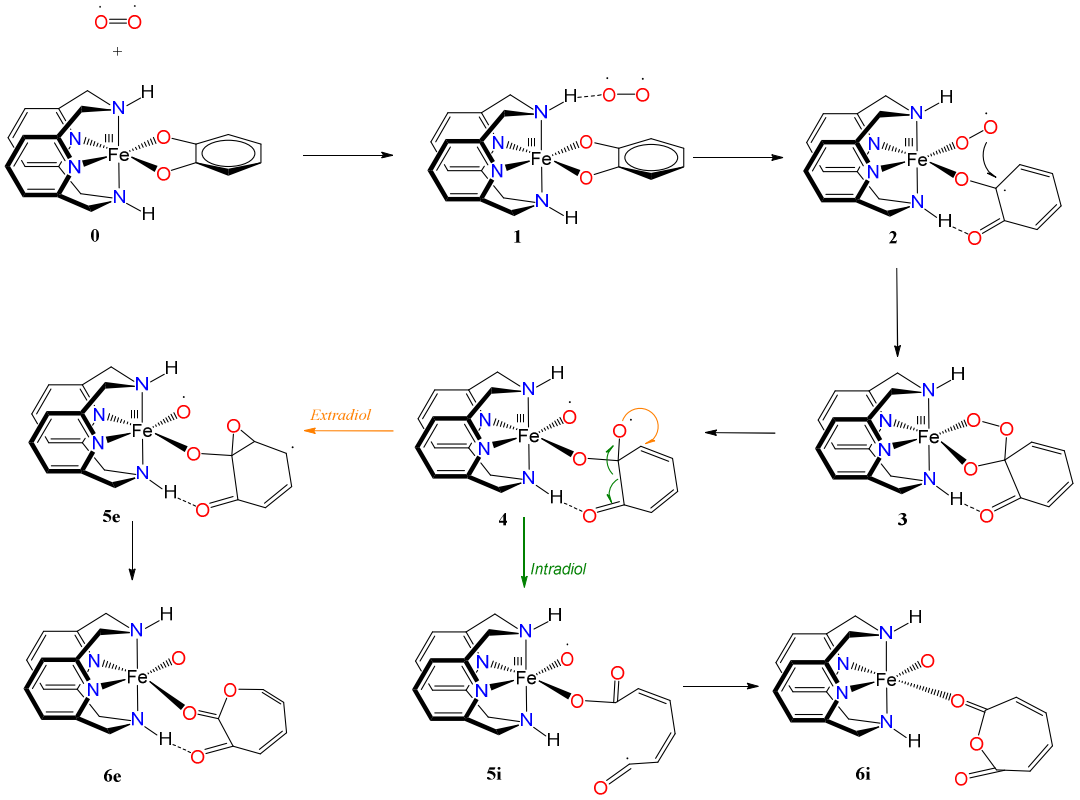

Figure 4-18 Proposed mechanism and nomenclature for intra- and extradiol catechol cleavage catalyzed by L-N_2H_2 iron(III) complex

In the first step of the binding of oxygen molecule, van der Waals complex (1), Figure 4-18, is obtained. Electron transfer from catechol, via iron(III) to oxygen, and coordination of oxygen, occur via concentrated process,[202] forming intermediate (2),Figure 4-18. In the next step, coordinated superoxide attacks the catechol resulting in bridging alkyl peroxide, (3), Figure 4-18. Oxygen-oxygen bond is cleaved homolytically, leading to the specie (4), Figure 4-18., which immediately decays in one of two possible proposed courses: intradiol or extradiol pathway. Intradiol path leads to the open chain radical intermediate, (5i), Figure 4-18., via dissociation of C-C bond. Final step includes cyclization leading to the structure designated as (6i) in the Figure 4-18. Extradiol path implies the formation of cyclic epoxide, (5e), Fig. 3., and further dissociation of C-C bond leads to the structure (6e), Figure 4-18. It should be noted that (6i) and (6e) dissociate forming two isomers, muconic anhydride and seven-membered ring lactone, respectively.

In order to fully understand the proposed mechanism, the spin-state energetics is investigated for all the structures denoted in Figure 4-18. Relative spin-state energetics of (0), (6i) and (6e) at S12g level of theory is given in the Table 4-26. Results of single point calculations with SSB-D, S12h, M06-L and MVS[211] DFAs can be found in the original publication. [212]

There are three experimentally available crystal structures of the complexes that are related to the investigated catalytic cycle. Two of them are the precursors of complex (0) with chloride ions instead of catechol, with L-N_2H_2 and L-N_2Me_2 ligands. The complex with catechol is structurally characterized only with L-N_2Me_2 ligand. Calculated bond distances for all complexes show reasonable agreement with experimentally determined bond lengths.[212] Experimental studies have concluded (based on the bond lengths of similar systems) that all of these complexes are in the HS ground state.[202,203] The calculated electronic energies show that complexes with the chloride ions as ligands are in the HS ground state, which corroborates the experimental conclusions. However, for the complex with catechol, the LS state is obtained as the ground state. Similar results are obtained previously at B3LYP* level of theory.[203] This indicates that the spin ground-state for this complex is not determined by the electronic energies, but instead a significant effect is to be expected from enthalpy and entropy corrections, that systematically favor a HS state. Irrespectively of coordinated ligand (L-N_2H_2 or L-N_2Me_2), HS intradiol product is thermodynamically favored Table 4-26.

Table 4-26 Electronic energies for the long range complex (0) and final products (6i) and (6e), relative to the ground state of (0), at the S12g, level of theory. The results are given in kcal/mol.

Ligand	L-N_2H_2			L-N_2Me_2		
molecule	0	6i	6e	0	6i	6e
LS	0	-28.3	-15.9	0	-25.8	-12.6
IS	5.0	-28.7	-15.5	4.3	-26.5	-13.3
HS	4.5	-30.0	-16.8	4.1	-27.4	-21.7

4.4.1.2. Reaction path with the L-N_2H_2 ligand

The first part of potential energy landscape for the catalytic cycle of the complex with L-N_2H_2 ligand (before the branching into intradiol and extradiol pathways) is represented in Figure 4-19. Two intrinsic reaction pathways are given in Figure 4-20.

Following the schematic representation shown in Figure 4-16, the complete catalytic dioxygenation reaction for all available spin states is calculated, starting from a $[Fe(LN_4H_2)(Cat)]^+$ complex (0), Figure 4-19. As mentioned before, the initial structure (0) is suggested to be in a HS state. A close lying LS and the HS state are obtained using S12g, with the LS slightly lower in energy. The reaction proceeds with initial formation of the van der Waals complex (1) that has negligible effect on relative spin state energetics. Since the complex (1) is coordinately saturated, the subsequent coordination of molecular oxygen needs to be accompanied by the decoordination of one part of catechol, in a strongly endergonic process, leading to structure (2). Oxygen that dissociated is now able to form an H-bond with the ligand fixating its position during the reaction. This step is a complex set of events that include catechol oxidation coupled with the iron mediated electron transfer to the O_2 molecule, accompanied by the large structural changes. Consequently, calculated spin state ordering in intermediate (2) is different, and the sextet state becomes the ground state. This results is in accordance with experimental results for the enzymatic reaction[213] and similar iron superoxo intermediates[214].

Following previous studies in the field, we will primarily focus on the reaction profile after oxygen coordination.[202,203] In the next step, after catechol is attacked by superoxo oxygen, the intermediate with five-membered ring (3) is formed. This corroborates well the scattered experimental results for the enzymatic process[215]. During the formation of peroxo intermediate, the quartet state becomes the lowest in energy, and governs the course of the reaction until the final point where muconic anhydride and seven-membered ring lactone dissociate from the iron center. After the formation of intermediate (3), the O-O bond becomes weakened, and subsequently it dissociates, leading the reaction profile to the region in which it can continue either in intradiol or

extradiol pathway. The sextet state is lowest in energy for the superoxo complex (2). However, due to the fact that barrier for the O-O bond dissociation (TS_{34}) is very high in energy on the PES, the sextet state has insignificant effect on the reaction mechanism.

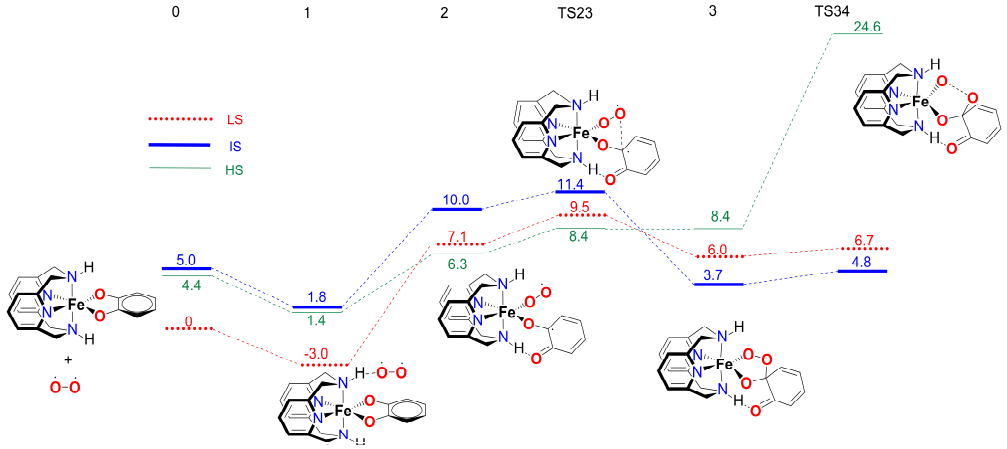

Figure 4-19 Calculated reaction profile, for the first part of the catechol dioxygenation mechanism, starting from the $[Fe(LN_4H_2)(Cat)]^+$ complex, (0). Electronic energies, obtained using S12g/TZ2P level of theory, are given relative to the ground state of the initial complex (0).

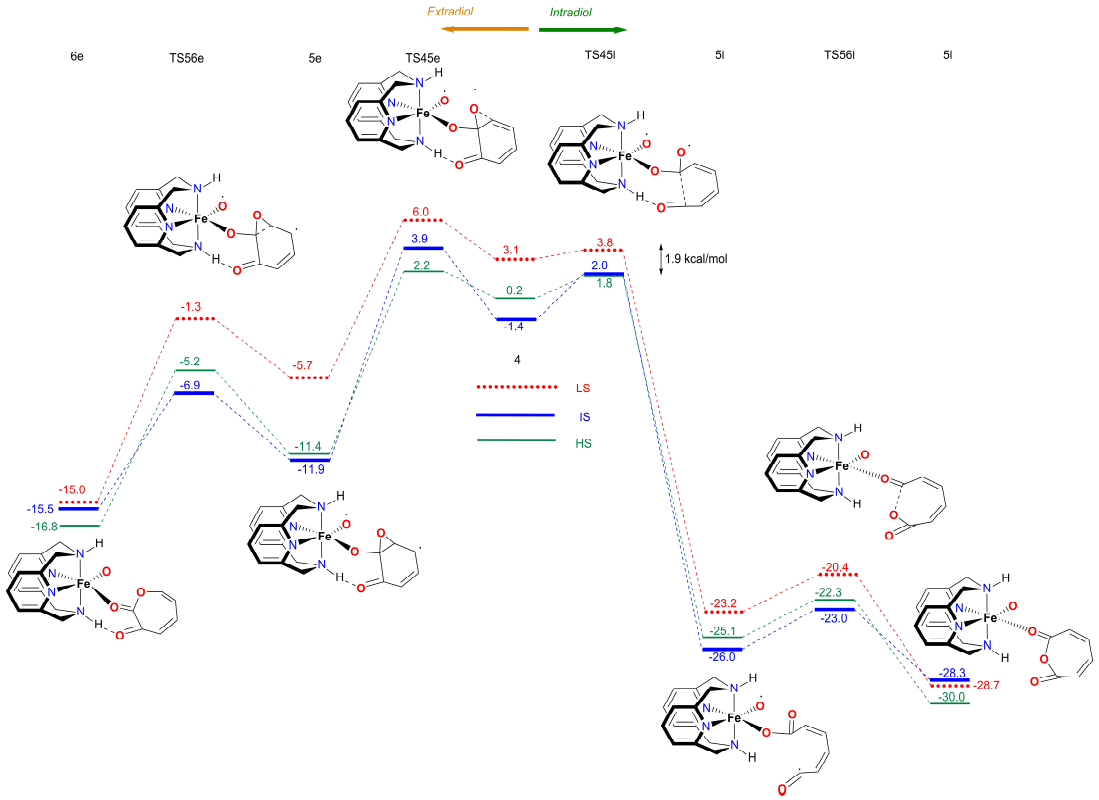

Figure 4-20 Calculated reaction profile for the second part of the catalytic mechanism with LN_4H_2 ligand, branching to the intradiol and extradiol pathway. Electronic energies, obtained using S12g/TZ2P level of theory, are given relative to the ground state of the initial complex (0), from the Figure 4-19.

The reaction profile that follows the cleavage of O-O bond in intermediate (3) is depicted in Figure 4-19. The intradiol pathway is presented on the Figure 4-20 (right), while extradiol pathway is shown on the same Figure (left). These two mechanisms are characterized by distinct structural transformations, reaction courses and final products. Our calculations indicate that intradiol mechanism starts with the C-C dissociation, which is then followed by a rearrangement and cyclization, creating the final product, seven-membered ring lactone. The extradiol pathway is initiated by the formation of the cyclic epoxide, followed by a different C-C bond dissociation that gives the extradiol product, muconic anhydride (see Figure 4-20). However, in most of the previous studies concerning the mechanism of intradiol catechol dioxygenaze[201] and its biomimetics,[202,203] the concerted mechanism was found for the formation of seven-membered lactone, whereas in this study the C-C bond dissociation occurs in the first step.

The ratio of the products is determined by the barriers for the two pathways, i.e. the relative energies of two transition states (TS_{45i}) and (TS_{45e}). Having in mind that the quartet state governs the course of the reactions, it determines the distribution of products. The energy difference between TS_{45i} and TS_{45e} in IS state is 1.9 kcal/mol. It indicates that both products should in principle be formed, which is in excellent agreement with the experiment.[210] The inspection of the reaction landscape shows that although the quartet and sextet states are almost equienergetic in some cases, Figure 4-20, quartet state governs the reaction until the dissociation of seven-membered ring products and formation of five coordinated iron oxo complex occur. This is in a good agreement with previous studies which concluded that iron oxo complexes tend to be in a close lying spin states, with the dominant HS state in a penta-coordinated environment, and IS when hexa-coordinated.

4.4.1.3. Reaction path with the L-N_2Me_2 ligand

In order to fully understand the behavior and intrinsic properties of the spin state governed reactions, the calculations have been carried out for biomimetic complex with L-N_2Me_2 ligand. Theoretical reaction profile with S12g DFA is shown in Figure 4-21 and Figure 4-22. The overall reaction pathway is very similar to the catalytic cycle of complex with the L-N_2H_2 ligand. The sextet state is the ground state for the superoxo intermediate (2), Figure 4-21, as well as for the final product, five-coordinate iron oxo complex. The quartet state governs the reaction mechanism and product distribution due to the fact that barrier for the O-O bond dissociation (TS_{34}) is very high in energy on a sextet PES. However, there are two notable differences. First, the step for the coordination of oxygene molecule, (1)→(2), is more exothermic. The obvious reason for this observation lies in the fact that after one of catechol oxygen's dissociates, it cannot form an H-bond, as in the previous investigated case, Figure 4-21. Secondly and most importantly, the energy difference between the particular TSs which determines the intradiol/extradiol selectivity is almost two times higher (3.4 kcal/mol) than in the case of complex with L-N_2H_2 ligand, Figure 4-22. This corroborates the experimental findings that iron(III) complex with a L-N_2Me_2 ligand is a selective intradiol cleaving biomimetic system.[209]

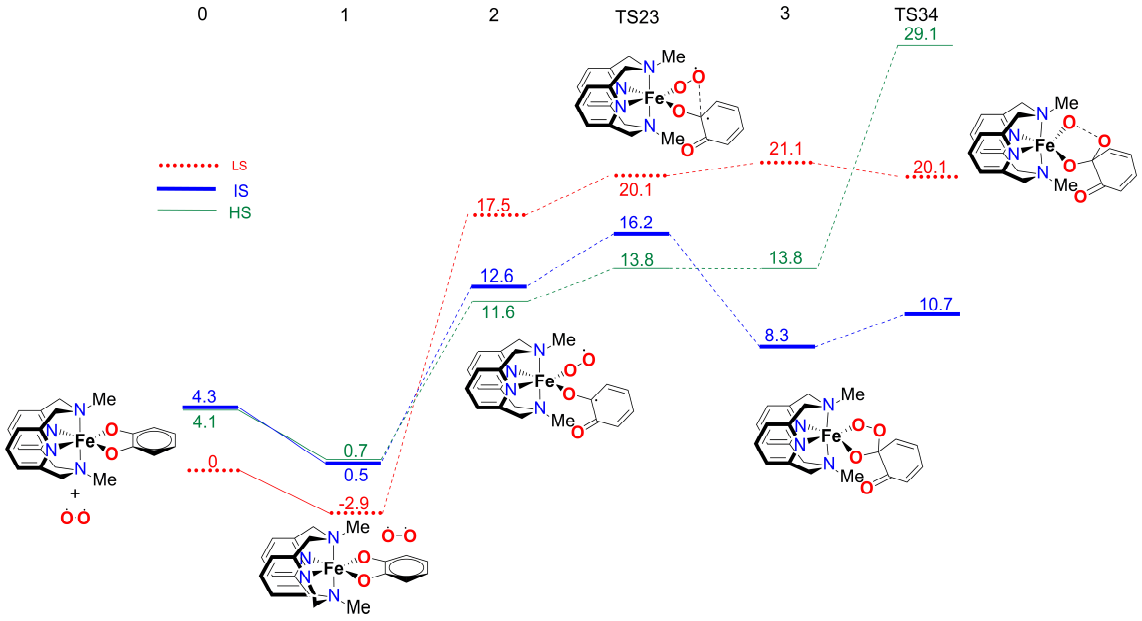

Figure 4-21 Calculated reaction profile, for the first part of the catechol dioxygenation mechanism, starting from the $[Fe(LN_4Me_2)(Cat)]^+$ complex, (0). Electronic energies, obtained using S12g/TZ2P level of theory, are given relative to the ground state of the initial complex (0).

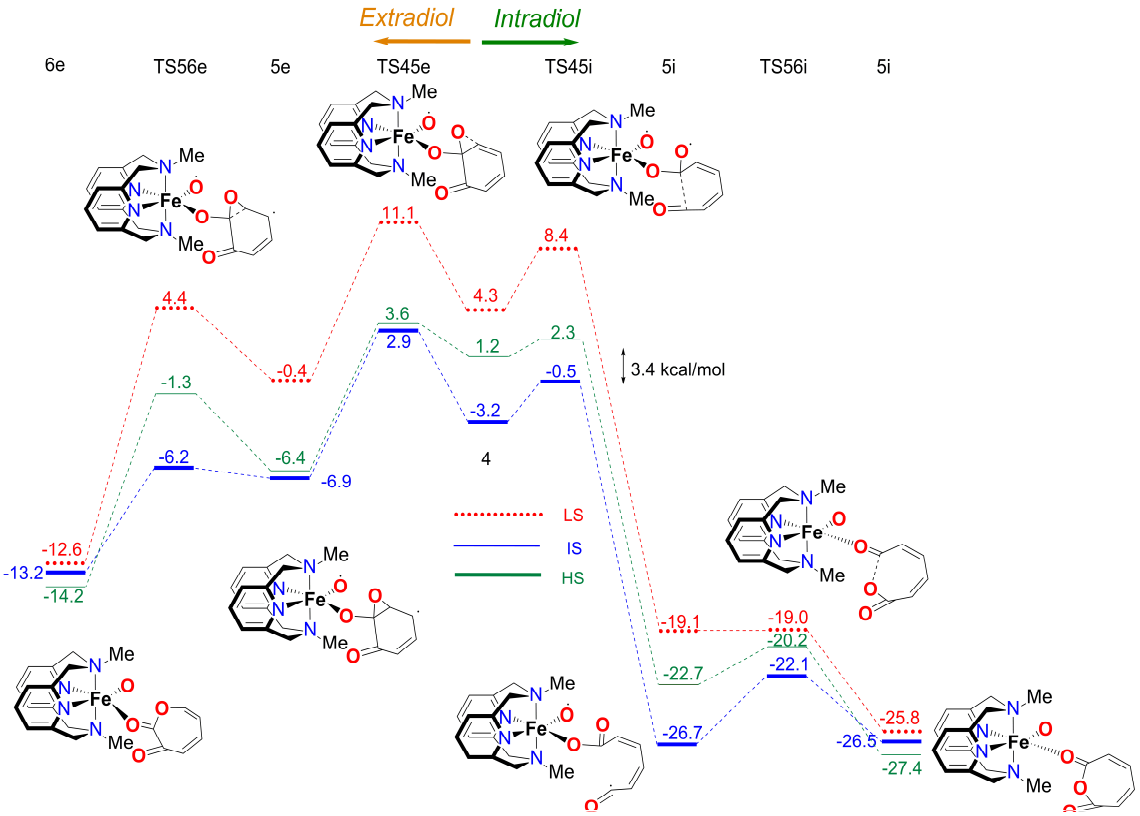

Figure 4-22 Calculated reaction profile for the second part of the catalytic mechanism with LN_4Me_2 ligand, branching to the intradiol and extradiol pathway. Electronic energies, obtained using S12g/TZ2P level of theory, are given relative to the ground state of the initial complex (0), from the Figure 4-21.

4.4.1.4. The difference in the product selectivity with complexes from L-N2H2 and L-N2Me2 ligand

The overall selectivity of the catalytic cycle is determined by the differences in the energies of the transition states for two reaction pathways, (TS_{45i}) for the intradiol and (TS_{45e}) for the extradiol direction. The difference in the intradiol/extradiol barriers can be explained in terms of the relative orientation of the substrate toward the bridging peroxide.[203] The extradiol pathway has a higher barrier, probably due to the necessity of reorientation of O (2p) orbital originated from O-O dissociation.[203] The reason of the difference in product selectivity for the two complexes, i.e. barrier heights at the branching point, can be found in the inspection of H-bonding of catechol substrate with

L-N_2H_2 ligand. During the intradiol pathway, H-bond with the L-N_2H_2 ligand is lost, as a consequence of C-C bond dissociation. This is not happening during the extradiol reaction path, explaining why the intradiol pathway is higher in energy and closer to the extradiol alternative with L-N_2H_2 ligand.

4.4.2. Conclusion

Density functional theory calculations have been performed on the reaction mechanism of the catechol cleaving dioxygenase biomimetic iron complexes, with L-N_2H_2 and L-N_2Me_2 ligands. Full details of the catalytic cycle, with all accessible spin states and two possible pathways, intradiol and extradiol, were determined. Our calculations show that the formation of both intradiol and extradiol products is substantially exothermic, but the intradiol product formation is thermodynamically more favorable. Although the sextet state is the ground state at the beginning and at the end of the catalytic cycle, only the quartet state is likely to be involved in an energetically plausible mechanism, completely determining the product distribution. The reason could be found in the very high barrier for the O-O bond dissociation of the specie in the sextet state. We demonstrated that the differences in the energies of the transition states for intradiol (TS_{45i}) and extradiol (TS_{45e}) pathways, Figure 4-20 and Figure 4-22, determine the selectivity and provides insight and deeper understanding of the experimental observations. Finally, the difference in in the intradiol/extradiol barriers is explained with the change in the H-bonding of catechol substrate with L-N_2H_2 ligand during the intradiol pathway.

4.4.3. Computational details

All DFT calculations were performed with the ADF suite of program(ADF 2016).[93,42] MOs were expanded in an uncontracted set of Slater type orbitals (STOs) of triple-ζ quality containing diffuse functions (TZ2P) [95] and two sets of polarization functions. Core electrons (1s for 2nd period, 1s2s2p for 3rd-4th period) were not treated explicitly during the geometry optimizations (frozen core approximation), as it was shown to have a negligible effect on the obtained geometries.[96] An auxiliary set of s, p, d, f, and g

STOs was used to fit the molecular density and to represent the Coulomb and exchange potentials accurately for each SCF cycle.

Geometries were optimized with the QUILD program[100] using adapted delocalized coordinates[101] until the maximum gradient component was less than 10^{-4} a.u. Energies and gradients were calculated using the S12g[47] DFA, with Becke grid[190,191] numerical accuracy of verygood quality. COSMO[97-99] dielectric continuum model was used for implicit treatment of the environment(with methanol as a solvent).[154,155] Scalar relativistic corrections have been included self-consistently by using the zeroth-order regular approximation (ZORA).[216-218] Nature of stationary points is confirmed by calculating analytical Hessians, with S12g/COSMO level of theory and Becke grid good integration parameters. Subsequent single point calculations that utilize all electron basis set have been performed on all optimized geometries, with S12g,[47] SSB-D[39] , M06-L[112,113], MVS[211] and S12h[47] levels of theory.

5. General Conclusion

The results presented in this thesis demonstrate modern theoretical approach for the accurate analysis of the spin states in transition metal systems. Recently developed DFAs were utilized, together with already proven levels of theory, in order to understand the connection between the spin state and the structure, properties and reactivity of a diverse class of transition-metal complexes that are biomimetic model systems and SCO candidates.

From the systematization of the influence of the geometrical parameters and implicit environment in studying challenging transition metal complexes and cytochrome p450 model systems, S12g emerged as excellent level of theory for both structural parameters and electronic structure of exotic transition metal systems. This has been repetitively demonstrated in the following years. As a accompanying conclusion, we turned the attention on the errors in combining gas phase and COSMO approaches in geometry optimization and single point calculations. Our recommendation was to avoid mixing these two methodologies. The influence of the spin state and the ligand charge on the binding modes for a Mn^{II}, Fe^{II}/Fe^{III}, Co^{II}, Ni^{II}, Cu^{II} and Zn^{II} for the 2,6-diacetylpyridine-bis(semioxamazide) ligand and its mono- and di-anionic analogues revealed the connection between the spin state of the central metal ion and the geometry of the formed complexes. The results were rationalized on the basis of molecular orbitals and they were interpreted as simple consequence of orbitals occupation. This simple rezoning also explained some other important experimental findings (the inability of N^{II} to form heptacoordinate complexes with dapsox ligand). Deeper understanding of complicated electronic structure of polypyrazolylborato complexes enabled us to rationalize the effects of substitution at the position 3 and 5 of pyrazolyl rings. This project resulted in clear and specific conclusions, and brought us a step closer to the ultimate goal: achieving explicit control of spin states of TM compounds through rational design of ligand coordination that will direct the synthesis of interesting and applicable SCO molecules and more selective and catalytically active biomimetic systems.

The obtained knowledge and the experience was a prerequisite to study und understand the mechanism of the catalytic cycle for catechol dioxygenase biomimetics. By using

DFA that showed best performance in the previous studies we unravelled the very complicated electronic structure and multiple spin state switchings between various intermediates in this important reaction. The model systems were selected not only because of their significance, but also due to their intriguing properties: similar biomimetic molecules give different products, and the abundance of short lived species with complicated electronic structure and close lying spin states in the catalytic cycle. The selectivity was attributed to the breaking of the hydrogen bond (in one of the structures) along the branching point of the catalytic mechanism. Provided results and rationalizations can assist in the design of more selective catechol dioxygenation biomimetics.

6. References

(1) Swart, M.; Costas, M. *Spin States in Biochemistry and Inorganic Chemistry: Influence on Structure and Reactivity*; Wiley, 2015.

(2) Worthington, S. E.; Cramer, C. J. *Journal of Physical Organic Chemistry* **1997**, *10*, 755.

(3) Scott, A. P.; Platz, M. S.; Radom, L. *J. Am. Chem. Soc.* **2001**, *123*, 6069.

(4) Harvey, J. In *Principles and Applications of Density Functional Theory in Inorganic Chemistry I*; Springer Berlin Heidelberg: 2004; Vol. 112, p 151.

(5) Clayden, J.; Greeves, N.; Warren, S. *Organic Chemistry*; OUP Oxford, 2012.

(6) Bersuker, I. B. *Electronic Structure and Properties of Transition Metal Compounds: Introduction to the Theory*; Wiley, 2010.

(7) Pfennig, B. W. *Principles of Inorganic Chemistry*; Wiley, 2015.

(8) Cook, S. A.; Lacy, D. C.; Borovik, A. S. In *Spin States in Biochemistry and Inorganic Chemistry*; John Wiley & Sons, Ltd: 2015, p 203.

(9) Deeth, R. J. In *Spin States in Biochemistry and Inorganic Chemistry*; John Wiley & Sons, Ltd: 2015, p 85.

(10) de Visser, S. P. In *Comprehensive Inorganic Chemistry II (Second Edition)*; Poeppelmeier, J. R., Ed.; Elsevier: Amsterdam, 2013, p 619.

(11) Ortiz de Montellano, P. R. *Chemical Reviews* **2009**, *110*, 932.

(12) Swart, M.; Gruden, M. *Accounts of Chemical Research* **2016**, *49*, 2690.

(13) Duboc, C.; Gennari, M. In *Spin States in Biochemistry and Inorganic Chemistry*; John Wiley & Sons, Ltd: 2015, p 59.

(14) Sousa, C.; de Graaf, C. In *Spin States in Biochemistry and Inorganic Chemistry*; John Wiley & Sons, Ltd: 2015, p 35.

(15) Griffith, J. S. *The Theory of Transition-Metal Ions*; Cambridge University Press, 1964.

(16) Van Vleck, J. H. *The theory of electric and magnetic susceptibilities*; Oxford University Press, 1952.

(17) Bethe, H. *Annalen der Physik* **1929**, *395*, 133.

(18) Cotton, F. A.; Wilkinson, G.; Murillo, C. A.; Bochmann, M. *ADVANCED INORGANIC CHEMISTRY, 6TH ED*; Wiley India Pvt. Limited, 2007.

(19) Greenwood, N. N.; Earnshaw, A. *Chemistry of the Elements*; Elsevier Science, 2012.

(20) Schläfer, H. L.; Gliemann, G. *Basic principles of ligand field theory*; Wiley-Interscience, 1969.

(21) Orgel, L. E. *An Introduction to Transition-metal Chemistry: Ligand-field Theory*; Methuen, 1966.

(22) Jørgensen, C. K. *Modern aspects of ligand field theory*; North-Holland Pub. Co., 1971.

(23) Ballhausen, C. J. *Introduction to ligand field theory*; McGraw-Hill, 1962.

(24) Koch, W.; Holthausen, M. C. *A chemist's guide to density functional theory*; Wiley-VCH, 2000.

(25) Wigner, E. *Physical Review* **1932**, *40*, 749.

(26) Thomas, L. H. *Mathematical Proceedings of the Cambridge Philosophical Society* **2008**, *23*, 542.

(27) Fermi, E. *Z. Phys.* **1928**, *48*, 73.

(28) Dirac, P. A. M. *Proceedings of the Royal Society A* **1931**, *123*, 714.

(29) Zettili, N. *Quantum Mechanics: Concepts and Applications*; Wiley, 2009.

(30) Perić, M. *Struktura i spektri molekula*; Srpska Akademija Nauka i Umetnosti, 2009.

(31) Szabo, A.; Ostlund, N. S. *Modern Quantum Chemistry: Introduction to Advanced Electronic Structure Theory*; Dover Publications, 1989.

(32) Piela, L. *Ideas of Quantum Chemistry*; Elsevier Science, 2006.

(33) Levine, I. N. *Quantum Chemistry*; Pearson Education, 2013.

(34) Parr, R. G.; Weitao, Y. *Density-Functional Theory of Atoms and Molecules (International Series of Monographs on Chemistry)*; Oxford University Press, 1994.

(35) Kohn, W.; Sham, L. J. *Physical Review* **1965**, *140*, A1133.

(36) Harvey, J. N. *Annual Reports Section "C" (Physical Chemistry)* **2006**, *102*, 203.

(37) Vosko, S. H.; Wilk, L.; Nusair, M. *Canadian Journal of Physics* **1980**, *58*, 1200.

(38) Cramer, C. J.; Truhlar, D. G. *Physical Chemistry Chemical Physics* **2009**, *11*, 10757.

(39) Swart, M.; Solà, M.; Bickelhaupt, F. M. *Journal of Chemical Physics* **2009**, *131*, 094103.

(40) Becke, A. D. *Physical Review A* **1988**, *38*, 3098.

(41) McQuarrie, D. A. *Quantum Chemistry*; University Science Books, 2008.

(42) te Velde, G.; Bickelhaupt, F. M.; Baerends, E. J.; Fonseca Guerra, C.; van Gisbergen, S. J. A.; Snijders, J. G.; Ziegler, T. *Journal of Computational Chemistry* **2001**, *22*, 931.

(43) Paulsen, H.; Duelund, L.; Winkler, H.; Toftlund, H.; Trautwein, A. X. *Inorg. Chem.* **2001**, *40*, 2201.

(44) Daul, C.; Zlatar, M.; Gruden-Pavlović, M.; Swart, M. In *Spin States in Biochemistry and Inorganic Chemistry*; John Wiley & Sons, Ltd: 2015, p 7.

(45) Swart, M. *Journal of Chemical Theory and Computation* **2008**, *4*, 2057.

(46) Swart, M.; Groenhof, A. R.; Ehlers, A. W.; Lammertsma, K. *Journal of Physical Chemistry A* **2004**, *108*, 5479.

(47) Swart, M. *Chemical Physics Letters* **2013**, *580*, 166.

(48) Swart, M.; Ehlers, A. W.; Lammertsma, K. *Molecular Physics* **2004**, *102*, 2467.

(49) Kepp, K. P. *Coordination Chemistry Reviews* **2013**, *257*, 196.

(50) Güell, M.; Luis, J. M.; Solà, M.; Swart, M. *The Journal of Physical Chemistry A* **2008**, *112*, 6384.

(51) Loew, G. H.; Harris, D. L. *Chemical Reviews* **2000**, *100*, 407.

(52) Ortiz de Montellano, P. R. *Cytochrome P450 structure, mechanism and biochemistry*; Plenum: New York, 1995.

(53) Harris, D.; Loew, G. *J. Am. Chem. Soc.* **1993**, *115*, 8775.

(54) Shaik, S.; Kumar, D.; de Visser, S. P.; Altun, A.; Thiel, W. *Chemical Reviews* **2005**, *105*, 2279.

(55) Schlichting, I.; Berendzen, J.; Chu, K.; Stock, A. M.; Maves, S. A.; Benson, D. E.; Sweet, B. M.; Ringe, D.; Petsko, G. A.; Sligar, S. G. *Science* **2000**, *287*, 1615.

(56) Limberg, C. *Angewandte Chemie-International Edition* **2003**, *42*, 5932.

(57) Ogliaro, F.; Harris, N.; Cohen, S.; Filatov, M.; de Visser, S. P.; Shaik, S. *J. Am. Chem. Soc.* **2000**, *122*, 8977.

(58) Filatov, M.; Harris, N.; Shaik, S. *Angewandte Chemie-International Edition* **1999**, *38*, 3510.

(59) Rittle, J.; Green, M. T. *Science* **2010**, *330*, 933.

(60) Park, M. J.; Lee, J.; Suh, Y.; Kim, J.; Nam, W. *J. Am. Chem. Soc.* **2006**, *128*, 2630.

(61) Hessenauer-Ilicheva, N.; Franke, A.; Meyer, D.; Woggon, W.-D.; van Eldik, R. *J. Am. Chem. Soc.* **2007**, *129*, 12473.

(62) Han, A.-R.; Jin Jeong, Y.; Kang, Y.; Yoon Lee, J.; Sook Seo, M.; Nam, W. *Chemical Communications* **2008**, 1076.

(63) Blomberg, M. R. A.; Borowski, T.; Himo, F.; Liao, R.-Z.; Siegbahn, P. E. M. *Chemical Reviews* **2014**, *114*, 3601.

(64) Ghosh, A.; Vangberg, T.; Gonzalez, E.; Taylor, P. *J. Porphyr. Phthalocyanines* **2001**, *5*, 345.

(65) Ghosh, A.; Persson, B. J.; Taylor, P. R. *J. Biol. Inorg. Chem.* **2003**, *8*, 507.

(66) Conradie, M. M.; Conradie, J.; Ghosh, A. *Journal of Inorganic Biochemistry* **2011**, *105*, 84.

(67) Ghosh, A.; Taylor, P. R. *Curr. Opin. Chem. Biol.* **2003**, *7*, 113.

(68) Kamachi, T.; Yoshizawa, K. *J. Am. Chem. Soc.* **2003**, *125*, 4652.

(69) Boone, A. J.; Chang, C. H.; Greene, S. N.; Herz, T.; Richards, N. G. J. *Coordination Chemistry Reviews* **2003**, *238–239*, 291.

(70) Noveron, J. C.; Olmstead, M. M.; Mascharak, P. K. *Inorg. Chem.* **1998**, *37*, 1138.

(71) Fallon, G. D.; Gatehouse, B. M.; Minari, P. J.; Murray, K. S.; West, B. O. *Journal of the Chemical Society Dalton Transactions* **1984**, 2733.

(72) Govindaswamy, N.; Quarless, D. A.; Koch, S. A. *J. Am. Chem. Soc.* **1995**, *117*, 8468.

(73) Sellmann, D.; Hofmann, T.; Knoch, F. *Inorganica Chimica Acta* **1994**, *224*, 61.

(74) Sellmann, D.; Kunstmann, H.; Knoch, F.; Moll, M. *Inorg. Chem.* **1988**, *27*, 4183.

(75) Sellmann, D.; Soglowek, W.; Knoch, F.; Ritter, G.; Dengler, J. *Inorg. Chem.* **1992**, *31*, 3711.

(76) Sellmann, D.; Utz, J.; Blum, N.; Heinemann, F. W. *Coordination Chemistry Reviews* **1999**, *192*, 607.

(77) Gruden, M.; Stepanovic, S.; Swart, M. *Journal of the Serbian Chemical Society* **2015**, *80*, 1399.

(78) Radoń, M.; Broclawik, E. *Journal of Chemical Theory and Computation* **2007**, *3*, 728.

(79) Ye, S.; Neese, F. *Inorg. Chem.* **2010**, *49*, 772.

(80) Liao, M.-S.; Scheiner, S. *Journal of Computational Chemistry* **2002**, *23*, 1391.

(81) Hamprecht, F. A.; Cohen, A. J.; Tozer, D. J.; Handy, N. C. *Journal of Chemical Physics* **1998**, *109*, 6264.

(82) Lee, C.; Yang, W.; Parr, R. G. *Physical Review B* **1988**, *37*, 785.

(83) Perdew, J. P.; Burke, K.; Ernzerhof, M. *Physical Review Letters* **1996**, *77*, 3865.

(84) Xu, X.; Goddard III, W. A. *Proceedings of the National Academy of Sciences USA* **2004**, *101*, 2673.

(85) Reiher, M.; Salomon, O.; Hess, B. A. *Theoretical Chemistry Accounts* **2001**, *107*, 48.

(86) Rydberg, P.; Sigfridsson, E.; Ryde, U. *J. Biol. Inorg. Chem.* **2004**, *9*, 203.

(87) Shaik, S.; Cohen, S.; de Visser, S. P.; Sharma, P. K.; Kumar, D.; Kozuch, S.; Ogliaro, F.; Danovich, D. *European Journal of Inorganic Chemistry* **2004**, 207.

(88) Shaik, S.; Cohen, S.; Wang, Y.; Chen, H.; Kumar, D.; Thiel, W. *Chemical Reviews* **2009**, *110*, 949.

(89) Li, D.; Wang, Y.; Han, K. *Coordination Chemistry Reviews* **2012**, *256*, 1137.

(90) Wittbrodt, J. M.; Schlegel, H. B. *Journal of Chemical Physics* **1996**, *105*, 6574.

(91) Lonsdale, R.; Harvey, J. N.; Mulholland, A. J. *Journal of Chemical Theory and Computation* **2012**, *8*, 4637.

(92) Lonsdale, R.; Harvey, J. N.; Mulholland, A. J. *The Journal of Physical Chemistry Letters* **2010**, *1*, 3232.

(93) Baerends, E. J.; Autschbach, J.; Berces, A.; Bo, C.; Boerrigter, P. M.; Cavallo, L.; Chong, D. P.; Deng, L.; Dickson, R. M.; Ellis, D. E.; Fan, L.; Fischer, T. H.; Fonseca Guerra, C.; van Gisbergen, S. J. A.; Groeneveld, J. A.; Gritsenko, O. V.; Grüning, M.; Harris, F. E.; van den Hoek, P.; Jacobsen, H.; van Kessel, G.; Kootstra, F.; van Lenthe, E.; Osinga, V. P.; Patchkovskii, S.; Philipsen, P. H. T.; Post, D.; Pye, C. C.; Ravenek, W.; Ros, P.; Schipper, P. R. T.; Schreckenbach, G.; Snijders, J. G.; Solà, M.; Swart, M.; Swerhone, D.; te Velde, G.; Vernooijs, P.; Versluis, L.; Visser, O.; van Wezenbeek, E.; Wiesenekker, G.; Wolff, S. K.; Woo, T. K.; Ziegler, T.; SCM: Amsterdam.

(94) Guerra, C. F.; Snijders, J. G.; teVelde, G.; Baerends, E. *Theoretical Chemistry Accounts* **1998**, *99*, 391.

(95) van Lenthe, E.; Baerends, E. J. *Journal of Computational Chemistry* **2003**, *24*, 1142.

(96) Swart, M.; Snijders, J. G. *Theoretical Chemistry Accounts* **2003**, *110*, 34.

(97) Klamt, A.; Jonas, V. *The Journal of Chemical Physics* **1996**, *105*, 9972.

(98) Klamt, A. *The Journal of Physical Chemistry* **1995**, *99*, 2224.

(99) Klamt, A.; Schuurmann, G. *Journal of the Chemical Society, Perkin Transactions 2* **1993**, 799.

(100) Swart, M.; Bickelhaupt, F. M. *Journal of Computational Chemistry* **2008**, *29*, 724.

(101) Swart, M.; Bickelhaupt, F. M. *International Journal of Quantum Chemistry* **2006**, *106*, 2536.

(102) Slater, J. C. *Physical Review* **1951**, *81*, 385.

(103) Handy, N. C.; Cohen, A. J. *Molecular Physics* **2001**, *99*, 403.

(104) Perdew, J. P. *Physical Review B* **1986**, *33*, 8822.

(105) van Voorhis, T.; Scuseria, G. *Journal of Chemical Physics* **1998**, *109*, 400.

(106) Gruening, M.; Gritsenko, O.; Baerends, E. J. *Journal of Physical Chemistry A* **2004**, *108*, 4459.

(107) Krieger, J. B.; Chen, J.; Iafrate, G. J.; Savin, A. In *Electron Correlations and Materials Properties*; Gonis, A., Kioussis, N., Eds.; Plenum: New York, 1999.

(108) Becke, A. D. *Journal of Chemical Physics* **2000**, *112*, 4020.

(109) Filatov, M.; Thiel, W. *Molecular Physics* **1997**, *91*, 847.

(110) Becke, A. D. *The Journal of Chemical Physics* **1997**, *107*, 8554.

(111) Tao, J. M.; Perdew, J. P.; Staroverov, V. N.; Scuseria, G. E. *Physical Review Letters* **2003**, *91*, 146401.

(112) Zhao, Y.; Truhlar, D. G. *Theoretical Chemistry Accounts* **2008**, *120*, 215.

(113) zhao, y.; Truhlar, D. G. *Journal of Chemical Physics* **2006**, *125*, 194101.

(114) Adamo, C.; Barone, V. *The Journal of Chemical Physics* **1999**, *110*, 6158.

(115) Becke, A. D. *Journal of Chemical Physics* **1993**, *98*, 5648.

(116) Stephens, P. J.; Devlin, F. J.; Chabalowski, C. F.; Frisch, M. J. *Journal of Physical Chemistry* **1994**, *45*, 11623.

(117) Adamo, C.; Barone, V. *Chemical Physics Letters* **1997**, *274*, 242.

(118) Zhang, D.; Busch, D. H.; Lennon, P. L.; Weiss, R. H.; Neumann, W. L.; Riley, D. P. *Inorg. Chem.* **1998**, *37*, 956.

(119) Gutman, C. T.; Brunold, T. C. *Inorg. Chem.* **2012**, *51*, 12729−12737.

(120) Lieb, D.; Friedel, F. C.; Yawer, M.; Zahl, A.; Khusniyarov, M. M.; Heinemann, F. W.; Ivanović-Burmazović, I. *Inorg. Chem.* **2013**, *52*, 222−236.

(121) Ivanović-Burmazović, I.; Anđelković, K. *Advances In Inorganic Chemistry* **2004**, *55*, 315.

(122) Šumar, M.; Ivanović-Burmazović, I.; Hodžić, I.; Andjelković, K. *Synthesis and Reactivity in Inorganic and Metal-Organic Chemistry* **2002**, *32*, 721.

(123) Liu, G.-F.; Filipović, M.; Heinemann, F. W.; Ivanovíc-Burmazović, I. *Inorg. Chem.* **2007**, *46*, 8825−8835.

(124) Andelković, K.; Ivanović, I.; Prelesnik, B. V.; Leovac, V. M.; Poleti, D. *Polyhedron* **1996**, *15*, 4361.

(125) Andjelković, K.; Bacchi, A.; Pelizzi, G.; Jeremić, D.; Ivanović-Burmazović, I. *Journal of Coordination Chemistry* **2002**, *55*, 1385.

(126) Ivanović-Burmazović, I.; Bacchi, A.; Pelizzi, G.; Leovac, V. M.; Andjelković, K. *Polyhedron* **1999**, *18*, 119.

(127) Ivanović, I.; Andelković, K.; Beljanski, V.; Prelesnik, B. V.; Leovac, V. M.; Momirović, M. *Journal of Coordination Chemistry* **1997**, *42*, 335.

(128) Bacchi, A.; Ivanović-Burmazović, I.; Pelizzi, G.; Andjelković, K. *Inorganica Chimica Acta* **2001**, *313*, 109.

(129) Pelizzi, G.; Bacchi, A.; Ivanović-Burmazović, I.; Gruden, M.; Andjelković, K. *Inorganic Chemistry Communications* **2001**, *4*, 311.

(130) Andelković, K.; Ivanović, I.; Niketić, S. R.; Prelesnik, B. V.; Leovac, V. M. *Polyhedron* **1997**, *16*, 4221.

(131) Swart, M. *International Journal of Quantum Chemistry* **2013**, *113*, 2.

(132) Remacle, F.; Grandjean, F.; Long, G. *Inorg. Chem.* **2008**, *47*, 4005.

(133) Dees, A.; Zahl, A.; Puchta, R.; van Eikema Hommes, N. J. R.; Heinemann, F. W.; Ivanović-Burmazović, I. *Inorg. Chem.* **2007**, *46*, 2459.

(134) Ivanović-Burmazović, I.; Hamza, M. S. A.; van Eldik, R. *Inorg. Chem.* **2006**, *45*, 1575.

(135) Sarauli, D.; Meier, R.; Liu, G.-F.; Ivanović-Burmazović, I.; van Eldik, R. *Inorg. Chem.* **2005**, *44*, 7624.

(136) Gutman, C. T.; Guzei, I. A.; Brunold, T. C. *Inorg. Chem.* **2013**, *52*, 8909−8918.

(137) Jackson, T. A.; Gutman, C. T.; Maliekal, J.; Miller, A.-F.; Brunold, T. C. *Inorg. Chem.* **2013**, *52*, 3356.

(138) Sarauli, D.; Popova, V.; Zahl, A.; Puchta, R.; Ivanović-Burmazović, I. *Inorg. Chem.* **2007**, *46*, 7848.

(139) Sarauli, D.; van Eldik , R.; Ivanović-Burmazović, I. *BioInorg. React. Mech.* **2012**, *8*, 107.

(140) Hoffmann, R.; Beier, B. F.; Muetterties, E. L.; Rossi, A. R. *Inorg. Chem.* **1977**, *16*, 511.

(141) Stepanovic, S.; Andjelkovic, L.; Zlatar, M.; Andjelkovic, K.; Gruden-Pavlovic, M.; Swart, M. *Inorg. Chem.* **2013**, *52*.

(142) Zlatar, M.; Gruden-Pavlović, M.; Güell, M.; Swart, M. *Physical Chemistry Chemical Physics* **2013**, *15*, 6631.

(143) Andjelković, L.; Gruden-Pavlović, M.; Daul, C.; Zlatar, M. *International Journal of Quantum Chemistry* **2013**, *113*, 859.

(144) Bray, M. R.; Deeth, R. J.; Paget, V. J.; Sheen, P. D. *International Journal of Quantum Chemistry* **1996**, *61*, 85.

(145) Kundu, T. K.; Bruyndonckx, R.; Daul, C.; Manoharan, P. T. *Inorg. Chem.* **1999**, *38*, 3931.

(146) Deeth, R. J.; Brooke Jenkins, H. D. *Journal of Physical Chemistry A* **1997**, *101*, 4793.

(147) Ghosh, A. *J. Biol. Inorg. Chem.* **2006**, *11*, 712.

(148) Gaspar, A. B.; Ksenofontov, V.; Reiman, S.; Gütlich, P.; Thompson, A. L.; Goeta, A. E.; Muñoz, M. C.; Real, J. A. *Chemistry-a European Journal* **2006**, *12*, 9289

(149) Gütlich, P.; Gaspar, A. B.; Garcia, Y. *Beilstein Journal of Organic Chemistry* **2013**, *9*, 342.

(150) McGrath, C. M.; O'Connor, C. J.; Sangregorio, C.; Seddon, J. M. W.; Sinn, E.; Sowrey, F. E.; Young, N. A. *Inorganic Chemistry Communications* **1999**, *2*, 536.

(151) Yan, J.-Q.; Zhou, J.-S.; Goodenough, J. B. *Physical Review B* **2004**, *69*, 1.

(152) Shaik, S.; Chen, H.; Janardanan, D. *Nature Chemistry* **2011**, *3*, 19.

(153) Swart, M.; Solà, M.; Bickelhaupt, F. M. *Journal of Computational Methods in Science and Engineering* **2009**, *9*, 69.

(154) Pye, C. C.; Ziegler, T. *Theoretical Chemistry Accounts* **1999**, *101*, 396.

(155) Swart, M.; Rösler, E.; Bickelhaupt, F. M. *European Journal of Inorganic Chemistry* **2007**, 3646.

(156) Trofimenko, S. *Chemical Reviews* **1993**, *93*, 943.

(157) Trofimenko, S. *Scorpionates: The Coordination Chemistry of Polypyrazolylborate Ligands*; Imperial College Press, 1999.

(158) Trofimenko, S. *Polyhedron* **2004**, *23*, 197.

(159) Güell, M.; Solà, M.; Swart, M. *Polyhedron* **2010**, *29*, 84.

(160) Halcrow, M. A. *Chemical Society Reviews* **2011**, *40*, 4119.

(161) Jesson, J. P.; Trofimenko, S.; Eaton, D. R. *J. Am. Chem. Soc.* **1967**, *89*, 3148.

(162) Jesson, J. P.; Trofimenko, S.; Eaton, D. R. *J. Am. Chem. Soc.* **1967**, *89*, 3158.

(163) Reger, D. L.; Gardinier, J. R.; Elgin, J. D.; Smith, M. D. *Inorg. Chem.* **2006**, *45*, 8862.

(164) Salmon, L.; Molnar, G.; Cobo, S.; Oulie, P.; Etienne, M.; Mahfoud, T.; Demont, P.; Eguchi, A.; Watanabe, H.; Tanakae, K.; Bousseksou, A. *New Journal of Chemistry* **2009**, *33*, 1283.

(165) Swart, M.; Güell, M.; Solà, M. In *Quantum Biochemistry: Electronic structure and biological activity*; Matta, C. F., Ed.; Wiley-VCH: Weinheim-Germany, 2010; Vol. 2, p 551.

(166) Forshaw, A. P.; Smith, J. M.; Ozarowski, A.; Krzystek, J.; Smirnov, D.; Zvyagin, S. A.; Harris, T. D.; Karunadasa, H. I.; Zadrozny, J. M.; Schnegg, A.; Holldack, K.; Jackson, T. A.; Alamiri, A.; Barnes, D. M.; Telser, J. *Inorg. Chem.* **2013**, *52*, 144.

(167) Tierney, D. L. *The Journal of Physical Chemistry A* **2012**, *116*, 10959−10972.

(168) Lobbia, G. G.; Bovio, B.; Santini, C.; Pettinari, C.; Marchetti, F. *Polyhedron* **1997**, *16*, 671.

(169) Chanaka, D.; Alwis, L. D.; Schultz, F. A. *Inorg. Chem.* **2003**, *42*, 3616.

(170) Alsfasser, R.; Powell, A. K.; Vahrenkamp, H. *Angewandte Chemie International Edition* **1990**, *29*, 898.

(171) D., Q.; T., K. L.; N., K.; G., S. T. *J. Am. Chem. Soc.* **1994**, *116*, 2585.

(172) Calabrese, J. C.; Trofimenko, S.; Thompson, J. S. *Journal of the Chemical Society, Chemical Communications* **1986**, 1122.

(173) Bergquist, C.; Fillebeen, T.; Morlok, M. M.; Parkin, G. *J. Am. Chem. Soc.* **2003**, *125*, 6189.

(174) Parkin, G. *Chemical Reviews* **2004**, *104*, 699.

(175) Cecchi, P.; Berrettoni, M.; Giorgetti, M.; Lobbia, G. G.; Calogero, S.; Stievano, L. *Inorganica Chimica Acta* **2001**, *318*, 67.

(176) Churchill, M. R.; Gold, K.; Maw, C. E. *Inorg. Chem.* **1970**, *9*, 1597.

(177) Mason, S. J.; Hill, C. M.; Murphy, V. J.; O'Hare, D.; Watkin, D. J. *Journal of Organometallic Chemistry* **195**, *485*, 165.

(178) Calogero, S.; Lobbia, G.; Cecchi, P.; Valle, G.; Friedl, J. *Polyhedron* **1994**, *13*, 87.

(179) Swart, M. *Chemical Communications* **2013**, *49*, 6650.

(180) Kitano, T.; Sohrin, Y.; Hata, Y.; Kawakami, H.; Horib, T.; Ueda, K. *Journal of the Chemical Society, Dalton* **2001**, 3564.

(181) Oliver, J. D.; Mullica, D. F.; Hutchinson, B. B.; Milligan, W. O. *Inorg. Chem.* **1980**, *19*, 165.

(182) Abrams, M. J.; Faggiani, R.; Lock, C. J. L. *Inorganica Chimica Acta* **1985**, *106*, 69.

(183) Fujiharaa, T.; Schönherrb, T.; Kaizaki, S. *Inorganica Chimica Acta* **1996**, *249*, 135.

(184) Hossain, F.; Rigsby, M. A.; Duncan, C. T.; Milligan, P. L.; Lord, R. L.; Baik, M.-H.; Schultz, F. A. *Inorg. Chem.* **2007**, *46*, 2596.

(185) Cho, S. H.; Whang, D.; Kim, K. *Bulletin of the Korean Chemical Society* **1991**, *12*, 107.

(186) Curnow, O. J.; Nicholson, B. K. *Journal of Organometallic Chemistry* **1984**, *267*, 257.

(187) Chan, M. K.; Armstrong, W. H. *Inorg. Chem.* **1989**, *28*, 3777.

(188) Wieghardt, K.; Schmidt, W.; Herrmann, W.; Kuppers, H. J. *Inorg. Chem.* **1983**, *22*, 2953.

(189) Hannay, C.; Hubin-Franskin, M. J.; Grandjean, F.; Briois, V.; Itie, J. P.; Polian, A.; Trofimenko, S.; Long, G. J. *Inorg. Chem.* **1997**, *36*, 5580.

(190) Becke, A. D. *Journal of Chemical Physics* **1988**, *88*, 2547.

(191) Franchini, M.; Philipsen, P. H. T.; Visscher, L. *Journal of Computational Chemistry* **2013**, *34*, 1819.

(192) Zlatar, M.; Schlaepfer, C.-W.; Daul, C. In *The Jahn–Teller-Effect Fundamentals and Implications for Physics and Chemistry*; Koeppel, H., Yarkoni, D. R., Barentzen, H., Eds.; Springer: Heidelberg, Dordrecht, London, New York, 2009; Vol. 97, p 131.

(193) Bruyndonckx, R.; Daul, C.; Manoharan, P. T.; Deiss, E. *Inorg. Chem.* **1997**, *36*, 4251.

(194) Gruden-Pavlovic, M.; Garcia-Fernandez, P.; Andjelkovic, L.; Daul, C.; Zlatar, M. *J. Phys. Chem. A* **2011**, *115*, 10801.

(195) Gruden-Pavlovic, M.; Zlatar, M.; Schlaepfer, C.-W.; Daul, C. *THEOCHEM* **2010**, *954*, 80.

(196) Costas, M.; Mehn, M. P.; Jensen, M. P.; Que, L. *Chemical Reviews* **2004**, *104*, 939.

(197) Brown, C. K.; Vetting, M. W.; Earhart, C. A.; Ohlendorf, D. H. *Annual Review of Microbiology* **2004**, *58*, 555.

(198) Lippard, S. J.; Berg, J. M.; University Science Books 1994, p 411.

(199) Silva, J. J. R. F. d.; Williams, R. J. P. *The Biological Chemistry of the Elements*; Oxford University Press, 2001.

(200) Ray, K.; Pfaff, F. F.; Wang, B.; Nam, W. *J. Am. Chem. Soc.* **2014**, *136*, 13942.

(201) Company, A.; Lloret-Fillol, J.; Costas, M. In *Comprehensive Inorganic Chemistry II (Second Edition)*; Poeppelmeier, J. R., Ed.; Elsevier: Amsterdam, 2013, p 487.

(202) Jastrzebski, R.; Quesne, M. G.; Weckhuysen, B. M.; de Visser, S. P.; Bruijnincx, P. C. A. *Chemistry – A European Journal* **2014**, *20*, 15686.

(203) Georgiev, V.; Noack, H.; Borowski, T.; Blomberg, M. R. A.; Siegbahn, P. E. M. *The Journal of Physical Chemistry B* **2010**, *114*, 5878.

(204) Chatterjee, S.; Sheet, D.; Paine, T. K. *Chemical Communications* **2013**, *49*, 10251.

(205) Panda, M. K.; John, A.; Shaikh, M. M.; Ghosh, P. *Inorg. Chem.* **2008**, *47*, 11847.

(206) Carvalho, A. T. P.; Barrozo, A.; Doron, D.; Kilshtain, A. V.; Major, D. T.; Kamerlin, S. C. L. *Journal of Molecular Graphics and Modelling* **2014**, *54*, 62.

(207) Gruden-Pavlović, M.; Stepanović, S.; Perić, M.; Güell, M.; Swart, M. *Physical Chemistry Chemical Physics* **2014**, *16*, 14514.

(208) Pandey, B.; Ansari, A.; Vyas, N.; Rajaraman, G. *J Chem Sci* **2015**, *127*, 343.

(209) Koch, W. O.; Krüger, H.-J. *Angewandte Chemie International Edition in English* **1996**, *34*, 2671.

(210) Raffard, N.; Carina, R.; Simaan, A. J.; Sainton, J.; Rivière, E.; Tchertanov, L.; Bourcier, S.; Bouchoux, G.; Delroisse, M.; Banse, F.; Girerd, J.-J. *European Journal of Inorganic Chemistry* **2001**, *2001*, 2249.

(211) Sun, J.; Perdew, J. P.; Ruzsinszky, A. *Proceedings of the National Academy of Sciences* **2015**, *112*, 685.

(212) Stepanovic, S.; Angelone, D.; Gruden, M.; Swart, M. *Organic & Biomolecular Chemistry* **2017**, *15*, 7860.

(213) Mbughuni, M. M.; Chakrabarti, M.; Hayden, J. A.; Bominaar, E. L.; Hendrich, M. P.; Münck, E.; Lipscomb, J. D. *Proceedings of the National Academy of Sciences* **2010**, *107*, 16788.

(214) Chiang, C.-W.; Kleespies, S. T.; Stout, H. D.; Meier, K. K.; Li, P.-Y.; Bominaar, E. L.; Que, L.; Münck, E.; Lee, W.-Z. *J. Am. Chem. Soc.* **2014**, *136*, 10846.

(215) Knoot, C. J.; Purpero, V. M.; Lipscomb, J. D. *Proceedings of the National Academy of Sciences* **2015**, *112*, 388.

(216) van Lenthe, E.; Ehlers, A.; Baerends, E.-J. *The Journal of Chemical Physics* **1999**, *110*, 8943.

(217) van Lenthe, E.; Baerends, E. J.; Snijders, J. G. *The Journal of Chemical Physics* **1994**, *101*, 9783.

(218) Lenthe, E. v.; Baerends, E. J.; Snijders, J. G. *The Journal of Chemical Physics* **1993**, *99*, 4597.

Biography

Stepan Stepanović (born in 1985, Belgrade) finished elementary school in Barič and recived medical secondary education in Belgrade. He graduated in 2011 at the Faculty of Chemistry, University of Belgrade, at study program Chemistry. He finished Master studies at the Faculty of Chemistry, University of Belgrade in 2012, and in the same year he started the PhD studies. He was employed as a research trainee at the Center for Chemistry of the Institute of Chemistry, Technology and Metallurgy in Belgrade at October 2012. He became a research associate in 2014 at the same institution. He is a member of the Serbian Chemical Society. He participated in teaching at the following courses, at the Faculty of Chemistry, university of Belgrade:

- Theory of Chemical Bonding
- Inorganic Chemistry

He is a member of COST Action CM1305 (ECOSTBio: Explicit Control Over Spin-states in Technology and Biochemistry) and has visited the University of Girona, Spain, for 2 months (November - December 2014), during the Short-Term Scientific Mission, COST-STSM-CM1305-21136. In 2015 he was awarded by EYCN (European Young Chemists Network) the best poster presentation during the 3rd Conference of Young Chemists of Serbia. He is coauthor on 13 scientific papers.

List of scientific papers that are part of the doctoral dissertation:

1. **Stepanović, S.**, Angelone, D., Gruden, M., Swart, M. *The role of spin states in the catalytic mechanism of the intra- and extradiol cleavage of catechols by O2*. Organic and Biomolecular Chemistry, **2017**, 15 (37), 7860-7868.

2. Gruden, M., **Stepanovic, S.**, Swart, M. *Spin state relaxation of iron complexes: The case for OPBE and S12g,* Journal of the Serbian Chemical Society, **2015**, 80 (11), 1399-1410.

3. Gruden-Pavlović, M., **Stepanović, S.**, Perić, M., Güell, M., Swart, M. *A density functional study of the spin state energetics of polypyrazolylborato complexes of*

first-row transition metals, Physical Chemistry Chemical Physics, **2014**, 16 (28), 14514-14522.

4. **Stepanović, S.**, Andjelković, L., Zlatar, M., Andjelković, K., Gruden-Pavlović, M., Swart, M. *Role of spin state and ligand charge in coordination patterns in complexes of 2,6-diacetylpyridinebis(semioxamazide) with 3d-block metal ions: A density functional theory study.* Inorganic Chemistry, **2013**, 52 (23), 13415-13423.

List of scientific papers thet are not included in the doctoral dissertation:

1. Browne, R. W., Chen, J., Draksharapu, A., Gruden, M., **Stepanovic, S.** *A non-heme iron photocatalyst for light driven aerobic oxidation of methanol.* Angewandte Chemie International Edition, **2018**, DOI: 10.1002/anie.201712678

2. Gruden, M., Andjeklović, L., Jissy, A.K., **Stepanović, S.**, Zlatar, M., Cui, Q., Elstner, M. *Benchmarking density functional tight binding models for barrier heights and reaction energetics of organic molecules.* Journal of Computational Chemistry, **2017**, 38 (25), 2171-2185.

3. Ajdačić, V., **Stepanović, S.**, Zlatović, M., Gruden, M., Opsenica, I.M. *Decarbonylative Dibromination of 5-Phenylthiophene-2-carbaldehyde with Bromine.* Synthesis (Germany), **2016**, 48 (24), 4423-4430.

4. Fitzpatrick, A.J., **Stepanovic, S.**, Müller-Bunz, H., Gruden-Pavlović, M.A., García-Fernández, P., Morgan, G.G. *Challenges in assignment of orbital populations in a high spin manganese(iii) complex.* Dalton Transactions, **2016**, 45 (15), 6702-6708.

5. Popović-Djordjević, J., **Stepanović, S.**, Došen-Mićović, L., Ivanović, E., Ivanović, M.D. *High-yielding method for preparation of carbocyclic or N-containing heterocyclic β-keto esters using in situ activated sodium hydride in dimethyl sulphoxide,* Green Chemistry Letters and Reviews, **2016**, 9 (1), 61-68.

6. Andjelković, L., **Stepanović, S.**, Vlahović, F., Zlatar, M., Gruden, M. *Resolving the origin of the multimode Jahn-Teller effect in metallophthalocyanines,* Physical Chemistry Chemical Physics, **2016**, 18 (42), 29122-29130.

7. Adhikary, J., Chakraborty, A., Dasgupta, S., Chattopadhyay, S.K., Kruszynski, R., Trzesowska-Kruszynska, A., **Stepanović, S.**, Gruden-Pavlović, M., Swart, M., Das, D. *Unique mononuclear MnII complexes of an end-off compartmental Schiff base ligand: Experimental and theoretical studies on their bio-relevant catalytic promiscuity,* Dalton Transactions, **2016**, 45 (31), 12409-12422.

8. Čobeljić, B., Pevec, A., **Stepanović, S.**, Spasojević, V., Milenković, M., Turel, I., Swart, M., Gruden-Pavlović, M., Adaila, K., Anelković, K. *Experimental and theoretical investigation of octahedral and square-planar isothiocyanato complexes of Ni(II) with acylhydrazones of 2-(diphenylphosphino)benzaldehyde,* Polyhedron, **2015**, 89, 271-279.

9. Perić, M., García-Fuente, A., Zlatar, M., Daul, C., **Stepanović, S.**, García-Fernández, P., Gruden-Pavlović, M. *Magnetic anisotropy in "scorpionate" first-row transition-metal complexes: A theoretical investigation,* Chemistry - A European Journal, **2015**, 21 (9), 3716-3726.

Biografija

Stepan Stepanović (rođ. 1985. godine u Beogradu) završio je osnovnu školu u Bariču i Srednju Medicinsku školu u Beogradu. Diplomirao je 2011. godine na Hemijskom fakultetu Univerziteta u Beogradu, na smeru Hemija. Završio je master studije na Hemijskom fakultetu Univerziteta u Beogradu 2012. godine, a iste godine je upisao i doktorske studije. Zaposlio se kao istraživač-pripravnik pri Centru za hemiju Instituta za hemiju, tehnologiju i metalurgiju u Beogradu, Oktobra 2012. godine. 2014. godine izabran je u zvanje istraživač-saradnik. Član je Srpskog hemijskog društva. Učestvovao je u izvođenju nastave na Hemijskom fakultetu Univerziteta u Beogradu iz sledećih predmeta:

- Teorija Hemijske Veze
- Neorganska Hemija

Član je COST akcije CM1305 (ECOSTBio: Explicit Control Over Spin-states in Technology and Biochemistry) i boravio je u Španiji, na Univerzitetu u Đironi 2 meseca (novembar - decembar 2014), tokom Short-Term Scientific Mission, COST-STSM-CM1305-21136. 2015 godine je nagrađen od strane EYCN (European Young Chemists Network) za najbolje postersko saopštenje na III konferenciji mladih hemičara Srbije. Koautor je na 13 naučnih radova.

Spisak naučnih radova koji čine deo doktorske disertacije:

1. **Stepanović, S.**, Angelone, D., Gruden, M., Swart, M. *The role of spin states in the catalytic mechanism of the intra- and extradiol cleavage of catechols by O2*. Organic and Biomolecular Chemistry, **2017**, 15 (37), 7860-7868.

2. Gruden, M., **Stepanovic, S.**, Swart, M. *Spin state relaxation of iron complexes: The case for OPBE and S12g,* Journal of the Serbian Chemical Society, **2015**, 80 (11), 1399-1410.

3. Gruden-Pavlović, M., **Stepanović, S.**, Perić, M., Güell, M., Swart, M. *A density functional study of the spin state energetics of polypyrazolylborato complexes of*

first-row transition metals, Physical Chemistry Chemical Physics, **2014**, 16 (28), 14514-14522.

4. **Stepanović, S.**, Andjelković, L., Zlatar, M., Andjelković, K., Gruden-Pavlović, M., Swart, M. *Role of spin state and ligand charge in coordination patterns in complexes of 2,6-diacetylpyridinebis(semioxamazide) with 3d-block metal ions: A density functional theory study.* Inorganic Chemistry, **2013**, 52 (23), 13415-13423.

Spisak naučnih radova koji nisu deo doktorske disertacije:

1. Browne, R. W., Chen, J., Draksharapu, A., Gruden, M., **Stepanovic, S.** *A non-heme iron photocatalyst for light driven aerobic oxidation of methanol.* Angewandte Chemie International Edition, **2018**, DOI: 10.1002/anie.201712678

2. Gruden, M., Andjeklović, L., Jissy, A.K., **Stepanović, S.**, Zlatar, M., Cui, Q., Elstner, M. *Benchmarking density functional tight binding models for barrier heights and reaction energetics of organic molecules.* Journal of Computational Chemistry, **2017**, 38 (25), 2171-2185.

3. Ajdačić, V., **Stepanović, S.**, Zlatović, M., Gruden, M., Opsenica, I.M. *Decarbonylative Dibromination of 5-Phenylthiophene-2-carbaldehyde with Bromine.* Synthesis (Germany), **2016**, 48 (24), 4423-4430.

4. Fitzpatrick, A.J., **Stepanovic, S.**, Müller-Bunz, H., Gruden-Pavlović, M.A., García-Fernández, P., Morgan, G.G. *Challenges in assignment of orbital populations in a high spin manganese(iii) complex.* Dalton Transactions, **2016**, 45 (15), 6702-6708.

5. Popović-Djordjević, J., **Stepanović, S.**, Došen-Mićović, L., Ivanović, E., Ivanović, M.D. *High-yielding method for preparation of carbocyclic or N-*

containing heterocyclic β-keto esters using in situ activated sodium hydride in dimethyl sulphoxide, Green Chemistry Letters and Reviews, **2016**, 9 (1), 61-68.

6. Andjelković, L., **Stepanović, S.**, Vlahović, F., Zlatar, M., Gruden, M. *Resolving the origin of the multimode Jahn-Teller effect in metallophthalocyanines,* Physical Chemistry Chemical Physics, **2016**, 18 (42), 29122-29130.

7. Adhikary, J., Chakraborty, A., Dasgupta, S., Chattopadhyay, S.K., Kruszynski, R., Trzesowska-Kruszynska, A., **Stepanović, S.**, Gruden-Pavlović, M., Swart, M., Das, D. *Unique mononuclear MnII complexes of an end-off compartmental Schiff base ligand: Experimental and theoretical studies on their bio-relevant catalytic promiscuity,* Dalton Transactions, **2016**, 45 (31), 12409-12422.

8. Čobeljić, B., Pevec, A., **Stepanović, S.**, Spasojević, V., Milenković, M., Turel, I., Swart, M., Gruden-Pavlović, M., Adaila, K., Anelković, K. *Experimental and theoretical investigation of octahedral and square-planar isothiocyanato complexes of Ni(II) with acylhydrazones of 2-(diphenylphosphino)benzaldehyde,* Polyhedron, **2015**, 89, 271-279.

9. Perić, M., García-Fuente, A., Zlatar, M., Daul, C., **Stepanović, S.**, García-Fernández, P., Gruden-Pavlović, M. *Magnetic anisotropy in "scorpionate" first-row transition-metal complexes: A theoretical investigation,* Chemistry - A European Journal, **2015**, 21 (9), 3716-3726.

Прилог 1.

Изјава о ауторству

Потписани-а Степан Степановић
број индекса ДХ34/2012

Изјављујем

да је докторска дисертација под насловом
Density functional approximations for spin state energetics in transition-metal complexes (Aproksimacije funkcionala gustine u proučavanju energija spinskih stanja kompleksa prelaznih metala)

- резултат сопственог истраживачког рада,
- да предложена дисертација у целини ни у деловима није била предложена за добијање било које дипломе према студијским програмима других високошколских установа,
- да су резултати коректно наведени и
- да нисам кршио/ла ауторска права и користио интелектуалну својину других лица.

Потпис докторанда

У Београду, _____

_____

Прилог 2.

Изјава о истоветности штампане и електронске верзије докторског рада

Име и презиме аутора Степан Степановић
Број индекса ДХ34/2012
Студијски програм Доктор хемијских наука

Наслов рада: Density functional approximations for spin state energetics in transition-metal complexes (Aproksimacije funkcionala gustine u proučavanju energija spinskih stanja kompleksa prelaznih metala)

Ментори др Маја Груден-Павловић, ванредни професор Хемијског факултета Универзитета у Београду и Prof. Dr. Marcel Swart, ICREA Research professor at Institut de Química Computacional i Catàlisi (IQCC), University of Girona

Потписани/а _____

Изјављујем да је штампана верзија мог докторског рада истоветна електронској верзији коју сам предао/ла за објављивање на порталу **Дигиталног репозиторијума Универзитета у Београду.**

Дозвољавам да се објаве моји лични подаци везани за добијање академског звања доктора наука, као што су име и презиме, година и место рођења и датум одбране рада.

Ови лични подаци могу се објавити на мрежним страницама дигиталне библиотеке, у електронском каталогу и у публикацијама Универзитета у Београду.

Потпис докторанда

У Београду, _____

_____

Прилог 3.

Изјава о коришћењу

Овлашћујем Универзитетску библиотеку „Светозар Марковић“ да у Дигитални репозиторијум Универзитета у Београду унесе моју докторску дисертацију под насловом:

Density functional approximations for spin state energetics in transition-metal complexes (Aproksimacije funkcionala gustine u proučavanju energija spinskih stanja kompleksa prelaznih metala)

која је моје ауторско дело.

Дисертацију са свим прилозима предао/ла сам у електронском формату погодном за трајно архивирање.

Моју докторску дисертацију похрањену у Дигитални репозиторијум Универзитета у Београду могу да користе сви који поштују одредбе садржане у одабраном типу лиценце Креативне заједнице (Creative Commons) за коју сам се одлучио/ла.

1. Ауторство
2. Ауторство - некомерцијално
3. Ауторство – некомерцијално – без прераде
4. Ауторство – некомерцијално – делити под истим условима
5. Ауторство – без прераде
6. Ауторство – делити под истим условима

(Молимо да заокружите само једну од шест понуђених лиценци, кратак опис лиценци дат је на полеђини листа).

Потпис докторанда

У Београду, _____

_____

1. Ауторство - Дозвољавате умножавање, дистрибуцију и јавно саопштавање дела, и прераде, ако се наведе име аутора на начин одређен од стране аутора или даваоца лиценце, чак и у комерцијалне сврхе. Ово ј најслободнија од свих лиценци.

2. Ауторство – некомерцијално. Дозвољавате умножавање, дистрибуцију и јавно саопштавање дела, и прераде, ако се наведе име аутора на начин одређен од стране аутора или даваоца лиценце. Ова лиценца не дозвољава комерцијалну употребу дела.

3. Ауторство - некомерцијално – без прераде. Дозвољавате умножавање, дистрибуцију и јавно саопштавање дела, без промена, преобликовања или употребе дела у свом делу, ако се наведе име аутора на начин одређен од стране аутора или даваоца лиценце. Ова лиценца не дозвољава комерцијалну употребу дела. У односу на све остале лиценце, овом лиценцом се ограничава највећи обим права коришћења дела.

4. Ауторство - некомерцијално – делити под истим условима. Дозвољавате умножавање, дистрибуцију и јавно саопштавање дела, и прераде, ако се наведе име аутора на начин одређен од стране аутора или даваоца лиценце и ако се прерада дистрибуира под истом или сличном лиценцом. Ова лиценца не дозвољава комерцијалну употребу дела и прерада.

5. Ауторство – без прераде. Дозвољавате умножавање, дистрибуцију и јавно саопштавање дела, без промена, преобликовања или употребе дела у свом делу, ако се наведе име аутора на начин одређен од стране аутора или даваоца лиценце. Ова лиценца дозвољава комерцијалну употребу дела.

6. Ауторство - делити под истим условима. Дозвољавате умножавање, дистрибуцију и јавно саопштавање дела, и прераде, ако се наведе име аутора на начин одређен од стране аутора или даваоца лиценце и ако се прерада дистрибуира под истом или сличном лиценцом. Ова лиценца дозвољава комерцијалну употребу дела и прерада. Слична је софтверским лиценцама, односно лиценцама отвореног кода.